

University of Alberta

OPERATION OF A GRID CONNECTED VARIABLE WIND TURBINE WITH A
FLYBACK CONVERTER

by

Jamal Ahmed Baroudi ©

A thesis submitted to the Faculty of Graduate Studies and Research
in partial fulfillment of the requirements for the degree of

Master of Science

Department of Electrical and Computer Engineering

Edmonton, Alberta

Fall, 2007



Library and
Archives Canada

Bibliothèque et
Archives Canada

Published Heritage
Branch

Direction du
Patrimoine de l'édition

395 Wellington Street
Ottawa ON K1A 0N4
Canada

395, rue Wellington
Ottawa ON K1A 0N4
Canada

Your file *Votre référence*
ISBN: 978-0-494-33195-8
Our file *Notre référence*
ISBN: 978-0-494-33195-8

NOTICE:

The author has granted a non-exclusive license allowing Library and Archives Canada to reproduce, publish, archive, preserve, conserve, communicate to the public by telecommunication or on the Internet, loan, distribute and sell theses worldwide, for commercial or non-commercial purposes, in microform, paper, electronic and/or any other formats.

The author retains copyright ownership and moral rights in this thesis. Neither the thesis nor substantial extracts from it may be printed or otherwise reproduced without the author's permission.

AVIS:

L'auteur a accordé une licence non exclusive permettant à la Bibliothèque et Archives Canada de reproduire, publier, archiver, sauvegarder, conserver, transmettre au public par télécommunication ou par l'Internet, prêter, distribuer et vendre des thèses partout dans le monde, à des fins commerciales ou autres, sur support microforme, papier, électronique et/ou autres formats.

L'auteur conserve la propriété du droit d'auteur et des droits moraux qui protègent cette thèse. Ni la thèse ni des extraits substantiels de celle-ci ne doivent être imprimés ou autrement reproduits sans son autorisation.

In compliance with the Canadian Privacy Act some supporting forms may have been removed from this thesis.

Conformément à la loi canadienne sur la protection de la vie privée, quelques formulaires secondaires ont été enlevés de cette thèse.

While these forms may be included in the document page count, their removal does not represent any loss of content from the thesis.

Bien que ces formulaires aient inclus dans la pagination, il n'y aura aucun contenu manquant.


Canada

To my parents:

Ahmed and Fatme

You have been of constant admiration in my life.

To my siblings:

Mohamed

Joumana

Jenan

Your support and encouragement throughout my professional preparation has been exceptional.

I love you all, my dear family.

Abstract

The use of small-scale grid connected wind turbines offers the opportunity for consumers to meet their energy needs and also possibly sell excess energy to the grid. The power electronic converter controls the generator and obtains optimal energy transfer from the generator to the grid. Many converter topologies offer two controllable rectifiers for AC-DC and DC-AC conversion with a separate transformer providing electrical isolation. This research proposes a unique energy converter for a small-scale variable wind turbine that employs a simple open-loop control. The converter uses a flyback DC-DC boost stage that includes a transformer for electrical isolation between the generator and grid. A single-phase inverter completes the transfer of power to the grid, resulting in a cost efficient design with just three power electronic switches. The benefits of a controlled system have been verified in simulation and the final test rig has been tested experimentally.

Acknowledgments

Successful completion of this thesis would not have been possible without the love and support from my parents, brother and sisters. They have proven the importance of having strong family bonds when I was faced with adversity during my graduate studies. My family has taken a genuine interest in my research and has provided continual encouragement throughout this process.

Outstanding individuals surrounded me at the University of Alberta. Most important to me was Dr. Knight, an exceptional supervisor that made this research project a positive experience. Dr. Knight has provided encouragement and knowledge to aid in my completion, while exhibiting great patience.

Numerous times Dr. Salmon has openly offered his wealth of experience and knowledge. He has freely offered equipment for the experimental setup and has played a considerable role in this research.

I am very thankful for the great friendships that have resulted from my time in the power lab. Sami Abdulsalam and Ian Roberge have been more than willing to give me a hand when needed. Special thanks given to Albert Terheide for being a great friend and willingly providing his expertise. He has helped throughout this process and most of with the experimental setup.

Additional thanks to the Natural Sciences and Engineering Research Council (NSERC) of Canada and the Informatics Circle of Research Excellence (ICORE) for generously funding this research.

I have gained valuable knowledge during my graduate experience and am grateful to have gained new friendships with fine individuals.

Table of Contents

1	Introduction.....	1
1.1	Wind Energy Today.....	1
1.2	State of the Art.....	3
1.3	Objective of Thesis.....	5
1.4	Outline of Thesis.....	6
2	Ideology of Wind Energy	7
2.1	Potential Wind Power.....	7
2.2	Grid Connected Wind Energy System.....	9
2.2.1	Wind Turbine Designs and Power Capture	10
2.2.2	Electric Generator Prospects	12
2.2.3	Energy Conversion	15
2.3	Control of Variable Speed Wind Turbines.....	19
2.3.1	Methodology of Control.....	19
2.3.2	Fixed and Variable Speed Control.....	20
2.4	Chapter Summary.....	21
3	Small-Scale Wind Energy Systems	22
3.1	Power Converters and Controllers.....	22
3.1.1	Power Converter Topologies and Cost Effectiveness.....	23
3.1.2	Possible Options for DC-DC Boost Stage.....	24
3.1.3	Controller Complexity Issues	26
3.2	Proposed Generator and Converter System	29
3.2.1	Chosen Converter Topology for Wind Conversion	30
3.2.2	Simple Control Methods.....	30
3.3	Chapter Summary.....	33
4	Simulation of Proposed Research	34
4.1	Simulation Setup and Parameters	34
4.2	Verification of Flyback Converter.....	35
4.3	Determination of Fixed Relationships.....	40
4.4	Wind Energy System Simulation	42

4.4.1	Simulation Algorithm	42
4.4.2	Fixed DC-Link Dynamic Results.....	47
4.4.3	Variable DC-Link Dynamic Results.....	50
4.4.4	Controller Step Response Results.....	52
4.5	Chapter Summary.....	54
5	Experimental Design.....	55
5.1	Wind Turbine Emulator.....	56
5.1.1	Permanent Magnet DC Motor.....	56
5.1.2	DC Power Supply.....	57
5.1.3	Speed Encoder.....	58
5.1.4	LabView Real-Time DC Current Control.....	58
5.2	Brushless Permanent Magnet Generator.....	60
5.3	Power Electronic Converter.....	61
5.3.1	Flyback Converter Design	61
5.3.2	Single-Phase Inverter.....	66
5.4	Grid Connection	67
5.5	Proposed Converter Controller	68
5.5.1	Generator Speed Measurement.....	68
5.5.2	Flyback Control and Driver Circuitry	70
5.5.3	Inverter Control and Algorithm	73
5.6	Chapter Summary.....	78
6	Experimental Results	79
6.1	Measurement Equipment.....	79
6.2	Controller Verification	81
6.2.1	Inverter Phase Angle Control.....	82
6.2.2	Fixed Relationship Control.....	85
6.3	Variable Wind Profile Response	87
6.4	Controller Step Response	91
6.5	Chapter Summary.....	95
7	Conclusions and Future Work.....	96
8	Bibliography	99

List of Tables

2.1	Average Wind Speeds and Available Wind Power in Alberta	8
4.1	Flyback Converter Simulation Parameters	34
4.2	Wind Energy System Simulation Parameters	35
5.1	Permanent Magnet DC Motor Properties	56
5.2	Permanent Magnet DC Motor Performance Specifications (at 1800 rpm).....	57
5.3	DC Power Supply Electrical Specifications.....	57
5.4	Brushless Servo Motor Specifications.....	60

List of Figures

2.1	Typical Topology of a Grid Connected Wind Energy System	10
2.2	Typical Coefficient of Performance Curve	11
2.3	Turbine Output Power Characteristic	11
2.4	Typical DFIG Wind Energy System.....	12
2.5	Single Phase Equivalent Circuit of an Induction Generator	13
2.6	Single Phase Equivalent Circuit of a Synchronous Generator.....	14
2.7	DFIG Wind Energy System with Matrix Converter	18
3.1	Three Possible DC-DC Converters for DC-link Boost.....	25
3.2	MPPT Search Operation	27
3.3	Proposed System and Control Topology	29
3.4	Turbine Torque and Control Operation	32
4.1	Simulated Flyback Converter with Snubber Circuit	36
4.2	Results for a Flyback Input of 60 V.....	37
4.3	Detailed Waveforms for a Flyback Input of 60 V	37
4.4	Results for a Flyback Input of 9 V	39
4.5	Detailed Waveforms for a Flyback Input of 9 V	39
4.6	Algorithm for Finding the Fixed Relationships for Current Control	40
4.7	Ideal DC-link Current vs. Mechanical Frequency.....	41
4.8	Simulation Algorithm Including Controller.....	44
4.9	Generator Conduction through Diode Rectifier	45
4.10	Simplified Generator Conduction Circuit.....	45
4.11	Simulation Results with a Constant DC-Link of 36 V	47
4.12	Simulation Results with a Constant DC-Link of 42 V	48
4.13	Simulation Results with Proposed Control – 1 ms Time Step.....	50
4.14	Simulation Results with Proposed Control – 5 ms Time Step.....	51
4.15	Simulation Results with Proposed Control – 10 ms Time Step	52
4.16	Proposed Controller Simulated 5 m/s Step-Down Response	53
4.17	Proposed Controller Simulated 5 m/s Step-Up Response.....	53

5.1	Experimental Test Rig Design Schematic	55
5.2	Algorithm for the LabView Wind Turbine Emulator	59
5.3	Final Flyback DC-DC Converter with Snubber.....	61
5.4	Transformer Design Algorithm	63
5.5	Observed Primary Current through the Flyback Transformer	64
5.6	Half-Bridge Connection of a 6-Switch Inverter	66
5.7	Grid Connection Circuit Schematic	67
5.8	Pulse Generation Circuit for Voltage to Frequency Measurement of PMG.....	68
5.9	Single-Rail Comparator Circuit Design.....	69
5.10	Theoretical Duty Ratio vs. Electrical Frequency Fixed Relationship	71
5.11	Flyback MOSFET Gate Driver Circuit with Current Sensing	72
5.12	Flyback Driver Chip Current Sensing Circuit.....	72
5.13	Inverter and Grid Output Circuit Diagram.....	74
5.14	Inverter Output Phasor Diagram.....	74
5.15	Theoretical Phase Angle vs. Electrical Frequency Fixed Relationship.....	75
5.16	LabView Inverter Phase Angle and Switching Algorithm	76
5.17	Sinusoidal Reference Transition for LabView FPGA PWM Switching.....	77
6.1	Generator Side Connection of Yokogawa Power Meter.....	80
6.2	High DC-Link and Grid Measurement Circuit.....	80
6.3	Yokogawa Connection for High DC-Link and Grid Measurement.....	81
6.4	Inverter PWM Switching at Positive Peak of Reference Signal	82
6.5	Inverter PWM Switching at Negative Peak of Reference Signal.....	83
6.6	Fourier Transform Results for Inverter Angle Verification	84
6.7	Inverter Output Phasor Diagram for Angle Verification.....	84
6.8	Comparison of Optimal Duty Ratio Relationships.....	85
6.9	Comparison of Optimal Inverter Angle Relationships.....	86
6.10	Comparison of Theoretical and Experimental Flyback Input DC Voltage	86
6.11	Optimal Power Curves at Various System Stages	87
6.12	Dynamic System Response with a Variable Wind Speed.....	88
6.13	V_{DC2} , Commanded Angle, and Duty Ratio with a Variable Wind Speed.....	89
6.14	Various System Power Results with a Variable Wind Speed	90
6.15	Flyback Efficiency and Energy Capture with a Variable Wind Speed	91

6.16	Dynamic System Response with a 1 m/s Wind Step Change	92
6.17	V_{DC2} , Commanded Angle, and Duty Ratio with a 1 m/s Wind Step Change	93
6.18	Dynamic System Response with a 2 m/s Wind Step Change	94
6.19	V_{DC2} , Commanded Angle, and Duty Ratio with a 2 m/s Wind Step Change	94

List of Symbols

A	wind turbine swept area
A_m	transformer magnetizing area
A_{wind}	core window area
A_{wire}	total winding wire area
A_{xsec}	cross sectional wire area
B	magnetic flux density
C	capacitance
C_L	load capacitance
C_O	flyback output capacitance
C_S	snubber capacitance
C_P	turbine coefficient of performance
C_i	flyback input capacitance
C_{sw}	capacitance across flyback switch
d	flyback duty ratio
d_w	winding wire diameter
E_A	generator induced voltage
f_{sw}	flyback switching frequency
I	current
I_D, I_A	stator current
I_2	rotor current
I_{DC}	DC-link current
I_F	field current
I_G	grid current
I_a	armature current
I_{pb}	phase current
I_q	quadrature axis current
i	instantaneous current
J	inertia
K	machine constant

K_E	machine voltage constant
K_T	machine torque constant
K_a, K_b	numerical constants
L	inductance
L_{Crit}	transformer critical magnetizing inductance
L_G	generator phase inductance
l	transformer wire length
N_1	number of transformer primary winding turns
N_2	number of transformer secondary winding turns
n	transformer turns ratio
P	power
P_{gen}	generator output Power
P_T	turbine output Power
P_w	potential wind power
Q_{Gate}	MOSFET gate charge
R	resistance
R_1, X_1	stator impedances
R_2, X_2	rotor impedances
R_A	armature resistance
R_F, X_F	field impedances
R_G	generator phase resistance
R_{Gate}	MOSFET gate resistance
R_L	load resistance
R_S	snubber resistance
R_m, X_m	magnetizing impedances
r	turbine radius
s	slip
T	torque
TSR	tip-speed ratio
T_S	switching period
T_{gen}	generator torque
T_{ind}	induced torque

T_{trb}	turbine torque
T_f	friction torque
t	time
V	voltage
V_p, V_φ	phase voltage
V_{DC}	DC-link voltage
$V_{DC,i}$	flyback input DC-link voltage
$V_{DC,o}$	flyback output DC-link voltage
V_F	field voltage
V_G	grid voltage
V_{inv}	inverter output voltage
V_L	line inductance voltage
V_S	snubber voltage
V_{comm}	commutation overlap voltage
V_d	diode forward bias voltage
V_{o1}	fundamental output voltage
V_{sw}	MOSFET switch voltage
v_w	wind speed
X_{LS}	inverter output line reactance
X_S	synchronous reactance
W	energy
δ	inverter phase angle
δt	change in time
φ	flux density
ρ	air density
ρ_C	resistivity of copper
θ	power factor angle
θ_e	electrical angle
τ	time constant
ω_e	electrical rotational frequency
ω_m	mechanical rotational frequency

Chapter 1

Introduction

The importance of wind energy generation and the affect it has in today's world is first described. Statistics are provided showing the viability of wind energy among traditional power generation and the promising future of this clean energy source. A general description of the components of a wind energy conversion system is outlined. Typical examples of generators and converter topologies are given for high power and low power systems. A converter topology chosen for this research is outlined along with the type of control that will be used to obtain optimal power extraction from the turbine. Finally, an outline of the complete thesis is given for the remainder of the chapters.

1.1 Wind Energy Today

Wind energy has arrived as a global market and over the past decade has rapidly developed into a mainstream power source in many countries worldwide. In 2005, global wind markets grew by 40.5%, generating some 12 billion Euro, or 14 billion USD, in new generating equipment. The world's wind energy generating capacity at the close of 2005 stood at over 59 GW, and is predicted to reach 1,000 GW by 2020, supplying 12% of the worldwide energy [1]. Wind energy has the potential to aid in responding to the crucial energy challenges facing society today. These challenges include the security of the supply of natural resources, alarming climate changes, increasing energy demand and erratic fossil fuel prices. Wind generation is a clean power source having numerous positive effects on the environment, and undoubtedly assists in reducing greenhouse gasses in the atmosphere. It is estimated that wind energy keeps more than 200 million tons of carbon dioxide out of the atmosphere every year [2].

Renewable energy technologies are often characterised by relatively higher capital costs while maintaining lower operating cost. Many technological advances in the turbine

blades, generators used and conversion methods have helped steadily decrease the cost of energy generation. Capital costs have substantially declined over the past two decades, with wind energy cost declining up to 200% [3]. This has forced wind energy production costs to drop down by 80% since 1980 to 5.0 US cents per kilowatt hour or less [4]. Not only has cost effectiveness increased, but also the support of the public has turned in favour of wind energy. Once thought as an eye sore and distractingly noisy, wind turbines are becoming readily accepted by communities due to their increasing environmental benefits and clean energy generation abilities. In the US, renewable energy sources have more credibility with the public (42%) than non-renewable such as fossil fuels (7%) and nuclear power (9%) [5].

The future of wind energy continues to look tremendously promising. The introduction of offshore wind farms is receiving positive attention. A main advantage of offshore generation is that wind speeds are more consistent and less turbulent over water. Currently about 600MW of offshore wind exists, all in Europe, with the first completed in 2003 in Denmark [6]. It is also predicted that through 2006 off-shore wind generation in the United Kingdom will have a capacity of 1500 MW, which is 15% of the UK's energy demand [7]. Turbine size and power rating also continue to increase with 3.6 MW generators currently available by GE Wind Energy. It is anticipated that by 2010, turbines of more than 5 MW will be available on the market [7]. Although wind energy has been dominant in the European countries, North America has entered the wind market with astounding yearly increases in wind power generation. The American Wind Energy Association projects wind energy will be able to provide 6% of the U.S. electricity demand by 2020. Canada is also showing tremendous growth and has increased its wind energy generation by 54% in 2005 [8]. It is estimated that by 2010, the cumulative installed capacity in Canada will have reached 5,000 MW. This means that 4,300 MW will be introduced during the period 2006-2010 listing Canada in the top five countries for that period [1].

The importance of minimizing the cost of the power electronic converter for small scale designs can be shown by investigating the current cost of these systems. A manufactured 1 kW wind turbine, that includes the converter, can be bought from the Bergey Windpower Company at a price of 2590 US dollars [9]. Without the converter, the cost decreases to 2082 US dollars. This means that the converter and control cost is set at 508 US dollars, nearly 20% of the overall cost. Decreasing the converter and control cost is advantageous and would have a significant affect on the entire system cost.

The statistics show wind energy will continue to grow globally through unrelenting research efforts and strong political support for clean renewable energy production. Research in wind energy conversion continues to grow due to the advances in power electronics used to aid in the conversion of a highly variable generator output voltage. Power electronics have made grid connection for wind turbines extremely viable. Their ability to stabilize the generated voltage through control algorithms, keeps the voltage at grid connection constant. Variable speed turbines are preferred since they allow for increased power efficiency and energy extraction from the variable wind source. There exists an optimum generator speed for every wind speed that seizes maximum electrical power from the wind passing through the turbine. As the wind speed changes it is important to have a speed controller that reacts to the changes in wind speed and controls the generator speed to match optimum points. Many power electronic devices have been used in various different combinations, some allowing for greater control and some achieving a low cost implementation.

1.2 State of the Art

Wind energy systems cover a wide range of power levels, with the large scale designs now reaching approximately 3.6 MW. Small scale turbines, designed for residential and commercial use, are of the low kilowatt power range. Typically, wind energy systems consist of a turbine, generator and an electronic converter. Various generators have been used including synchronous generators, induction generators, permanent magnet synchronous generators, and more recently doubly-fed induction machines. Early research invoked the use of a diode rectifier along with a thyristor rectifier and a reactive power compensator for power conversion [10]. As power electronic technology advanced, researchers have replaced thyristor rectifiers with inverters using fast switching semiconductor devices. A DC to DC converter may be placed in between the diode rectifier and inverter, which increases the systems controllability [11]. System control is further enhanced when back to back controlled rectifiers are used [12, 13, 14, 15, 16]. Controllers based on a Maximum Power Point Tracking (MPPT) technique constantly search for the maximum power point at all wind speed to maximize performance [14, 15, 16]. Other control methods include vector control

of both generator and grid-side converters [13] and the implementation of a fuzzy logic control scheme [12]. Recently, researchers have proposed implementing a matrix converter since it completes the wind energy conversion in just one stage with 18 unidirectional devices. Control of the matrix converter involves complex space vector pulse width modulation [17]. A more comprehensive literature review is given in Chapters 2 and 3.

Systems that employ the use of induction generators or doubly-fed induction generators require a controlled rectifier for AC to DC conversion due to their demand for reactive power. Contrarily, synchronous generators are self-excited machines, meaning they require no external reactive power, allowing for the advantageous use of a diode rectifier. The switches of a controlled rectifier are much more expensive than the diodes used in a diode rectifier, and therefore they are more commonly used in large scale designs. This research focuses on a low power wind energy system and therefore a diode rectifier is the more economical choice. Research has shown the usefulness of adding an intermediate DC to DC converter stage to the diode rectifier. However, the converters studied (such as the boost converter) do not provide electronic isolation, a desirable property for grid connected systems. The flyback converter is an option that has not yet been exploited in wind power applications. The flyback allows for intermediate boost capability that can be manipulated, and contains a high frequency transformer that can provide electronic isolation. Recently the matrix converter has gained research interest in wind energy systems. However, these converters are expensive due to the high number of electronic switches used and the complexity of its switch control. Due to the high cost of the matrix converter it is better suited for large scale systems.

The control methods described above are quite complex and require digital signal processors for practical implementation, which is another cost burden on the system. This thesis investigates if a fixed relationship control strategy could perform with less cost and complexity for a small scale system. Fixed relationship control uses predefined correlations between the generator speed and load designed for maximum power extraction.

1.3 Objective of Thesis

The objective of this research is to design a power electronic controller for a small scale grid connected wind energy system that aims to achieve maximum power transfer at all wind speeds while keeping the cost to an absolute minimum. A permanent magnet synchronous generator is chosen due to its superior efficiency and allowance for connection to a diode rectifier. The use of a diode rectifier guarantees minimum cost through the first stage of conversion. The power electronic converter will invoke the use of a flyback converter and a controlled rectifier for single phase grid connection. The flyback is chosen for the intermediate stage since it provides electronic isolation for the grid. Together the flyback converter and single phase inverter only contain three controllable electronic switches, again maintaining minimal cost of the system.

A fixed relationship control scheme will be used to obtain maximum efficiency from the turbine, allowing for simple control implementation through analog circuit components. The overall goal of minimizing cost and maintaining maximum efficiency is achieved through the selection of converter components and control strategy. Since the use of an actual wind turbine is unavailable, the wind turbine connection to the generator is emulated through computer software and a DC motor. The process by which the goals of this research are achieved is outlined below.

- Extensive literature review on past wind energy converters.
- Completion of design of the wind turbine emulator, flyback converter, and speed controller for simulation and experimental implementation.
- Simulation of the flyback converter along with fixed and variable DC-link simulation of the overall system using the wind turbine emulator.
- Construction of the test rig and experimental testing of the entire system and its control.

1.4 Outline of Thesis

This thesis completely describes and illustrates the manner in which the objectives of the research are obtained. Although the focus of the research is on the small-scale design of a wind energy system, it is important to investigate all power ranges to better understand the operation of these systems. Therefore, an extensive literature is first performed on large and small scale systems, specifically investigating generator, converters, and control schemes used. The results of the extensive literature review of existing wind system designs and past research is provided. More specifically, wind turbine characteristics, typical generators and possible converter topologies are described. The majority of this background information is given in Chapter 2. A more detailed analysis of small-scale wind energy systems is necessary since this research focuses on the lower power range. Possible DC-DC boost stage converters are investigated for addition to a diode rectifier. The details of two control strategies, Maximum Power Point Tracking (MPPT) and fixed relationship control, are also described. With the small-scale emphasis set in the beginning of Chapter 3, the remainder of the chapter defines the proposed conversion system. The details and reasons for the chosen generator, converter, and control scheme are reported.

Simulation design and results are shown in Chapter 4, with emphasis placed on the advantages of having a controlled input DC-link voltage rather than leaving it fixed. In addition, the flyback converter is modelled and simulated for verification of its operation and the necessity of the snubber circuit. A fully operational experimental system is the primary focus of this research. A wind emulator is created since a real wind turbine is unavailable, and ensuring practicality is a main concern. The full flyback converter design, including snubber circuit, transformer and driver circuit, is covered in Chapter 5. In addition, this chapter outlines the control design for both the flyback and single phase inverter. All results obtained for the experimental test rig are placed in Chapter 6. The system control is tested while under the influence of a variable wind profile. Results show power outputs at various stages of the converter and the controller performance in obtaining optimal efficiency. Conclusions and future work that may extend the scope of this research are expressed in Chapter 7.

Chapter 2

Ideology of Wind Energy

Developing an efficient grid connected wind energy system entails careful planning and understanding of all aspects of the system. The generator and converter must be designed for maximum efficiency whilst ensuring cost effectiveness. Many designs have incorporated various types of generators that are accompanied by numerous converter design possibilities. The influx of power electronics to the wind energy industry has enabled a significant number of control methods that may be applied to achieve maximum power capture at a wide range of wind speeds. The variable nature of wind power and the importance of optimal control is described in the next section. The wind energy system components, including possible generator types, converter topologies, and control schemes, are also described in this chapter.

2.1 Potential Wind Power

Wind is a product of two separate forces that continually interact with one another. Pressure gradients, produced by uneven solar heating, accelerate the air. The rotation of the earth also produces an additional, but separate, acceleration on the moving air. The action of these two forces creates the wind [18]. As a result wind profiles vary widely over different regions all over the globe. It is due to this varying wind that the system converter must be controlled to obtain maximum power extraction from the wind throughout the wind speed range.

The calculation of the wind power available is better understood by first determining the kinetic energy of a moving volume of air. The mass of air used in determining the kinetic energy is simply the air density multiplied by the volume of air considered. The volume of air is defined as a surface area multiplied by the distance travelled by the air.

$$KE_{air} = \frac{1}{2} \rho A d v_w^2 \quad (2.1)$$

In equation 2.1 the distance travelled by the air can be replaced by the velocity multiplied by the time it takes for the air to move through that distance. Therefore the potential wind power that is available for capture by a wind turbine is simply the kinetic energy over that time.

$$P_w = \frac{1}{2} \rho A v_w^3 \quad (2.2)$$

In Alberta, it is observed that the average wind speeds vary over the region (Table 2.1 [19]). Accompanying the average wind speeds are the available instantaneous wind power for each month in each city. The calculation of the available instantaneous power is based upon the average wind speed and air density for each month for a randomly chosen wind turbine produced by General Electric. A 1.5 MW wind turbine with a rotor diameter of 77 m is used in calculating the area in equation 2.2. The air density for each month is also taken into account since it varies with city altitude and temperature. From these power results it is evident that wind energy is extremely practical in Alberta and should be exploited, especially in the southern region.

Table 2.1: Average Wind Speeds and Available Wind Power in Alberta

Month	Location					
	Edmonton		Calgary		Lethbridge	
	Avg. Wind Speed (m/s)	Power (MW)	Avg. Wind Speed (m/s)	Power (MW)	Avg. Wind Speed (m/s)	Power (MW)
January	3.33	107.06	4.44	238.10	6.11	626.05
February	3.33	105.44	4.17	193.26	5.26	465.12
March	3.61	131.58	4.44	231.95	5.28	392.94
April	4.17	196.32	4.72	272.19	5.83	519.15
May	4.17	191.50	5.00	316.26	5.56	440.57
June	3.89	153.54	4.72	262.72	5.28	371.2
July	3.61	122.09	4.17	179.22	4.44	220.15
August	3.61	122.51	3.89	145.72	4.17	181.40
September	3.61	125.10	4.17	182.38	4.72	268.67
October	3.61	127.34	4.17	185.65	5.83	515.45
November	3.33	103.49	4.17	191.12	5.83	530.55
December	3.33	106.25	3.89	158.31	6.11	623.71

It is known, through equation 2.2, that the available power is related to the wind speed via a cubic relationship. This implies that the average wind speed of a region does not determine the average power of that area. For example the same wind turbine may be placed in two separate regions with identical average wind speeds. However the first region may experience high fluctuations in wind speed where as the second may undergo very little deviation from the average wind speed. In this case, the turbine in the first region will capture a greater amount of energy, this can be attributed to the cubic relationship between power and wind speed. Instantaneous power is highly dependant on instantaneous wind speed. Instances of high wind speeds will create brief periods of high energy capture. On the other hand it is very rare to find a site with frequent or constant high wind speeds; low wind speeds are more common and are very important in system design as well. It is ideal to design a converter that is able to operate at low cut-in wind speed to maximize wind energy capture.

Often wind turbine generators are placed in locations where extremely high wind speeds have historically occurred. These high wind speeds have the ability to mechanically or electrically damage the wind energy system. Thus it is important to develop a control that allows for the system to cut out at extreme wind speeds to prevent extensive damage. Methods of cut-out control include forcing an aerodynamic stall or feathering the turbine blades [20]. Clearly each wind turbine installation must consider the sites' past wind speed averages and extremes in order to prevent damage to the system and guarantee that the highest efficiency is achieved.

2.2 Grid Connected Wind Energy System

Grid connected wind energy systems typically consist of a wind turbine, generator, power electronic converter and grid connection (shown in Figure 2.1). The generator is connected to the turbine through a shaft allowing it to transform the turbine mechanical energy into electrical energy. A power electronic converter, usually consisting of two stages, is responsible for transferring power to the grid. Control is applied to the converter to ensure maximum power transfer and the compliance of power quality standards. This is the typical process of conversion that will be applied for this research and the experimental test rig.

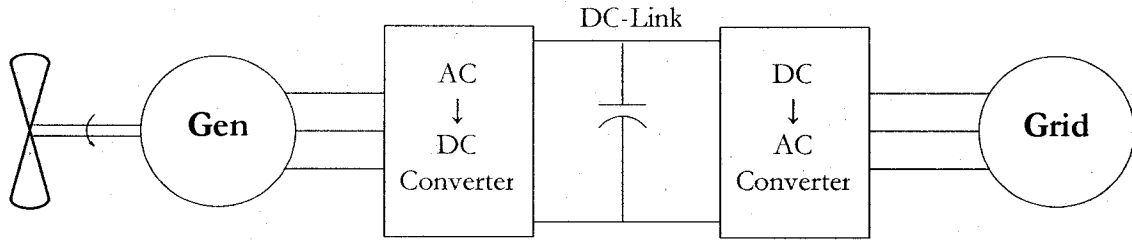


Figure 2.1: Typical Topology of a Grid Connected Wind Energy System

2.2.1 Wind Turbine Designs and Power Capture

Over the past century wind turbine designs have evolved into many different forms. There are two main types, horizontal axis and vertical axis rotating wind turbines. In horizontal axis designs, the axis of rotation is parallel to the ground and roughly perpendicular to the wind stream. Conversely, vertical axis turbines have an axis of rotation that is vertical to the ground. Three blade horizontal axis turbines have become the most widely used in grid connected wind energy systems.

Each turbine design has an efficiency known as the coefficient of performance (C_p), a value quantifying the percentage of potential wind power that is captured for transfer through the generator. The coefficient of performance is influenced by the tip-speed ratio (TSR); the ratio of the speed of the rotating tip to the speed of the wind.

$$TSR = \frac{\omega_m r}{v_w} \quad (2.3)$$

There is a theoretical upper limit to the coefficient of performance of 0.593, known as the Betz limit [21]. However, in practice real wind rotors have maximum coefficient of performance values in the range of 0.25-0.45 [22]. The turbine efficiency varies with the wind turbines TSR and will reach a maximum at one specific TSR value. In order to achieve maximum power capture the TSR should be kept at the optimal operating point for all wind speeds. To keep the TSR at its optimal value the generator mechanical speed must be altered proportionally with the wind speed, hence giving rise to the name variable speed wind turbine. Research has shown that, under identical wind conditions, a variable speed wind turbine can capture 9-11% more energy than a fixed-speed turbine [23].

Figure 2.2 depicts a typical C_p versus TSR curve for a wind turbine. The curve shows a maximum coefficient of performance of approximately 0.41 at a single TSR value of about 7.8. Likewise, the turbine power output can be plotted versus the turbine rotational speed for different wind speeds, an example of which is shown in Figure 2.3 for a small scale wind turbine. The curves indicate that the maximum power point increases and decreases as wind speed rises and falls.

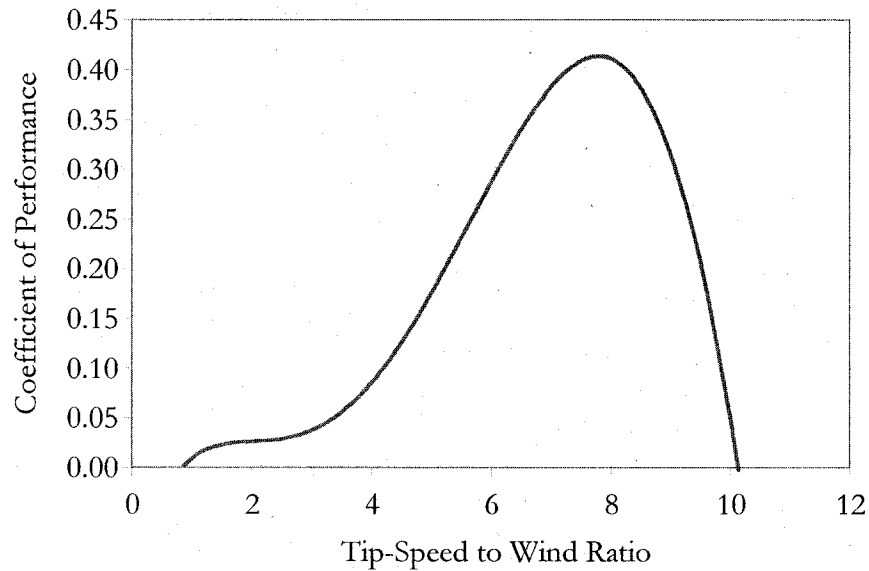


Figure 2.2: Typical Coefficient of Performance Curve

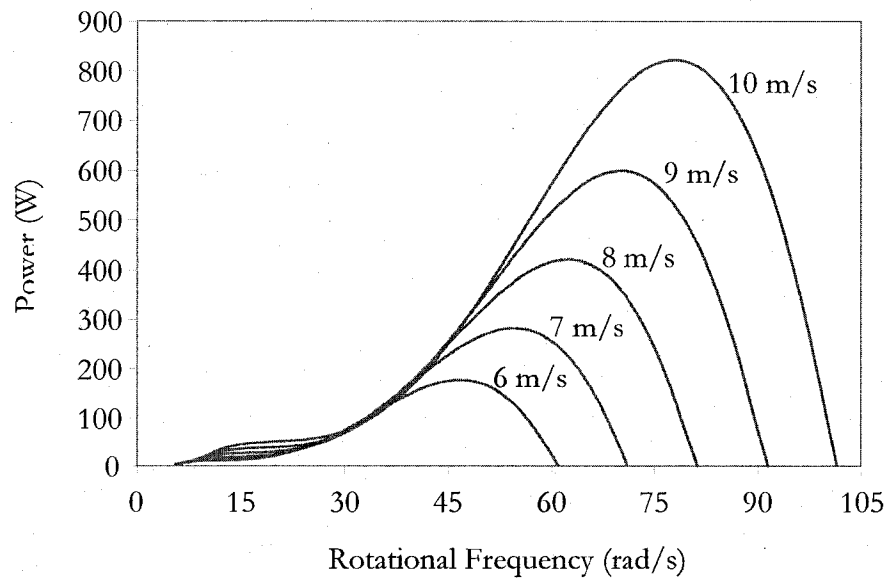


Figure 2.3: Turbine Output Power Characteristic

2.2.2 Electric Generator Prospects

Wind energy systems have been carefully researched over the past several years. Large and small scale wind turbines may be connected to a variety of electrical generators to convert the created mechanical energy to electrical power. The most common generators used are the induction generator, synchronous generator and doubly fed induction generator. While these machines are highly used in large scale systems, the permanent magnet synchronous generator is commonly used in small scale grid connected systems. All generators listed above are described in further detail below to provide a comparative study before a generator is chosen for the experimental setup.

Doubly Fed Induction Generators

The doubly fed induction generator (DFIG) has recently received a great deal of attention in wind energy conversion. In this case, a wound rotor induction generator is used which makes it possible to control the generator by accessing the rotor terminals, shown in Figure 2.4. Wound rotor induction generators require extra maintenance due to the wear associated with their brushes and slip rings. However, it is able to transfer maximum power over a wide speed range in both sub- and super-synchronous modes. These generators are excellent for high power applications in the MW power range. More importantly the converter power rating is reduced since it is connected to the rotor, whilst the majority of the power flows through the stator.

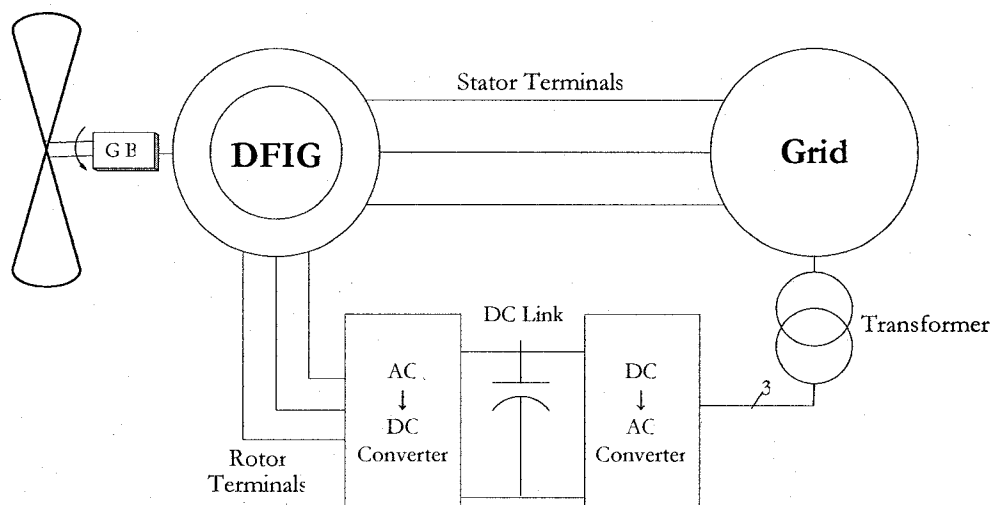


Figure 2.4: Typical DFIG Wind Energy System

Operation of a DFIG with variable wind speed applications offers several advantages, including the ability to control rotor speed to follow the ideal TSR and improve turbine efficiency as the wind speed varies. Other advantages include a reduction in mechanical stress and torque oscillations that may be converted to electrical disturbances transmitted to the grid [24]. These disturbances may include variation in grid voltage that can cause a reduction in power quality. For DFIG schemes, numerous converter schemes have been researched including back-to-back pulse width modulation (PWM) converters. Other possibilities are the use of a rotor-side diode rectifier accompanied by a grid-side controllable inverter and more recently the utilization of a single matrix converter.

Induction Generators

Induction generators are advantageous since they are relatively inexpensive, robust and require low maintenance. A squirrel-cage induction generator consists of a wound stator and a series of conducting bars laid into slots in the face of the rotor and short circuited at either end by end-rings.

The nature of induction generators is unlike that of synchronous generators. Induction generators need bi-directional power flow in the generator-side converter since they require external reactive power support from the grid. An equivalent circuit for one phase of an induction generator is given in Figure 2.5 [21]. The stator impedances are labelled R_1 and X_1 , whereas R_2 and X_2 are the rotor impedances. The magnetizing branch resistance (R_m) represents the losses due to eddy currents and X_m represents the magnetizing reactance.

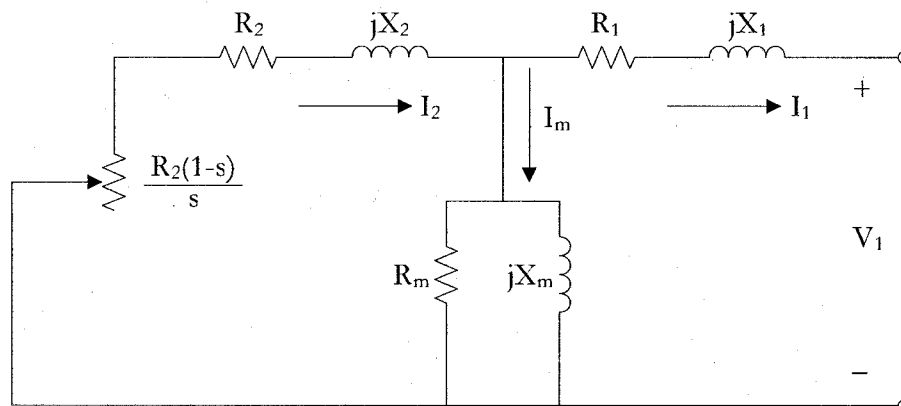


Figure 2.5: Single Phase Equivalent Circuit of an Induction Generator

The magnetizing reactance demands reactive current from the grid, without this reactive power the induction generator cannot operate. So when the connection to the utility is broken, the induction generator no longer receives reactive power and is not able to produce real power. In order to receive reactive power from the grid, the power electronic converter must allow bi-directional power flow. More specifically, the generator side converter must be a controllable rectifier. Therefore, the use of a diode rectifier may only be possible if a capacitive bank is used to provide the reactive power needed. However, incorporating a capacitive bank comes at an increase in cost. Most commonly back-to-back PWM converters are used in conjunction with an induction generator as they allow bi-directional power flow. However, this increases the number of controllable switches and cost.

Synchronous Generators

Synchronous generators offer a number of advantages over induction generators when used for wind generation systems. Synchronous generators are self excited machines that do not require reactive power from an external source or the grid. Self excitation implies that the direct-current (DC) field voltage (V_F), which supplies the field current (I_F) (energizing the rotor magnets), is created by the generator itself. Figure 2.6 depicts the full equivalent circuit of a single phase of a three-phase synchronous generator, including the rotor field circuit [25]. The field circuit is modelled by a DC power source (V_F) supplying the coils inductance (X_F) and resistance (R_F) in series. Each phase has an internally generated voltage (E_A) with a series inductance (X_s) and resistance (R_A). The field resistance is adjustable and is used to control the flow of field current.

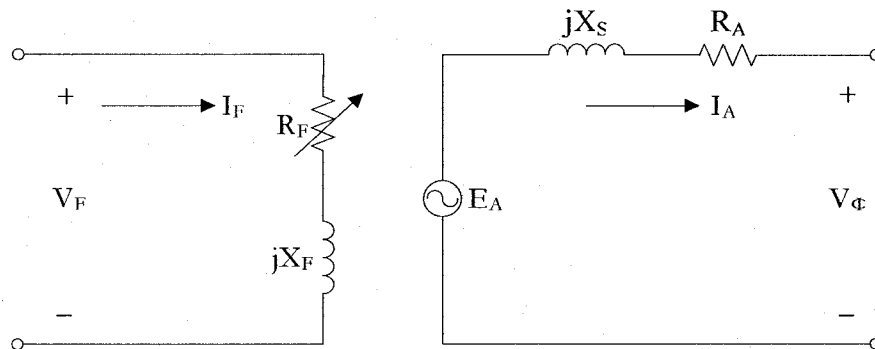


Figure 2.6: Single Phase Equivalent Circuit of a Synchronous Generator

The efficiency of a synchronous generator is usually high, because it employs the whole stator current for the electromagnetic torque production [26]. The converter cost can also be reduced by using a diode rectifier for the generator side since it does not require reactive power from the grid. In addition to supplying real power, the synchronous generator has the ability to supply either inductive or capacitive reactive power to a load.

Permanent Magnet Synchronous Generators

A permanent magnet synchronous generator is similar to the synchronous generator except the rotor field is produced by permanent magnets rather than through a field coil. This implies that there are no I^2R losses in the rotor, ultimately helping to increase the efficiency of the generator. Windings remain on the stator and a constant magnetic field is generated. Through application of Faraday's Law, the magnet induces a voltage across the stator windings each time it rotates past the windings. The induced voltage in the windings can be increased by using a stronger magnet in the rotor

Permanent magnet excitation is generally favoured in newer smaller scale turbine designs, since it allows for higher efficiency and smaller wind turbine blade diameter. Whilst recent research has considered larger scale designs, the economics of large volumes of permanent magnet material have limited their practical application. However the cost of constructing the permanent magnets continues to decrease. The primary advantage of permanent magnet synchronous generators is they do not require any external excitation current. This allows for the use of a diode bridge rectifier at the generator terminals. Much research has been performed using the diode rectifier; however, this leaves many options for the remainder of the power converter, including the possible use of mid stage DC-DC converter.

2.2.3 Energy Conversion

Grid connected converters typically involve two stages of energy conversion, a generator-side and supply side converter connected by a DC-link. In certain situations an intermediate DC-DC converter stage is added to allow for additional control by adding just one more power electronic switch, which is of minimal increase in cost. Many variations have been

studied, some of which will be further described together with possible advantages and disadvantages associated with their implementation.

Diode Rectifier + Inverter

The employment of a diode rectifier is common with permanent magnet synchronous generators used in small scale wind energy system designs. Since diodes are far less expensive than switches used in controllable rectifiers, the diode rectifier reduces the overall cost of the converter. It also guarantees unity power factor operation of the generator, which in turn includes benefits such as greater efficiency, larger power density, and improved power quality. The grid-side inverter (see Figure 2.1) may be constructed of thyristors (also known as semiconductor controlled switches (SCR)) or PWM controlled hard-switching devices.

Thyristors are triggered into the on-state and allow current flow by applying a pulse of positive gate current for a short duration. The thyristor then operates like a diode and only switches off when the current through it tries to reverse and becomes negative. At this point the gate regains control and must be triggered again to turn the switch back on. Using a thyristor based grid-side inverter allows continuous control of the inverter triggering, regulating turbine speed through the DC-link voltage; hence, obtaining optimum energy capture [10]. Advantages of this scheme include lower device cost and higher available power rating over hard switched inverters. A major drawback to this type of inverter is the reactive power demand which is usually supplied by the grid. Having a reactive power demand does not allow the grid inverter to operate at unity power factor. The thyristor also has the consequence of creating harmonic distortion which is absorbed by the grid.

Hard switched devices, such as the insulated gate bipolar transistor (IGBT), allow complete switching control. The most common method, sinusoidal PWM, compares a reference sinusoidal waveform with a high frequency triangular carrier waveform to determine the on and off instances of the switch. The peak amplitude of the sinusoidal waveform directly determines the modulation index. In turn, the modulation index affects the switching sequence and the magnitude of the output voltage or the DC-link, depending on which one is free to be controlled. These switches have lower power dissipation, and are fairly easy to implement and control. Advances in the design and production of semiconductor technology have made hard switches available for high power applications, such as grid connected wind energy systems.

Controlled Rectifier + Inverter

A converter consisting of a controlled rectifier and a controllable inverter may be used with any of the aforementioned generators. By replacing the generator-side diode rectifier with a controlled rectifier the converter has additional options for generator control. Once again thyristor switches or PWM hard-switching devices may be used for the controlled rectifier. The generator-side converter switching may be controlled in such a manner that produces maximum electrical torque from the generator while minimizing current. This type of a converter opens up more control options for the supply-side converter. Vector control may be implemented to simultaneously control the DC-link voltage and reactive power transfer to and from the grid. Finally, a generator-side controlled rectifier is able to meet the reactive power demands of an induction generator based wind turbine.

Diode Rectifier + DC Boost + Inverter

A DC boost stage can be added as an intermediate stage between the diode rectifier and the grid-side inverter. Adding the extra stage does not significantly affect the cost of the converter since the boost stage may only contain as little as one switch. The DC boost stage gives the advantage of generator-side DC-link voltage manipulation through simple control of the duty ratio of the boost converter switch. The duty ratio is simply the ratio of switch on time to switch off time over one switching cycle. The inverter therefore no longer needs to regulate the DC-link voltage and now has much more flexibility in its control options.

The inverter control can be implemented to keep the grid-side DC-link voltage constant and vary the reactive power in a manner that attains maximum real power transfer to the grid [27]. The real and reactive power delivered to the grid may also be coordinated via vector control of the current. As for the boost converter, variable speed control of the wind turbine is attained through control of the switch duty ratio. Optimum values of DC-link voltage and current can be identified corresponding to the maximum available turbine power for every shaft speed. These optimum values may then be met by varying the duty ratio of the switch essentially altering the DC-link voltage and current. It can be seen that the increased power generation from the increased controllability, can outweigh the incremental cost of the DC boost stage.

Matrix Converter

The matrix converter is capable of converting the variable AC from the generator into constant AC to the grid in one stage. The matrix converter consists of nine bidirectional switches, arranged in a manner such that any input phase may be connected to any output phase at any particular time. Each individual switch is capable of rectification and inversion, which allows for bi-directional power flow. Recently the use of a matrix converter in a doubly fed induction generator based wind energy system has been studied, as depicted in Figure 2.7.

Two distinct advantages arise from this topology, the converter requires no bulky energy storage or DC-link, and control is performed on just one converter. Although a single controller may be employed, the complexity is greatly increased as simultaneous control of 9 bi-directional switches is necessary. The matrix converter may be controlled using double space vector PWM, employing the use of input current and output voltage space vector modulation [17]. One of the major drawbacks of a matrix converter is that 18 total unidirectional switches are required, causing an increase in converter semiconductor cost and switching control complexity. Therefore, due to an increase in cost and complexity, the use of a matrix converter may be more practical in high power wind applications rather than small scale wind energy systems.

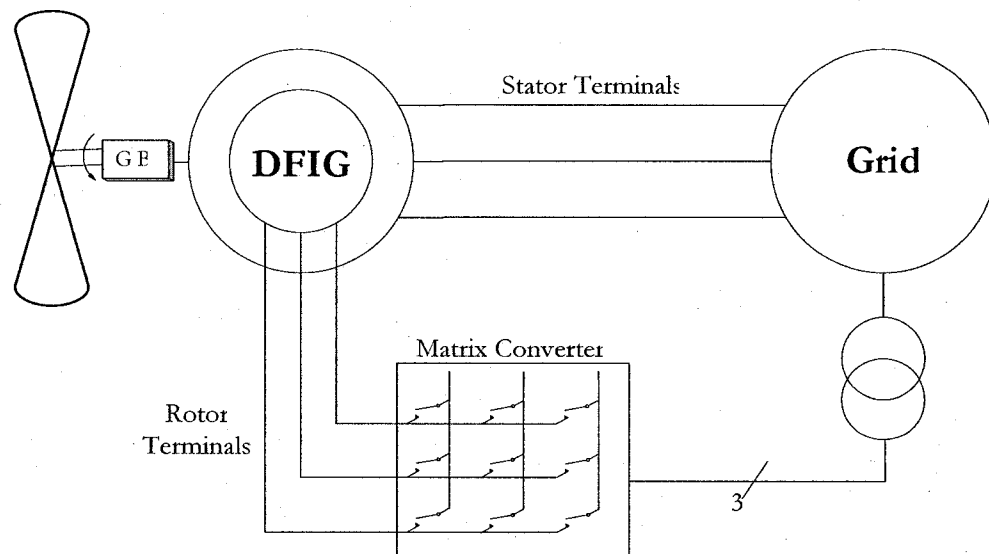


Figure 2.7: DFIG Wind Energy System with Matrix Converter

2.3 Control of Variable Speed Wind Turbines

Speed control of variable speed wind turbines has been accomplished through both mechanical and electrical manipulation of the turbine and generator. Mechanical control schemes include turbine blade pitch control, and gear changing between the turbine and generator. Electronic control may be performed using the power electronic converter of the wind energy system in order to achieve maximum power transfer and quality to the grid or through electronic pole changing method as in induction generator based wind systems. Both mechanical and electrical means of switching are further outlined in the following sections.

2.3.1 Methodology of Control

Pitch controlled wind turbines use an electronic controller that checks the power output of the turbine several times per second. When the power output is too high the controller enables the blade pitch mechanism to pitch (turn) the rotor blades slightly out of the wind. The opposite is true when the wind drops; in this case the blades are turned back into the wind. However a variable-pitch turbine is significantly more expensive than a fixed-pitch turbine.

There are two pole changing techniques used in induction generators, both require special design of the induction generator, which in turn increases cost. In the first technique, the stator winding is designed to be reconfigurable and the number of poles is changed by rearranging the coils of the winding. The second technique uses two stator windings, one used for low speed operations and the other for high speed operation when needed. This method of control does offer the advantage of a wide speed range but at an added generator cost.

The cost of power electronic devices has continually reduced and their use leads to a wide range of control possibilities. Anemometers may be used to measure wind speed. Although these devices allow for accurate measure of the wind velocity they undoubtedly increase the cost of the converter. Some common control methods include active and reactive power control through vector control of PWM inverters. The maximum power point tracking (MPPT) control of PWM inverters influences turbine speed to maximize

power output at all wind speeds. MPPT is fairly accurate but slow considering the wind speeds may change rapidly. Other possible controllers may draw on wind prediction methods through autoregressive statistical models [23]. Fuzzy logic controllers have also been researched due to its advantages such as parameter insensitivity, fast convergence and acceptance of noisy and inaccurate signals [12]. The use of power electronic converters in wind energy systems will continue to grow due to their extensive controllability.

2.3.2 Fixed and Variable Speed Control

All speed control schemes can be grouped into three distinct methods of control – fixed speed, two speed and variable speed control. Fixed speed and variable speed control dominate the wind energy market today. As of the end of 2005, Germany, the world leader in wind energy production, had 687 total installations. Out of the total installed wind turbines 80% were variable speed, 15% were fixed speed, and 5% were two fixed rotor speeds [28].

In a constant speed scheme the wind turbine speed is controlled to remain at a predetermined constant rotational speed. This implies that the optimum TSR value will only occur at one wind speed (referring to equation 2.3), which in turn indicates that maximum turbine efficiency will only transpire at a single wind speed. The inability to capture maximum power over a wide range of wind speeds is a major drawback for constant speed turbine designs. The wind energy is wasted when the wind speed is higher or lower than the value selected as the optimum. The use of pitchable rotors does improve efficiency over a range of wind speeds, however variable pitch turbine designs add significant cost to the wind energy system.

The two-speed design captures more energy, reduces losses in the rotor and reduces gear noise [29]. Two-speed generation may be accomplished by varying the gear ratio between the turbine and generator. The system is designed to have the peak power points, at each of two gear ratios, on either side of the annual average wind speed of the installation site. Two-speed generation may also be achieved through pole changing by varying the connection of the single stator pole winding. The stator connection which produces a higher pole number for low-speed operation is changed to one-half as many poles for high-speed operation [29].

Variable speed turbines may be controlled or left uncontrollable, with the latter having the benefit of low cost and easy implementation. However uncontrollable variable speed turbines suffer as they seldom capture maximum efficiency. Controlled variable speed wind systems force the turbine to operate at the optimum TSR over a range of wind speeds. They are able to adapt to the inconsistent force of the wind and begin power generation at low wind speeds. Variable speed operation may also reduce mechanical stresses and absorb the effects of wind gusts, creating an “elasticity” that reduces torque pulsations [13]. These advantages explain the dominance of variable speed turbine operation in the German market and are crucial factors in keeping wind energy competitive with traditional forms of energy production.

2.4 Chapter Summary

Grid connected wind energy systems are comprised of a turbine, generator and power electronic converter. All aspects of design must be tailored to the wind conditions of the specific location of installation. Various converter topologies may be implemented, each with numerous control possibilities. Ultimately a balance of controllability and cost effectiveness must be reached to achieve maximum generating efficiency along with economic viability. The process of energy conversion and the outlined wind energy conversion components aid in the selection of the generator and converter for the experimental design. Since the scope of this research is based on small-scale design, further background is explained in the next chapter.

Chapter 3

Small-Scale Wind Energy Systems

Small-scale grid connected wind energy systems are the focus of this research. Details of small-scale designs are outlined in the first section of this chapter. More specifically, designs involving permanent magnet synchronous generators will be studied, outlining possible converter and control schemes available. Cost effectiveness is an important issue and a balance must be achieved between system cost and efficiency. Three possible intermediate stage boost converters are examined, each having the ability to increase controllability at a reduced cost. Two controller schemes, Maximum Power Point Tracking (MPPT) and fixed relationship control, are presented as possible control options. A final design for simulation and implementation is chosen through investigation of the advantages and disadvantages of the possible converter systems and control schemes. The proposed system to be used in the experimental test rig is described in detail. The generator, power electronic converter and control scheme for both the inverter and flyback converter are described.

3.1 Power Converters and Controllers

The use of permanent magnet synchronous generator widens the range of the available power electronic converters. Since these generators do not require reactive power from the system for operation, diode rectifiers may be used for the variable AC-DC conversion. Some researchers have chosen to forgo this cost benefit and choose a controlled rectifier for the first stage of power electronic conversion. Although controlled rectifiers increase the overall cost they also enhance the controllability of the system. Most commonly, an inverter is used to perform the DC-AC conversion before grid connection and an optional intermediate DC-DC boost stage may also be applied. The converter schemes varying controllability and cost effectiveness are further analyzed with hopes of choosing the most cost effective scheme for experimental application.

3.1.1 Power Converter Topologies and Cost Effectiveness

Cost effectiveness is important in wind energy conversion as it competes with traditional generation methods in the highly competitive power industry. Large wind energy systems commonly include a controllable AC-DC converter in the initial stage of energy conversion. To achieve a precise and smooth AC-DC conversion, position sensors are needed to detect the phase of the synchronous generator. These sensors are relatively expensive for small systems, typically below 10 kW [11]. Similarly, if sensorless control is employed along with maximum power tracking, the system becomes increasingly complicated and will most likely need an expensive DSP (Digital Signal Processor) to achieve its objective [14,30].

A controllable AC-DC converter does have advantages as more control options become available for the rest of the systems. Methods of MPPT control can be performed by the controllable rectifier allowing for a reduction of control responsibilities for the inverter stage. As an alternative, the inverter may be chosen to control real and reactive power flow to the grid. Conversely, the addition of six controllable switches increases the cost of the overall system and is uneconomical for small-scale systems. It is due to the cost drawbacks mentioned that small-scale systems commonly utilize a diode rectifier in their design. The diode rectifier is cost efficient and allows for a high input power factor.

A diode rectifier used as the first stage of conversion hinders the controllability of the design and leaves all control demands to be dealt with by the inverter. Furthermore, during low wind speeds the generator tends to spin at a fairly slow rate and may not induce a voltage large enough to overcome the reverse bias created by the DC-link and the diode rectifier. Even at high wind speeds the DC-link voltage can be well below the limit needed to ensure sinusoidal PWM switching for the inverter stage. The inverter conversion equations for both a half-bridge single phase and full bridge inverter are given in equations 3.1 and 3.2 respectively [31].

$$V_{O1,pk} = m_a \frac{V_{DC}}{2} \quad (3.1)$$

$$V_{O1,pk} = m_a V_{DC} \quad (3.2)$$

As an example, a wind energy system may be connected to a single phase 120 V grid using a half-bridge inverter. In this case, through equation 3.1, it can be shown that a minimum DC-link voltage of 340 V is needed for sinusoidal PWM control of the inverter. This 340 V value is found for a modulation index of one, the maximum it can be for sinusoidal PWM. Sinusoidal PWM is defined for all modulation index values between zero and one. This scheme offers the benefit of an inexpensive design with the least amount of complexity.

In order to achieve a balance between cost effectiveness and system performance, one solution is to insert the DC boost stage in between the diode rectifier and inverter. This allows the converter to increase the DC-link voltage to the required level for sinusoidal PWM switching of the inverter. The DC-DC converter controls the diode rectifier DC-link voltage and therefore controls the generator terminal voltage and current. The DC-link control is commonly achieved through manipulation of the duty ratio of the switching device within the converter. Through the governing torque equation of a permanent magnet DC generator,

$$T = K\phi I_a, \quad (3.3)$$

controlling the generator current will produce generator torque and speed control. Therefore control of the DC-link voltage subsequently allows for maximum power transfer over a wide wind speed range.

3.1.2 Possible Options for DC-DC Boost Stage

Although there are many options to choose from for an intermediate DC-link boost stage, three options will be discussed in detail. The converters that will be discussed are the boost, buck-boost and flyback converter (Figure 3.1). It is also noted that each converter adds a controllable switch to the converter allowing for control of the DC-link. In addition the variability of these converters in wind energy systems will be analyzed and addressed. The analysis of these possible converters proves the viability of an intermediate DC-link boost stage for wind energy systems.

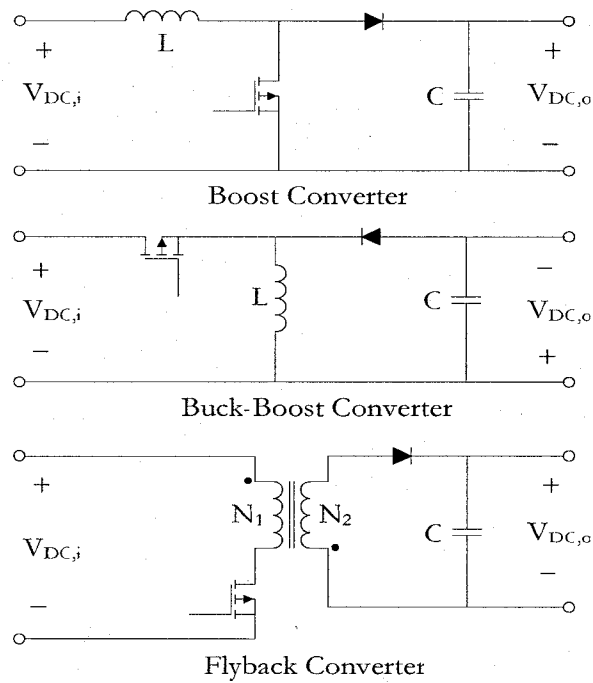


Figure 3.1: Three Possible DC-DC Converters For DC-Link Boost

The boost converter allows for control by varying the duty ratio of the switch to manipulate the rectifier DC-link voltage. At low wind speeds the voltage can be reduced to ensure some power flow; effectively reducing, and in some cases, eliminating the cut-in wind speed of the system. The use of a boost converter has been researched and proven worthy in stand-alone wind applications [32, 33]. However, since grid connection is the focus, the output voltage is required to be 340 V. A single stage boost converter, with an input voltage ranging from 10 to 50 V, is not practically capable of boosting to this high 340 V level, especially on the input voltage range. Instead, the use of multiple boost converters, in a cascade form, would be able to boost up to the required voltage level.

The buck-boost converter has two modes of operation, depending on the desired outcome. It is able to step the DC-link voltage down (buck), or increase the DC-link voltage (boost). Similar to the boost converter, the buck-boost converter is able to adjust the output voltage based on the duty cycle of the switching transistor. The driving circuitry for the switch is slightly more complicated since the switch does not have a terminal ground. The buck-boost converter has been proven useful for grid applications [11], and for stand-alone battery charging applications [34]. It is advantageous to have isolation from the grid for the wind energy system in order to protect the wind generator. This electrical isolation is usually

performed via a transformer. The boost and buck-boost converter topologies do not supply electrical isolation for the grid. Therefore it is recommended that a transformer be included in the overall converter design to ensure generator protection.

Unlike the previous two converters, the flyback converter has a transformer built into its circuit design, providing electrical isolation. The transformer's magnetizing inductance is used to store energy from the primary and transfer the energy to the secondary when the switch is off. Similarly the output voltage is controlled by changing the duty ratio of the switching transistor. The high frequency transformer within the flyback converter induces less cost than using a 60 Hz transformer at the output of the inverter. This decrease in cost is attributed to the reduction of transformer size for high frequency applications. The flyback also contains just one switch, further heightening the cost effectiveness in controlling and boosting the rectifier DC-link voltage. The use of this flyback converter is restricted to small scale designs that do not exceed 1 kW. Due to the transformer turns ratio, this topology has the ability to boost the voltage in a single stage. The addition of a center tap on the secondary winding allows for the use of a two-switch inverter for grid power transfer. Therefore, the converter may potentially contain just 3 switches, a great cost advantage.

3.1.3 Controller Complexity Issues

Turbine efficiency depends on the ratio between rotational speed and wind speed, known as the turbine TSR. The goal of speed control is to keep the TSR constant at its optimal point over a wide wind speed range. The constant variability of the wind creates the need for control of the generator electrical load. Controlling the generator electrical load to achieve maximum efficiency may be performed through many different means. The control strategies that have been researched and implemented lie within two categories: those with direct wind speed determination and those excluding this measurement.

An ideal control of wind turbines encompasses a direct measurement of the wind velocity through an anemometer. By directly measuring the wind, the desired rotational speed is easily extracted and compared with the current mechanical speed of the generator. In attempt to maintain maximum power extraction, the controller uses the discrepancy between the desired and actual speed to adjust the electrical load and therefore, the velocity of the generator. The controller may become imprecise since the anemometer measurement

may not be accurate due to the wind turbine tower shadowing, which inherently affects speed measurement. Two main control concepts that do not require speed measurements are maximum power point tracking schemes and systems that use a predefined fixed relationship control approach. The two control schemes are further analyzed in the following sections.

Maximum Power Point Tracking

As is shown in Figure 2.3, the power versus rotational speed curve has a single maximum point located in a relatively flat section of the curve. In maximum power point tracking, depicted in Figure 3.2, the generator load is incrementally increased or decreased causing a change in generator speed. If the change in speed results in an increase in generated power, load change continues in the same direction until maximum power capture is achieved. This method is insensitive to errors in wind speed measurements and wind turbine design [29].

Unfortunately wind speed changes much faster than the turbine rotational speed due to the large inertia of the turbine. Since the controller searches for the maximum power point every time the wind speed changes, the slow change in turbine speed hinders its ability to reach the optimum power point quickly. In fact, there may be instances where the optimum point is not reached before the wind speed subsequently changes. Traditional MPPT has been substantiated for large grid connected wind energy systems by Schiemenz and Stiebler [15].

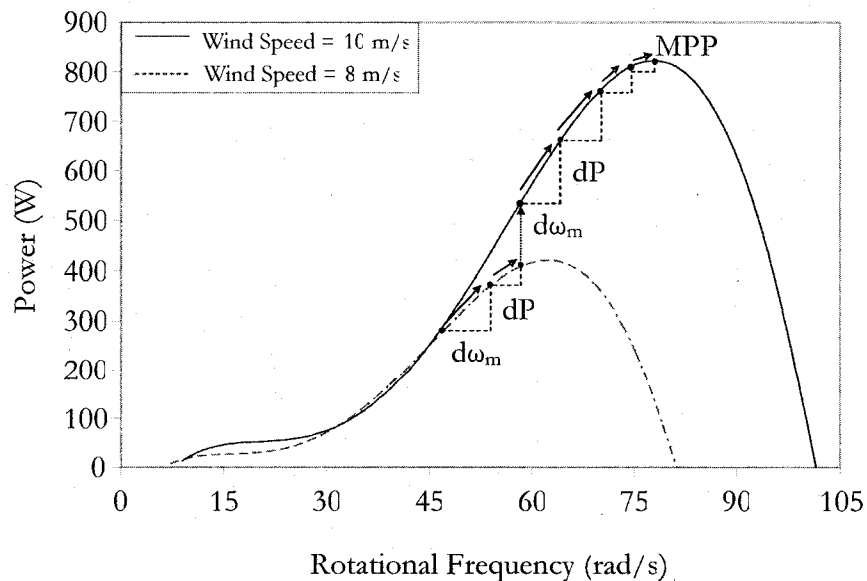


Figure 3.2: MPPT Search Operation

In an attempt to speed up the conventionally slow MPPT controller, Bhomik and Spee [16] employed a heuristic model of both the turbine and generator in order to estimate the wind speed. In addition, local MPPT is utilized to attain fine tuning of the desired TSR tracking. This controller improves the response time; however it is implemented using a digital signal processor and high level computer language, which increases the cost and complexity of the overall system. With the focus of this research placed on low cost and complexity, an attractive control scheme may be that which employs the use of fixed relationships. The details of this type of control scheme are outlined in the next section, shown below.

Fixed Relationship Controller

Fixed relationship control involves a predefined relationship between generator load and generator rotational speed. By measuring the generator speed as a control input, the optimal generator electrical load is immediately determined. The optimal velocity of the generator can be easily defined by first identifying the wind turbine power as,

$$P_T = \frac{1}{2} \rho A C_p v_w^3 \quad (3.4)$$

Substituting equation 2.3 for TSR gives a redefined power equation in terms of generator mechanical speed.

$$P_T = \frac{1}{2} \rho A C_p \frac{r^3}{TSR^3} \omega_m^3 \quad (3.5)$$

Since the optimal TSR value is known and is assumed constant through system control, the peak power versus mechanical speed is identified as a cubic correlation. Past researchers, such as De Broe et al. [34] used a fixed relationship between generator frequency and the switch duty ratio of a DC-DC converter to achieve turbine optimization. They have shown that fixed relationship control is a simple and a cost effective means to achieving maximum efficiency over a wide speed range.

3.2 Proposed Generator and Converter System

As was mentioned, the objectives and goals of this research is to design and implement a small scale wind energy system that achieves maximum power extraction at all wind speeds above the generator cut in wind speed. This system is to achieve maximum performance at minimal cost. The proposed system uses a brushless permanent magnet DC generator driven by LabView Real-Time software that emulates a wind turbine. A common shaft connects the AC permanent magnet synchronous generator to the DC generator.

The converter consists of a diode rectifier, flyback converter for DC-DC boost and control, and a single phase inverter for grid connection. The flyback contains a transformer with a center tapped secondary winding. This allows for the use of a single phase inverter with just two switches, further reducing the cost and control complexity. The flyback converter is controlled to follow a predefined fixed relationship between the generator electrical frequency and rectifier DC-link voltage. The control is implemented using LabView Real-Time computer software and corresponding hardware needed for communication with the system devices. The proposed system for this research is shown in Figure 3.3, with simple fixed relationship control based on the generator electrical frequency. This simple open-loop control will be used to control the flyback duty ratio and inverter phase voltage phase angle to achieve optimal power flow.

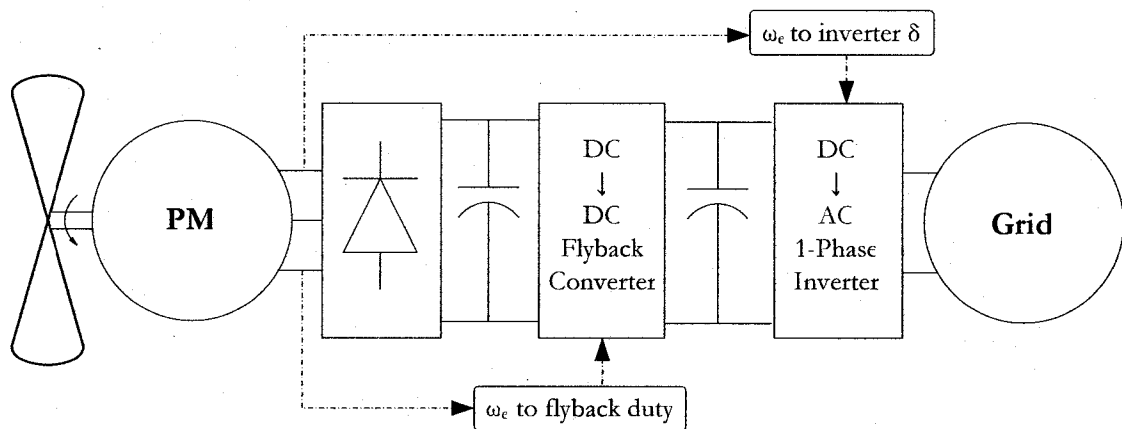


Figure 3.3: Proposed System and Control Topology

3.2.1 Chosen Converter Topology for Wind Conversion

For a small scale wind energy system, a permanent magnet generator is a commonly chosen since it provides reduced losses in the rotor, higher efficiency, allows for a smaller wind turbine diameter, and requires no external excitation. The generator supplies power to the grid via a power electronic converter encompassing a diode bridge rectifier, flyback converter and single phase inverter. The flyback converter is chosen since it provides adequate boost ability to match the requirements of the inverter and controllability of the DC-link voltage, while providing electrical isolation for the grid.

The single phase inverter along with the flyback converter is an attractive choice for the converter, due to the low controllable switch count. This low switch count reduces the cost for the overall system. The diode rectifier is also essential to making the wind energy system cost effective. In using the diode rectifier there is no need for a controlled rectifier since the DC-link control is performed by the flyback converter. Using simple control methods for both the flyback and inverter will further elevate this systems status as a practical and extremely cost efficient system.

3.2.2 Simple Control Methods

Two stages of control will be applied to the overall converter system. Both the inverter and flyback have separate control responsibilities. However, the controllers are integrated in their effort to transfer power from the generator to the grid. The flyback ensures maximum power from the wind turbine through torque control of the generator. The inverter ensures optimal power transfer to the grid over the entire wind speed range. Both controller schemes are designed to be as simple as possible by employing fixed relationships. Controller simplicity allows for possible implementation using discrete analog components that maintain the goal of cost minimization.

Inverter Control

The inverter is controlled through a sinusoidal PWM switching technique, meaning a modulation index below unity must be maintained. Since the output of the inverter is connected to the grid, its output voltage is held to a constant 120 V. From equation 3.1 it

can be shown that the grid side DC-link voltage must be at least $340 V_{DC}$. This value is achieved right at the boundary of sinusoidal PWM operation, where the modulation index is one. If the modulation index is decreased, where sinusoidal PWM is still maintained, then this voltage will increase. It is beneficial to sustain a modulation index near unity as the flyback converter boost capabilities are designed for a specific output voltage, and a large output DC-link voltage will require increased boost capacity from the converter. The inverter controller will continually monitor the electrical frequency of the generator and adjust the phase angle of the reference signal of the PWM switching. This variation of the phase angle will allow maximum power flow to the grid.

Flyback Control

The proposed controller does not require direct measurement of the wind speed; instead the controller uses a fixed relationship method to achieve maximum power transfer. Only one control input is needed, the electrical rotational speed of the generator, to determine the switching duty ratio of the flyback that must be applied to achieve maximum power. Through a predefined optimal value of TSR, a fixed relationship between the electrical frequency and duty ratio is constructed and employed in the control. This change in duty ratio will ultimately result in an alteration in the DC-link voltage. Thus, in turn, manipulation of the DC-link voltage leads to the torque control of the generator. Since the generator and turbine are connected by a single shaft, the control of the wind turbine is therefore achieved through simple control of the duty ratio. The predefined fixed relationship is first determined through theoretical analysis of the system and later adjusted during experimental testing, accounting for any theoretical assumptions that are made.

In using a fixed-relationship control method, it has already been stated that the system is never aware of the actual wind speed at any time of operation. A change in wind speed will subsequently result in a change in torque causing the turbine speed to change. In controller design, the desired TSR value is set to extract maximum wind power from the turbine. However, the value for maximum power does not necessarily correspond to the point of maximum torque. Another option is to select a reference TSR value slightly higher than the actual optimal TSR of the turbine to improve the system response during the brief periods of wind gusts. Rapid system response to fast changing wind is highly beneficial and allows the system to quickly return to the ideal operating point.

In comparison to operation at the ideal TSR, a slightly higher TSR will result in a slightly higher generator terminal voltage, a marginally lower generator current and a slight increase in turbine speed. Operating at this shifted TSR value does not significantly affect the power capture since the coefficient of performance does not change significantly in the vicinity of the optimal TSR value, shown in Figure 2.2. The performance of the controller, for both cases described above, is depicted in Figure 3.4. On the graph the point “a” represents the operating point at the ideal TSR value for 9 m/s. If a sudden wind gust increases the wind speed to 10 m/s, the operating point of the system suddenly moves to point “b”.

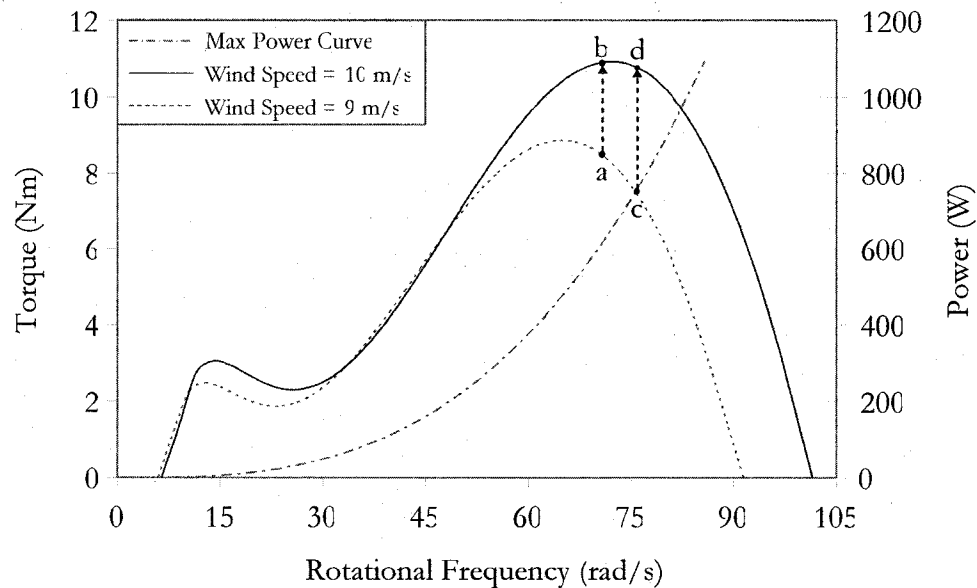


Figure 3.4: Turbine Torque and Control Operation

The change in torque is indicated by the dotted arrow pointing upward. Conversely the operating point “c” is at a slightly deviated TSR value, as it is to the right of point “a”, at a higher rotational speed. In this case the same wind gust will move the operation to “d” also causing a change in torque. It is clear from the figure that the operation from “c” to “d” induces a greater change in torque than the ideal progression from “a” to “b”. Therefore, based on the following equation:

$$T_{Turb} = T_{Gen} + J \frac{d\omega_m}{dt} \quad (3.6)$$

(the equation describing the torque balance between the turbine and generator), when the system experiences a larger change in torque due to an increase in wind speed, than the system will be able to accelerate at a faster rate to reach the next steady state operating point.

The system should be designed for the ideal situation to ensure maximum power extraction. However if the designed controller cannot handle sudden changes in wind speed, then the second approach of a slightly shifted model may be advantageous. This slight shift does not significantly affect power output and does not jeopardize power extraction at lower wind speeds.

3.3 Chapter Summary

The proposed system has been outlined and includes a permanent magnet generator and complete power electronic grid connected converter. A diode rectifier, flyback converter and single phase inverter are chosen to reduce cost without compromising the performance of the system. The inverter will control the grid side DC-link voltage through sinusoidal PWM control. The flyback converter current control is based upon a fixed relationship between the generator electrical speed and DC-link current, eliminating the need for wind speed measurements and further reducing costs and complexity. The system is first verified through simulation and then experimentally tested to further validate the design and determine its practicality. Simulation design and results are given in Chapter 4 where as the experimental design and results are given in Chapters 5 and 6 respectively.

Chapter 4

Simulation of Proposed Research

The simulation of the proposed system and the results obtained are presented in this chapter. The validity of the proposed flyback converter design is performed using the Matlab SimuLink software. This chapter outlines the system setup and parameters, along with the derivation of the fixed relationships used for the controller. Furthermore, the method of implementation for all fixed relationships used in the simulation is presented. A complete simulation algorithm describes the simulation process and all dynamic results, for both fixed and variable DC-link operation.

4.1 Simulation Setup and Parameters

All simulations are performed through SimuLink, a computer software package provided through Matlab. The flyback converter is simulated using a linear transformer, an IGBT as the primary side switch, and two diodes. A snubber circuit is used to limit the voltage spikes that occur during switching. The flyback converter is operated at the desired frequency of 1 kHz. Table 4.1 shows a complete list of the parameters used in the simulation of the flyback DC-DC converter.

Table 4.1: Flyback Converter Simulation Parameters

Circuit Properties		Transformer Properties	
Nominal Power	1 kW	Turns Ratio (n_2/n_1)	14
Switching Frequency	1 kHz	Primary Resistance	3.8 mΩ
Diode Forward Voltage Drop	0.8 V	Secondary Resistance	0.7056 Ω
Switch Forward Voltage Drop	1.0 V	Primary Inductance	11.459 μH
Snubber Capacitance	50 μF	Secondary Inductance	2.246 mH
Snubber Resistance	100 Ω	Magnetizing Resistance	360 Ω
Output Capacitance	0.3 mF	Magnetizing Inductance	5.157 mH

The full system simulation is devised into three components that are connected to each other. A wind profile, along with the generator speed, is fed into the turbine model. The outputs of the turbine model are shaft torque and speed. The mechanical torque is applied to the generator model to determine the new generator speed and rotational angle. The generator model outputs a three phase voltage which is connected to the power electronic converter beginning with the diode rectifier. A controller model manipulates the DC-link voltage during all wind speeds in accordance to the control signal inputs and the predefined fixed relationships. The parameters for the turbine, generator and converter simulation models are given in Table 4.2.

Table 4.2: Wind Energy System Simulation Parameters

Turbine Radius	1.0 <i>m</i>
System Inertia	0.4 <i>kg·m²</i>
System Damping	0.16 <i>Nm/kRPM</i>
Air Density	1.266 <i>kg/m³</i>
Friction	0.1 <i>Nm</i>
Poles	8
Phase to Phase Winding Inductance	3.3 <i>mH</i>
Phase to Phase Winding Resistance	0.51 Ω
Peak Phase to Phase Voltage Constant (K_E)	86 <i>V/kRPM</i>
Peak Per Phase Torque Constant (K_T)	0.71 <i>Nm/A</i>
Diode Bridge Forward Voltage Drop	1.0 <i>V</i>

4.2 Verification of Flyback Converter

The flyback converter in its purest form, shown in Figure 3.1, is first simulated to verify its switching and voltage boosting capabilities. However, it is immediately noted that a resistor-capacitor-diode (RCD) snubber circuit is necessary to suppress voltage spikes across the switching device. Voltage spikes can be caused by any stray inductance within the circuit or from the transformer leakage inductance. In addition to voltage protection, the snubber circuit limits the rate of rise of current flowing through the switching device. Figure 4.1 shows the simulated flyback converter circuit with the insertion of the snubber circuit.

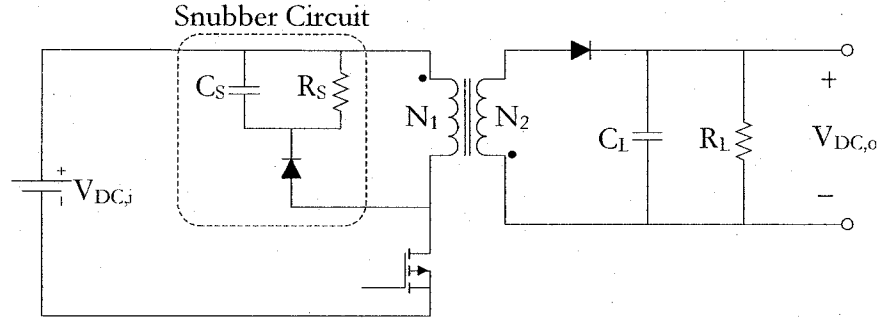


Figure 4.1: Simulated Flyback Converter with Snubber Circuit

The magnetizing inductance of the transformer is set above a critical value to ensure full transfer of current from the primary winding to the secondary winding during switch off time. Full transfer of current between the two windings is essential in the operation of the flyback converter, because it guarantees the output voltage reaches the necessary level for the grid side inverter. The critical magnetizing inductance is calculated using equation 4.1, given below. It is noted that the effective resistance and switch duty ratio are both dependant on the wind speed. The resistance is lowest at the minimum wind speed, therefore the critical magnetizing inductance is calculated for the minimum wind speed (2 m/s) used in the full system simulation.

$$L_{Crit} = \frac{1}{n^2} \frac{(1-d)^2 R_{eff}}{2f_{sw}} \quad (4.1)$$

$$R_{eff} = \frac{V_{DC,o}^2}{P_{Gen}} \quad (4.2)$$

The flyback is tested at both the high and low voltage extremes that are expected from the wind generator during operation over the entire wind range. In addition, the load resistance is varied to confirm the flyback operation under a varying load. The flyback is first simulated at the high voltage limit of 60 V; this voltage is slightly higher than the voltage generated at the maximum wind speed of 10 m/s used in the full system simulation. The results in Figure 4.2 show the load voltage and the magnetizing current in the transformer. The magnetizing current is further looked at by reducing the time scale on the waveform and is displayed in Figure 4.3. Accompanying the magnetizing current in this figure are detailed depictions of both the primary and switch voltages.

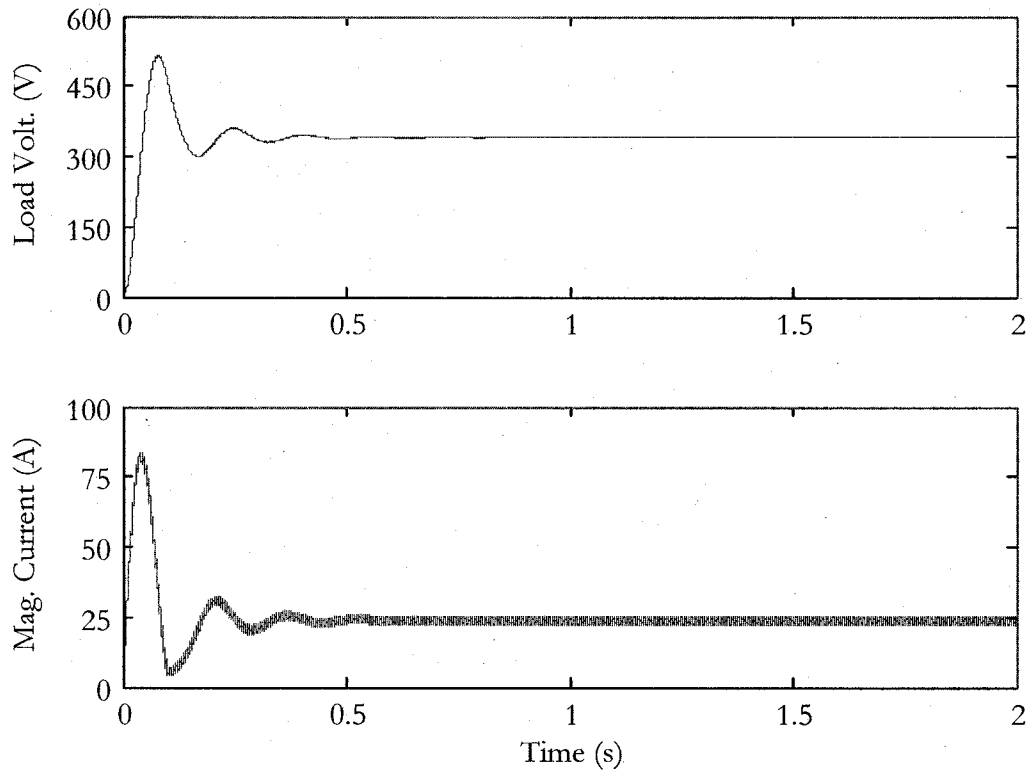


Figure 4.2: Results for a Flyback Input of 60 V

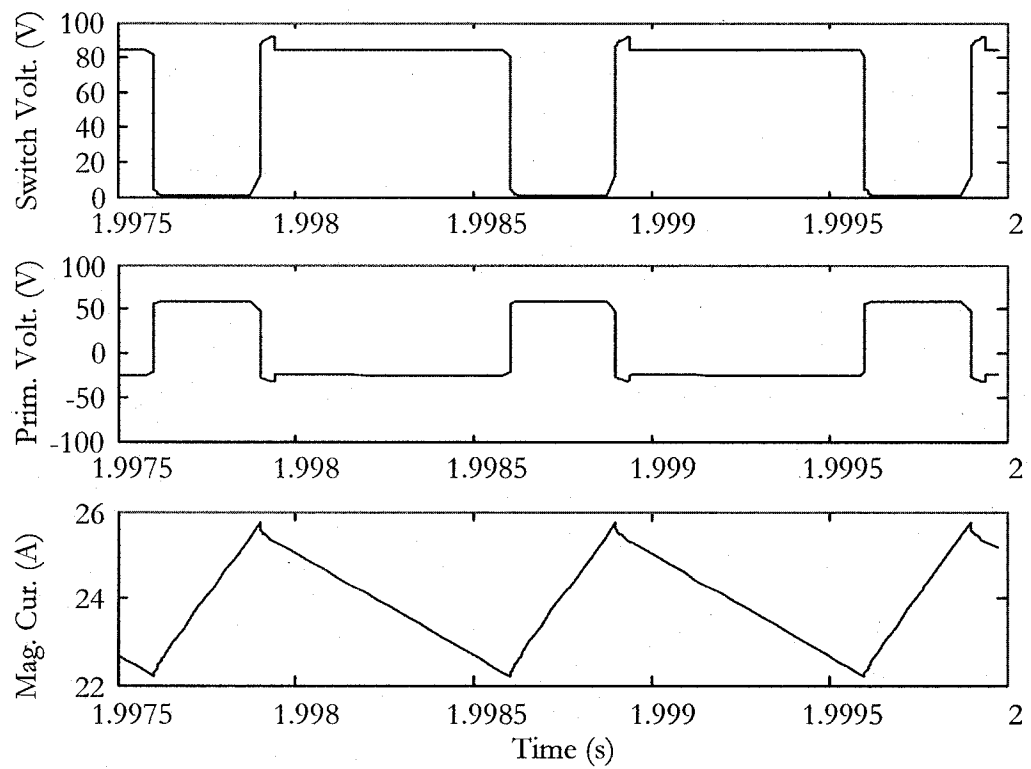


Figure 4.3: Detailed Waveforms for a Flyback Input of 60 V

In Figure 4.2 the load voltage reaches the expected voltage of 340V. However, the duty ratio is set to a value higher than the theoretical value calculated using the ideal equation 4.3. The ideal equation does not take into account the snubber circuit and diode voltage drops therefore justifying this necessary increase in duty ratio.

$$V_{DC,o} = V_{DC,i} \frac{N_2}{N_1} \frac{d}{1-d} \quad (4.3)$$

There is a short transient due to the initial charging of the capacitance, however the voltage settles off quickly. The magnetizing current remains quite constant with a small ripple shown in Figure 4.3. The triangular wave shape shows that while the switch is on, the magnetizing current increases, then decreases during switch off time. This implies that the current stored in the magnetizing branch is indeed transferred to the secondary winding during the switch off time. The switch voltage reaches the expected levels with very small voltage spikes, indicating that the snubber circuit is performing optimally. The switch voltage during off time is equal to the addition of the input DC-link voltage and the primary winding voltage, shown below.

$$V_{sw} = V_{DC,i} + \frac{N_1}{N_2} V_{DC,o} \quad (4.4)$$

The primary winding voltage is equivalent to the input DC-link voltage while the switch is on and also shows no large spikes during switching. These simulation results show that the flyback is operating as expected.

Next, the results for the other extreme case (at low voltages, coinciding with low wind speeds of approximately 2 m/s) are examined. Figure 4.4 shows that once again the flyback is able to produce the necessary output voltage. The magnetizing current shows a similar triangular waveform that is characteristic of transferring energy from the primary winding to the secondary winding while the switch is no longer conducting. Slight voltage spikes are evident on the switch and primary winding. However, the snubber circuit does limit the spikes to a respectable value (well within the range of typical ratings for semiconductor switching devices), preventing it from breaking down. It is noted that as the wind speed increases these spikes reduce and become virtually nonexistent.

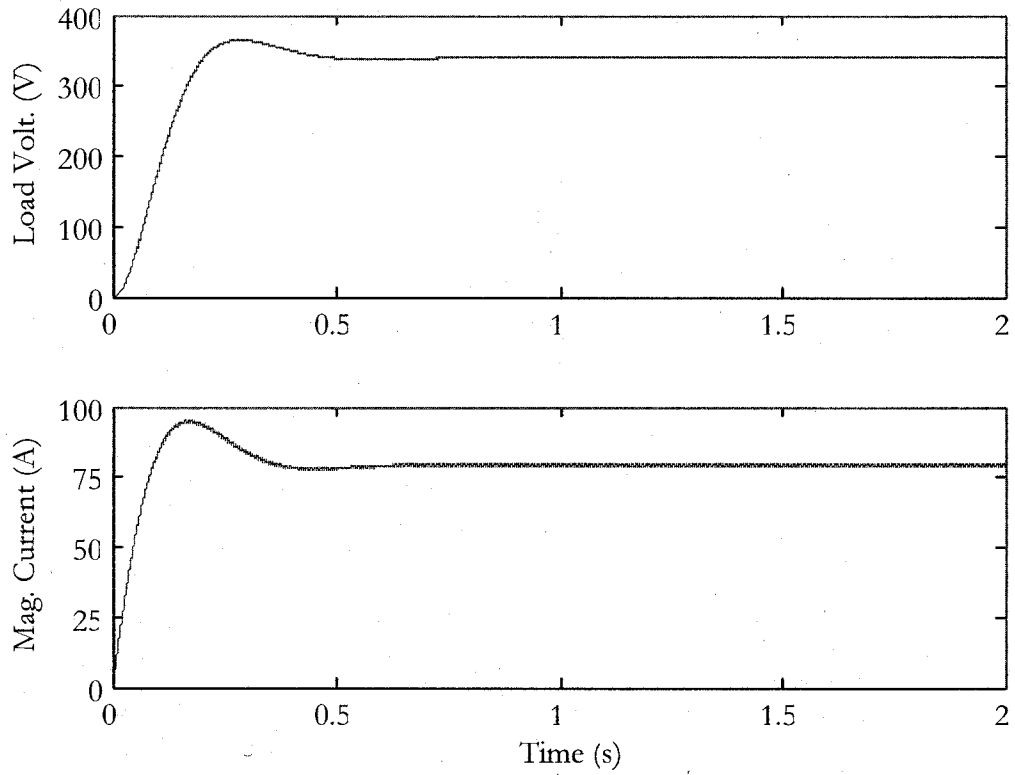


Figure 4.4: Results for a Flyback Input of 9 V

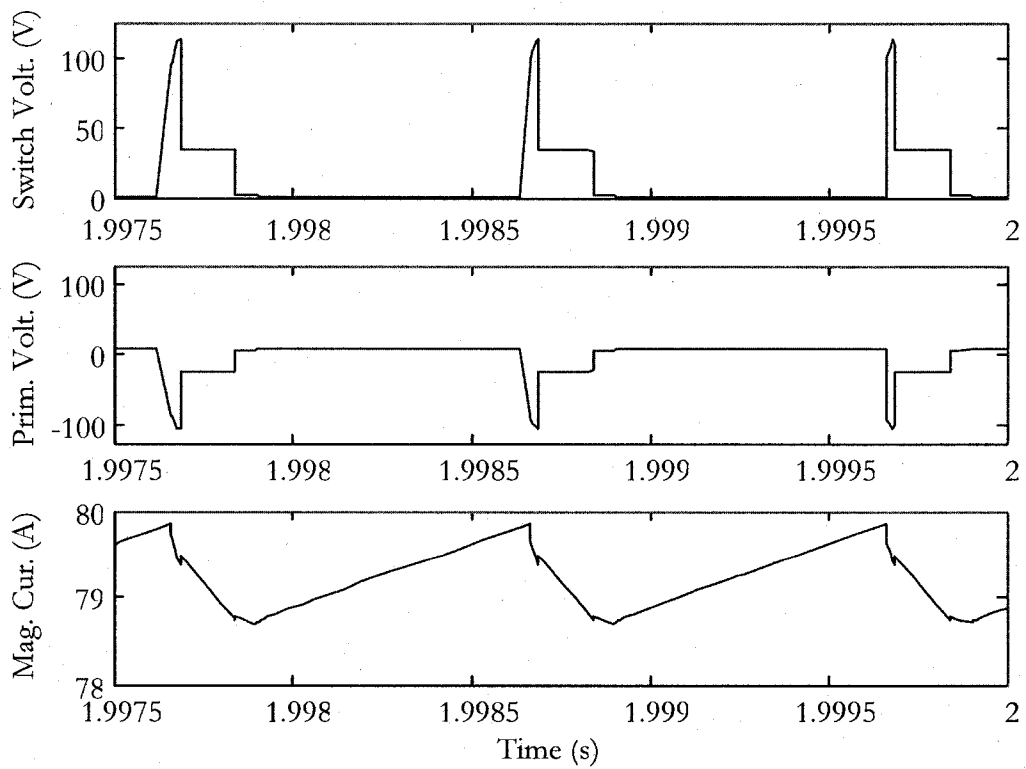


Figure 4.5: Detailed Waveforms for a Flyback Input of 9 V

4.3 Determination of Fixed Relationships

Fixed relationships described through mathematical functions are used throughout the full system simulation. The first function describes the relationship between the coefficient of performance and TSR. Using Microsoft Excel, the relationship shown in Figure 2.2, is approximated by a fifth order polynomial equation to provide the best fit for the curve. Figure 4.6 shows the mathematical process taken in developing the fixed relationships for the current controller.

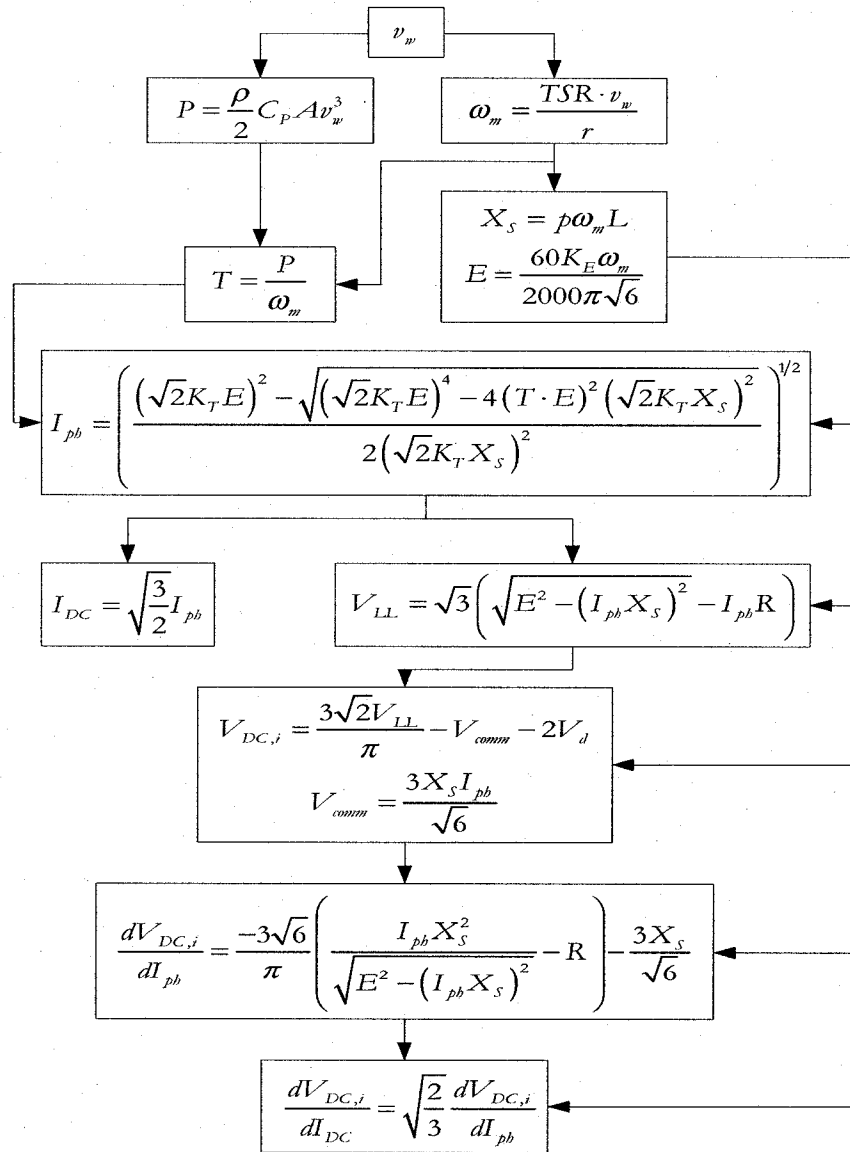


Figure 4.6: Algorithm for Finding the Fixed Relationships for Current Control

The process shown in Figure 4.6 is repeated for all wind speeds ranging from 1 m/s to 11 m/s by stepping through this algorithm in 0.5 m/s increments. With both the coefficient of performance and TSR values fixed at their optimal levels of 0.414 and 7.8 respectively, the generated power and mechanical speed can be calculated. The torque, generator reactance and induced voltage are calculated next, which allows for the determination of the generator phase current. The DC-link current is resolved by using the formula describing the current conversion through a diode rectifier. From this, a fixed relationship between the DC-link current and mechanical speed over all wind speeds is defined and shown in Figure 4.7. Finally, the line-to-line voltage is established, which gives way to the calculation of the DC-link voltage through the diode rectifier voltage conversion calculation. By taking the derivative of the DC-link voltage, with respect to the phase current, a ratio describing the change in DC-link voltage to the variation in DC-link current is found. This establishes the second fixed relationship for the current controller. The change in DC-link voltage, needed to maintain optimal power extraction at all wind speeds, is determined via this second predefined relationship.

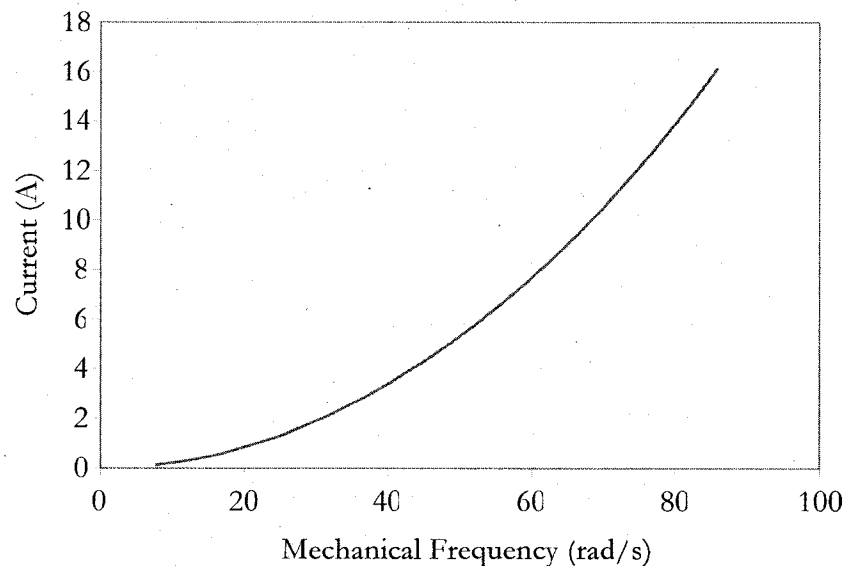


Figure 4.7: Ideal DC-Link Current vs. Mechanical Frequency

The data obtained from the algorithm used to create the above curve can be entered into the software program LabFit. The program then uses the data points to search for an equation that best fits the curve with minimal error over the entire range. The equation

obtained is therefore a very close approximation to the curve displayed and does not compromise the accuracy of the simulation. Using this software, the mathematical equation obtained for this curve is given in equation 4.5 and is used in the simulation.

$$I_{DC} = \frac{5.72 \times 10^{-3}}{-2.77 \times 10^{-5} - 1.25 \omega_m} \quad (4.5)$$

The same software program is also used to create a fixed equation for the $dV_{DC,i}/dI_{DC}$ ratio, as it changes with varying mechanical speed due to the fluctuating wind speed. The fixed relationship between this ratio and mechanical speed used in the current controller is given in equation 4.6. It is important to note that these equations allow for the use of simple mathematical function blocks in the Matlab simulations rather than using look-up tables.

$$\frac{dV_{DC,i}}{dI_{DC}} = \frac{50.1 + 0.637 \omega_m}{-102.32 + 3.31 \times 10^{-3} \omega_m^2} \quad (4.6)$$

4.4 Wind Energy System Simulation

The validity of the control scheme is tested by incorporating the controller with a simulation that modelled the wind turbine, permanent magnet synchronous generator and diode rectifier. This system is subjected to a varying wind profile that ranged from 2 m/s to 10 m/s. The flyback converter and grid side inverter are not simulated at this point as the main objective is to ensure the controller incorporated the correct fixed relationships that maximized power extraction from the wind turbine.

4.4.1 Simulation Algorithm

The simulation continually evaluates the calculations shown in the algorithm in Figure 4.7. Over each simulation time step, all system parameters are calculated and updated as the software steps through a varying wind speed. The simulation algorithm depicts the calculations performed for the turbine, generator, diode rectifier and control models.

In the simulation model, a wind speed profile is generated and received by the turbine model. The TSR is calculated based on the mechanical speed of the previous simulation cycle and the current wind speed. Turbine modeling is further carried out with the calculation of the coefficient of performance, power and torque. The simulation then moves into the generator modeling; in which the generator, turbine and friction torques are combined to determine the updated mechanical speed. The generator torque is based on the previous state of the outputted three phase currents. The quadrature axis transformation (equation 4.7) is performed on the three phase currents to obtain the quadrature current needed for the torque calculation.

$$I_q = \frac{2}{3} \left[I_a \cos(\theta_e) + I_b \cos\left(\theta_e - \frac{2\pi}{3}\right) + I_c \cos\left(\theta_e + \frac{2\pi}{3}\right) \right] \quad (4.7)$$

Next, the electromotive force for each phase of the generator is calculated based on the new mechanical speed and electrical phase angle. The differences between the per-phase induced voltages are determined and the greatest difference (E_{diff}) is compared with the DC-link voltage. If the induced voltage in the machine results in an E_{diff} which is greater than the DC-link voltage then conduction occurs through the diode rectifier. Otherwise the diodes are reversed biased resulting in zero line current and power extraction from the generator.

A closer look at the interaction between the generator and diode rectifier shows that the difference between E_{diff} and the DC-link voltage results in V_{diff} . The simulation uses this voltage difference in determining the generator line current during diode conduction. This voltage can be described as the voltage drop across the impedances of the two connecting phases of the generator during the conduction period (equation 4.8). The effect of commutation overlap, equation 4.9, is also included since in practical systems this transfer of current from one phase to another is not instantaneous and causes the current in the system to lag the voltage.

$$V_{diff} = E_{diff} - V_{comm} - 2V_d - V_{DC} \quad (4.8)$$

$$V_{comm} = \frac{3\omega_e L_G I_{pb}}{\sqrt{6}} \quad (4.9)$$

Figure 4.8 depicts the process in which energy is transferred to the DC-link from the generator via the diode rectifier. As can be seen from the figure, during conduction, two diodes are forward biased allowing current to flow to the DC-link through two generator phases. In the example shown, phases 'a' and 'b' are conducting since the difference between their induced voltages is greatest. The conduction of energy through the generator and diode rectifier is further simplified in Figure 4.9. The DC current in this figure varies with time, a sharp comparison to the nature of the current in the computer simulation. The two generator phases are represented by their equal resistances and inductances, and a switch is added to portray the beginning of conduction at zero time.

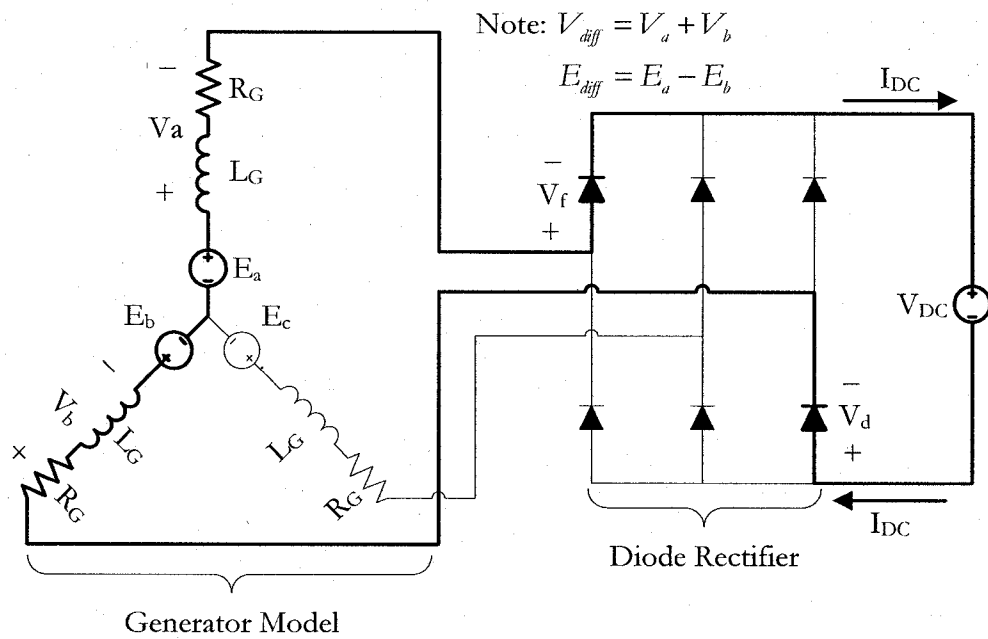


Figure 4.9: Generator Conduction through a Diode Rectifier

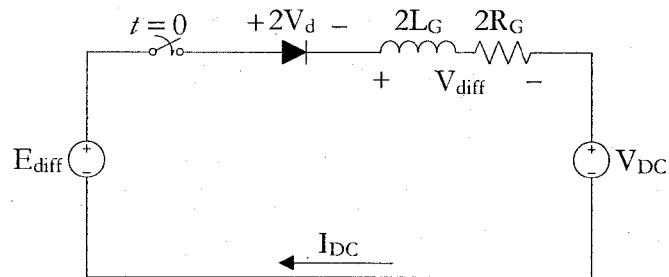


Figure 4.10: Simplified Generator Conduction Circuit

From Figure 4.10 another equation for V_{diff} can be identified that provides a means to identifying a solution for the DC-link current. The voltage across the generator resistance and inductance is represented by equation 4.10.

$$V_{diff} = 2R_G i(t) + 2L_G \frac{di(t)}{dt} \quad (4.10)$$

The common and well recognized solution for the current through a resistor-inductor network has been established (equation 4.11).

$$i(t) = K_a + K_b e^{-\frac{t}{\tau}} \quad (4.11)$$

The constants are derived by first substituting equation 4.11 into equation 4.10 and easily determining K_a and τ . Since the current through the inductor is initially zero, the second constant, K_b is also determined. The solutions for K_a , K_b , and τ are revealed in equations 4.12, 4.13, and 4.14 respectively, giving a final solution for the reference DC-link current.

$$K_a = \frac{V_{diff}}{R_G} \quad (4.12)$$

$$K_b = i(0) - \frac{V_{diff}}{2R_G} \quad (4.13)$$

$$\tau = \frac{L_G}{R_G} \quad (4.14)$$

Finally, the controller model uses the measured DC-link current to determine the error between the measured value and the reference DC-link current obtained through the fixed relationship. With this DC-link current error, a corresponding shift in DC-link voltage is determined via the second predetermined relationship. In conclusion the result is a new DC-link voltage that guarantees maximum power extraction. The simulations resulting data points are recorded at a limited time intervals due to large simulation times and memory storage restrictions.

4.4.2 Fixed DC-Link Dynamic Results

The system is simulated under fixed DC-link conditions, under the influence of a variable wind speed profile. The results obtained are compared with the results from the controlled DC-link cases, providing justification for the use of a variable speed controller. The wind profile used in all system simulations is given by

$$v_w = \left| 8 \sin\left(\frac{t}{36}\right) + 0.8 \sin\left(\frac{t}{4}\right) + 2 \right|. \quad (4.15)$$

The simulation is tested with a constant DC-link voltage of 36 V. If this were a practical system with a turbine that has a coefficient of power curve given in Figure 2.2, corresponding to an optimal wind speed of 7.19 m/s. Ideally, this system may be placed in a region that historically depicts an average wind speed matching this wind speed. The results for the mechanical speed, turbine TSR, DC voltage and DC power are given in Figure 4.11.

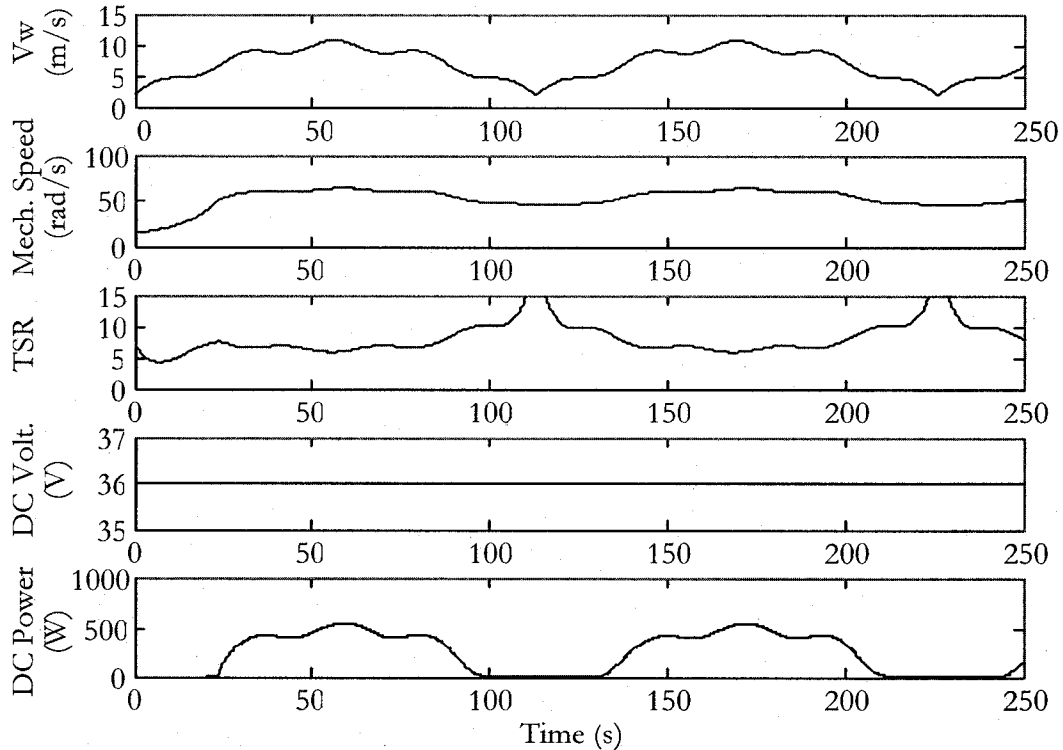


Figure 4.11: Simulation Results with a Constant DC-Link of 36 V

The power curve is further analyzed and the average power over 250 s of simulation time is determined to be 233.8 W. The maximum power transferred by the system at the maximum wind speed of 10 m/s is also identified as 554 W. Although these power results are respectable, the system very rarely operates at the optimum TSR and coefficient of performance. This is evident by the TSR curve as it deviates above and below the ideal TSR value of 7.8 during wind speeds above 5 m/s. During times of extreme low wind speeds the system no longer transfers power as the TSR continues to rise. This indicates that the mechanical speed of the generator has not slowed enough in coordinance with the decreasing wind speed.

The system is again run with a fixed DC-link, however in this case the value is increased to 42 V. Once again referring to a turbine with a coefficient of power curve in Figure 2.2, a system operating at this voltage is best suited for a region with an average wind speed of 8.93 m/s. As can be seen from the figure below, at a wind speed of approximately 9 m/s, the TSR nears the optimal value of 7.8. The results for this constant DC-link case are given in the same manner as the previous and are depicted in Figure 4.12.

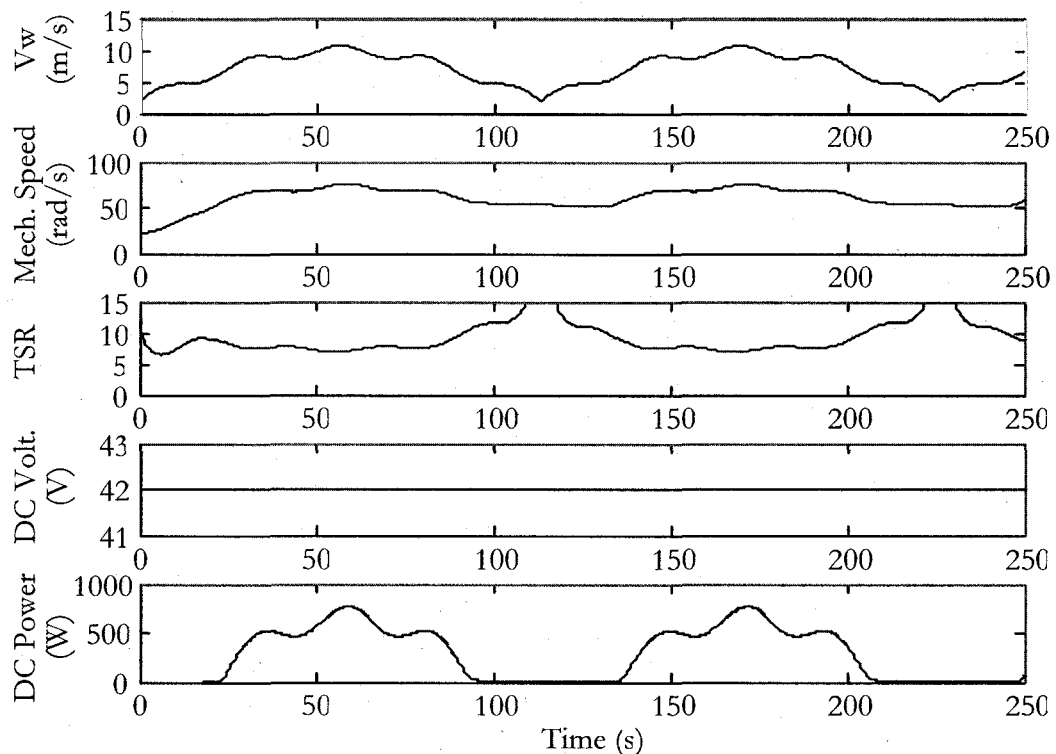


Figure 4.12: Simulation Results with a Constant DC-Link of 42 V

In this higher voltage case, the maximum and average DC power show an increase to 756.4 W and 268.7 W respectively. The higher DC-link voltage allows the mechanical speed to reach higher speeds. According to Figure 2.3, this results in higher power output during high wind speeds. For example, at maximum wind speed of 10 m/s, the mechanical speed in the 42 V DC-link case is higher than that in the previous case. Looking at Figure 2.3, the higher the mechanical speed the more power extracted from the turbine as long as the system is operating upon the left side of the TSR curve, (which it is during high wind speeds). It is also noted that the lower DC-link voltage case has a slightly lower cut-in wind speed. Thus the system extracts power over a wider range of wind speeds.

As the wind speed increases in both cases the generator speed change is fairly slow and small. Due to a constant DC-link, the generator attempts to match its generator voltage with the value of the DC-link voltage. As the wind speed increases above the cut-in value, the generator speed increases. This increase in generator speed causes an increase in the generated voltage. However the generator terminal voltage is fixed, due to the fixed DC-link voltage, resulting in an increase in generator current. As a result, equation 4.16 shows an electrical torque is produced which limits the generator speed, not allowing it to vary much during high wind speeds.

$$T = K\phi I_a \quad (4.16)$$

At low wind speeds, typically below 5 m/s, the generator terminal voltage dips below that of the DC-link voltage. Once this occurs, the diode bridge rectifier becomes reversed bias, cutting off current to the DC-link resulting in zero power extraction. Since the DC-link voltage is lower in the first case, the generator is able to operate at lower speeds before the terminal voltage falls below the DC-link voltage. This explains the lower power extraction cut-in wind speed for the first case.

The constant DC-link simulation results show that the system rarely operates at the optimal point over the wide range of wind speeds. This is a major drawback in using a constant DC-link, as the full system potential is not exploited. Therefore, in order for a wind energy system to compete with traditional methods of power generation, it must employ an optimal power controller. The system is next tested with the proposed controller, and results, along with comparisons are given in the next section.

4.4.3 Variable DC-Link Dynamic Results

The proposed current controller is injected into the system, allowing for control of the DC-link voltage. Initially, the entire system is run at a specified time step used for evaluating all system models over the simulation time. However, results pertaining to the DC-link voltage and power experienced high ripple, and are deemed unacceptable. Since the mechanical speed of the generator change is slow, with respect to the change in wind speed, it is not necessary to have the controller update the DC-link voltage at every time step. The Matlab simulation software allows different components of the simulation to be performed at different rates. The global system, excluding the controller, is modelled with a simulation time step of $1\mu\text{s}$. However, the current controller is modelled with a step size of 1ms , coinciding with the switching frequency of the flyback converter. The same variables plotted in the constant DC-link case are again evaluated for the controlled case, and a comparison is made between both forms of operation.

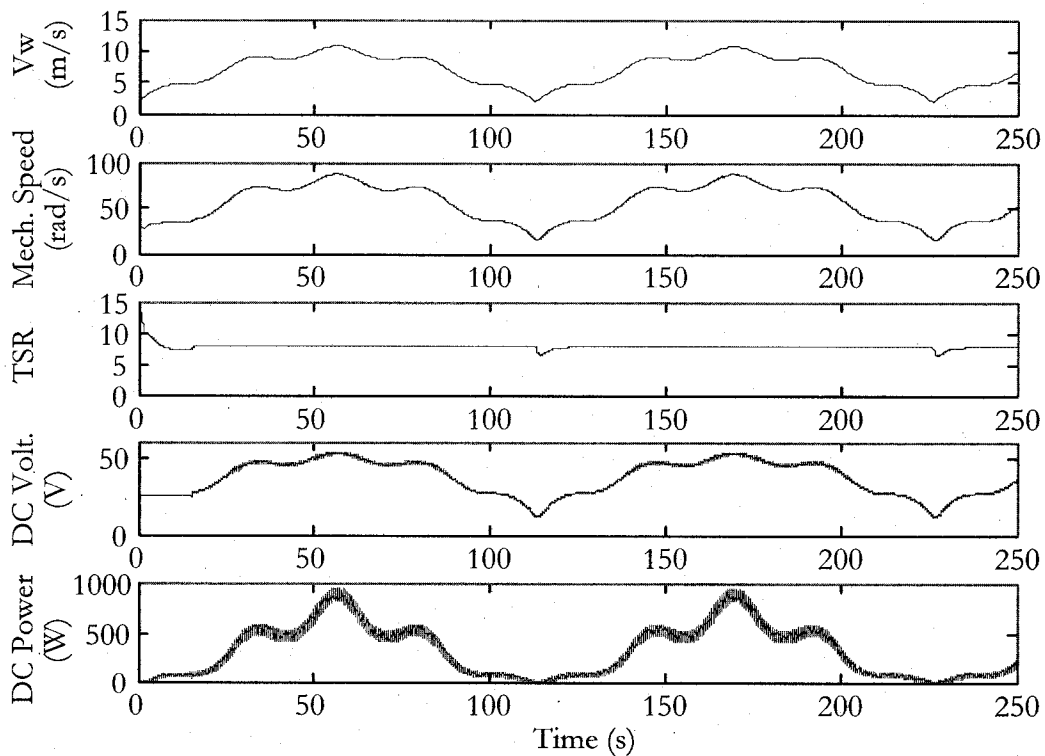


Figure 4.13: Simulation Results with Proposed Control – 1 ms Time Step

In Figure 4.13 it is immediately evident that the current controller is performing extremely well. The TSR remains fairly constant at its optimal value throughout much of the wind speed range. The average power extracted from the turbine is 324 W, a sharp increase from the constant DC-link method. The maximum power also increases to 953.8 W at 10 m/s, showing that the system operates at its optimal point at this maximum wind speed. The generator terminal voltage is no longer limited since the DC-link voltage is now variable. This allows the mechanical speed to track the wind speed and keep the turbine operating at the highest coefficient of performance possible. This lowers the cut-in wind speed, giving way to power extraction at wind speeds below 5 m/s. It is clear that over time, more power is extracted from the controlled wind energy system.

The controller time step is increased to determine if the ripple in the DC-link further subsides. However, it became evident as the controller time step is increased to 5 ms and 10 ms the ripple in the DC power grew. Although all three sets of results gave roughly the same average power output, the maximum power increased due to the increase in waveform ripple (results are shown in Figure 4.14 and Figure 4.15).

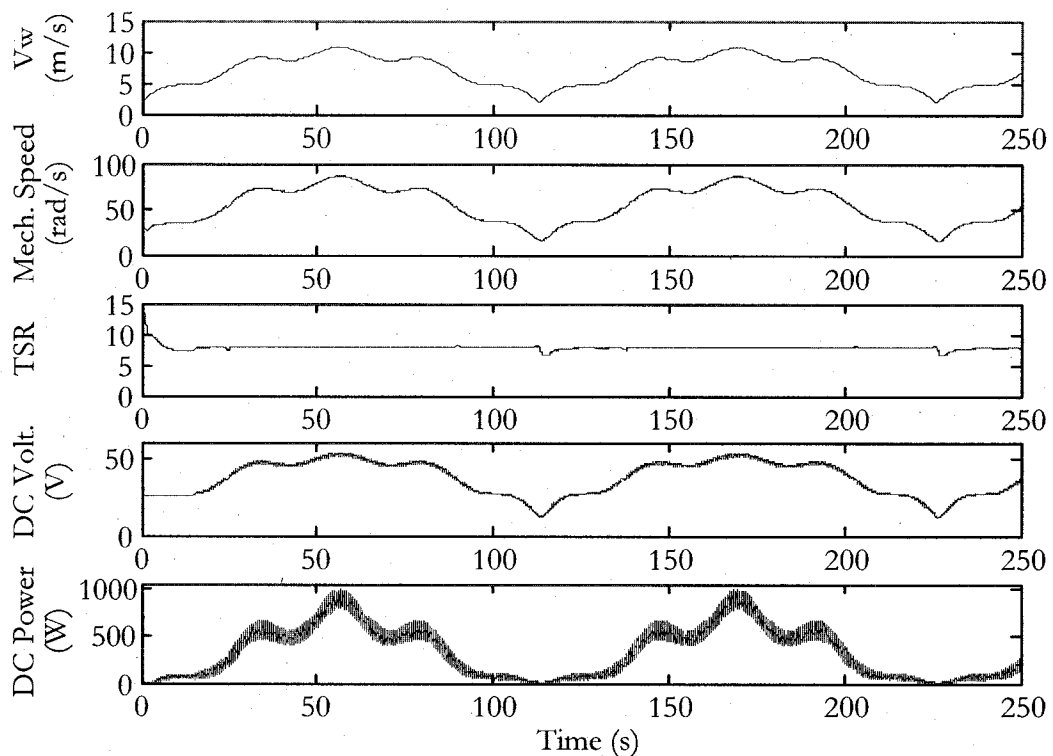


Figure 4.14: Simulation Results with Proposed Control – 5 ms Time Step

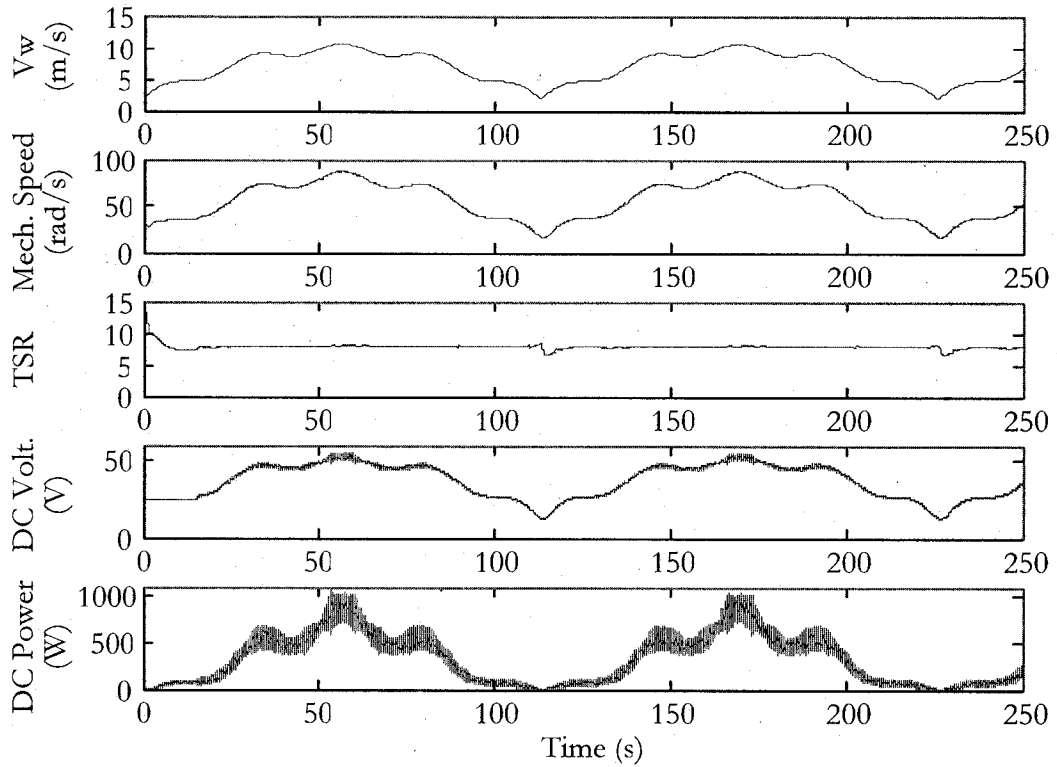


Figure 4.15: Simulation Results with Proposed Control – 10 ms Time Step

4.4.4 Controller Step Response Results

The proposed controller is tested for its ability to respond to a step change in wind speed. The wind is first stepped down from the maximum 10 m/s to 5 m/s and the DC-link voltage, DC power, TSR and generator mechanical speed are recorded. As can be observed in Figure 4.16, a sudden decrease in wind speed causes an increase in TSR, which is expected according to equation 2.3. Due to the high inertia of the system, the generator speed gradually decelerates during a shift in wind speed and the controller settles the machine to the optimal speed. As the figure shows the TSR reaches the optimal operating point after a transient time of 0.5 s.

Similarly the controller is also tested under the condition of a step-up in wind speed. In this case the wind speed is stepped from an initial wind speed of 5 m/s to the maximum wind speed of 10 m/s. This condition slightly resembles a sudden wind gust that a practical system may endure. Once again the TSR shows a sudden change, decreasing below 5, depicted in Figure 4.17. The controller performs well as the new optimum point for generator speed and voltage are reached within approximately 0.6 s.

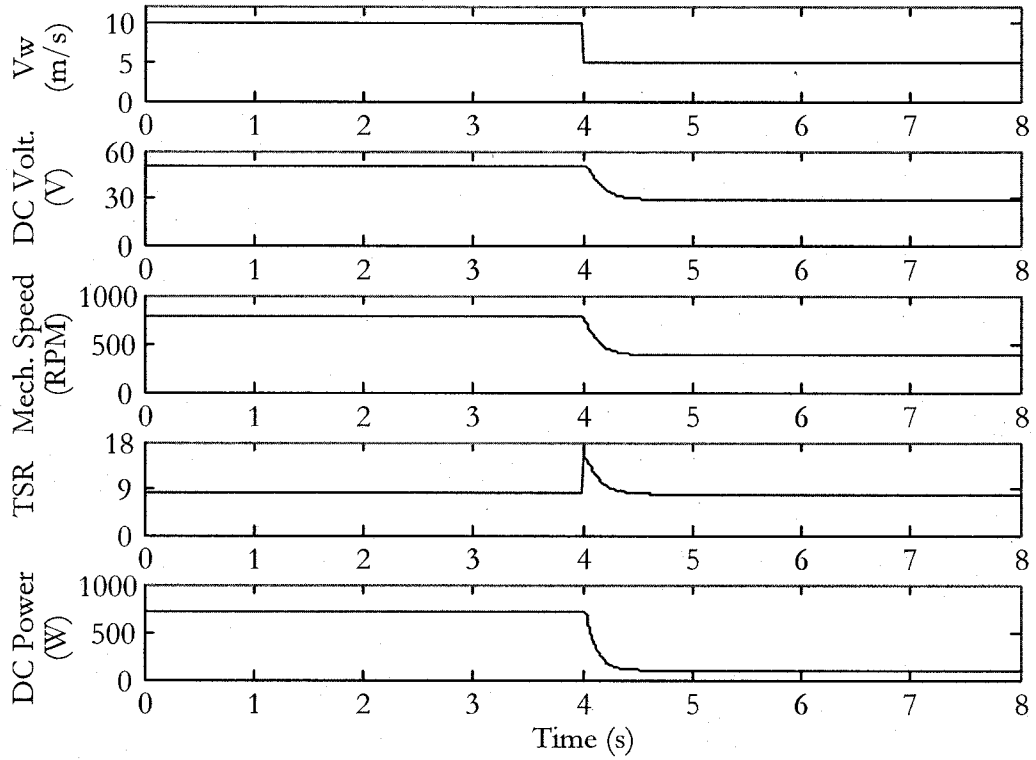


Figure 4.16: Proposed Controller Simulated 5 m/s Step-Down Response

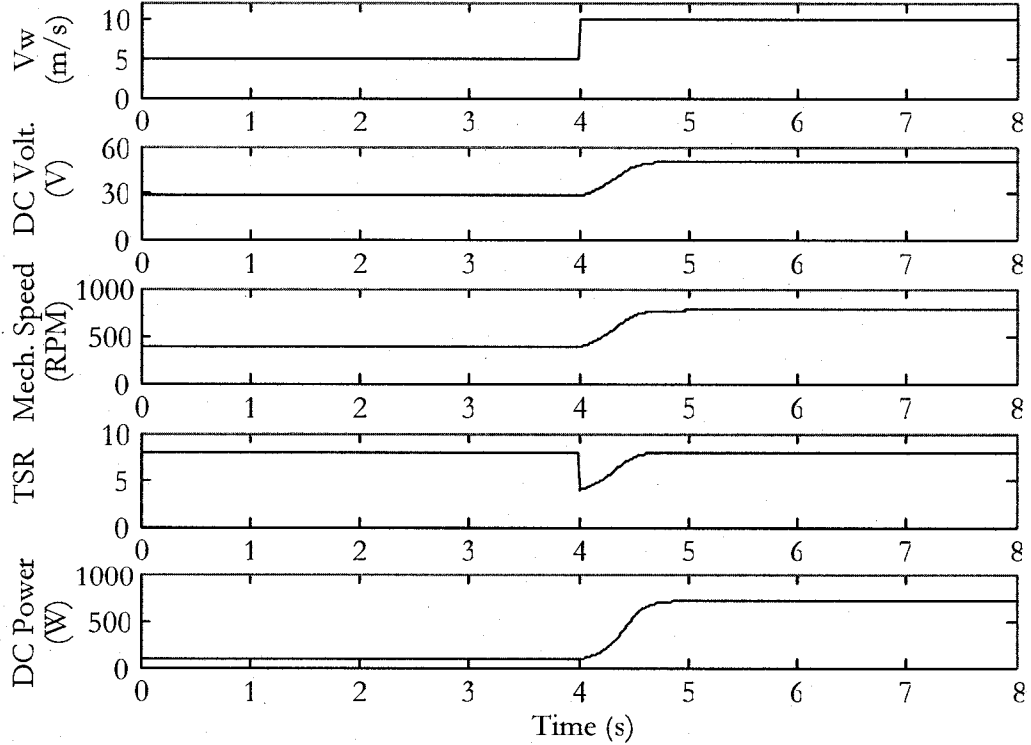


Figure 4.17: Proposed Controller Simulated 5 m/s Step-Up Response

4.5 Chapter Summary

The flyback converter is simulated and tested with a snubber circuit and shows it is capable of providing the demanded voltage boost at a 1 kHz switching frequency. The wind energy system is also simulated under both constant DC-link voltage and variable DC-link voltage conditions. Results have shown that the current controller is capable of tracking the optimal TSR through fixed relationships without the costly use of a speed encoder. The controlled system proves to be superior as it extracts more average power, and reaches the highest maximum power. These results paved the way for the design of an experimental test rig and verification of turbine control.

Chapter 5

Experimental Design

The design and experimental verification of the proposed wind energy system are presented in this chapter. The experimental test rig is shown in Figure 5.1 in which a LabView PXI chassis with real-time software is employed for wind turbine emulation. A brushless permanent magnet synchronous generator is coupled with a DC motor. The DC motor is connected to a DC power supply with controllable voltage and current limits. The generator supplies optimal power to the grid via the proposed power electronic converter. LabView data acquisition hardware and the real-time software are again used to perform the theoretical current control of the flyback converter switching ratio for maximum power transfer.

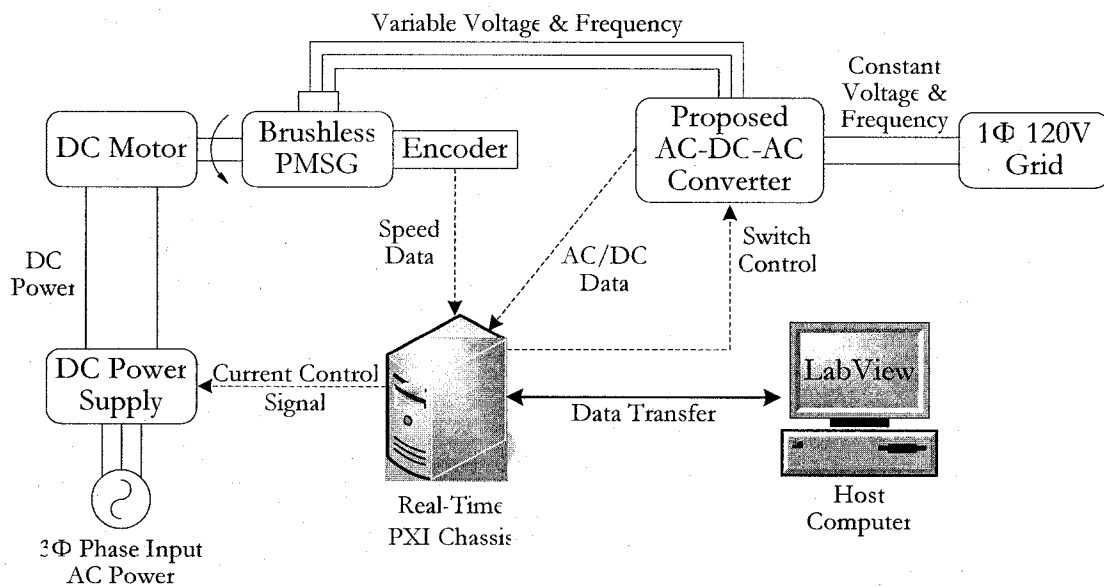


Figure 5.1: Experimental Test Rig Design Schematic

5.1 Wind Turbine Emulator

The test rig does not incorporate an actual wind turbine and the shaft characteristics of a wind turbine are emulated. The wind turbine emulation is performed with a LabView based data acquisition and control, a controllable DC power supply, a permanent magnet DC motor and a generator encoder. The mechanical speed is obtained from the encoder and fed to the LabView control, which in turn outputs a current control signal to the DC supply. This current control signal produces a DC motor torque corresponding to the emulation wind speed.

5.1.1 Permanent Magnet DC Motor

A permanent magnet DC motor is chosen due to the distinct advantages over shunt DC motors. A permanent magnet DC motor does not require an external field circuit, and because no field windings are needed, they can be smaller. Since the poles are made of permanent magnets, the flux in the motor remains fixed. This allows for a linear relationship between the induced torque and armature current, shown in equation 5.1.

$$T_{ind} = K\phi I_a \quad (5.1)$$

Since the torque and current are directly proportional, controlling the current will control the torque. The desired turbine torque for a given wind speed can be set by using a controllable DC power supply that alters the input current to the motor. The motor specifications and performance are given in Table 5.1 and Table 5.2 respectively.

Table 5.1: Permanent Magnet DC Motor Properties

Full Load Rotational Speed	1750 <i>rpm</i>
Full Load Current	14.0 <i>A</i>
Armature Voltage	180 V_{DC}
Efficiency	88.8%
Torque	12.202 <i>Nm</i>
Power	3.0 <i>HP</i>
Duty	Continuous

Table 5.2: Permanent Magnet DC Motor Performance Specifications (at 1800 rpm)

Torque (Nm)	Current (A)	Efficiency (%)
0	0.56	0
4.75	5.53	89.3
11.86	13	91.0

5.1.2 DC Power Supply

The controllable DC power supply allows for easy implementation of the wind emulator through the LabView Real-Time software. The power supply integrates well with the data acquisition hardware in the LabView PXI chassis, and allows for both voltage limit and current limit control. By varying the current limit value, the current output to the permanent magnet DC motor is adjusted. This change in current directly affects the DC motor torque and allows the motor speed to follow the wind profile, successfully emulating the wind turbine.

Remote control of the voltage and current may be performed via either resistive or voltage programming. Voltage programming is chosen for this test rig. The voltage and current limits may be controlled via a 0-5 V_{DC} signal or a 0-10 V_{DC} signal depending on the switch configuration on the rear of the power supply. The electrical specifications and performance of the controllable DC power supply are outlined in Table 5.3.

Table 5.3: DC Power Supply Electrical Specifications

Output Ratings:	
Output Voltage	300 <i>V</i>
Output Current	20 <i>A</i>
Output Power	6000 <i>W</i>
Output Ripple:	
Voltage	30 <i>mV</i>
Current	50 <i>mA</i>
Performance:	
Efficiency	91%

5.1.3 Speed Encoder

It is important to first note that the encoder is only used for the wind turbine simulation and not the flyback converter control, which would result in an increase in the control cost. The encoder outputs the speed information of the generator in the form of a square wave signal that steps from 0 V to 5 V at rate of 2000 lines/rev. The speed signal is interfaced with the LabView software through the data acquisition hardware. The software counts the number of pulsed 5 V lines over one second giving the speed in lines per second. Then a conversion is performed to extract the speed in radians per second, a value needed for the rest of the wind turbine emulation. The conversion is shown in equation 5.2.

$$\omega_m \text{ (rad/s)} = \frac{\omega_m \text{ (lines/s)}}{2000 \text{ (lines/rev)}} 2\pi \text{ (rad/rev)} \quad (5.2)$$

5.1.4 LabView Real-Time DC Current Control

As is shown in Figure 5.1, the Real-Time PXI chassis communicates with the host computer through Ethernet connection. Information is sent back and forth over this connection, giving complete control of the Real-Time system through an external computer. LabView files that access all the input and output capabilities of the modules on the PXI are written on the host computer and downloaded to the chassis for use. The FPGA module is used to perform all the control applications in the proposed system, including the wind turbine emulation.

The encoder data is inputted to the FPGA as a digital signal, and a counter is set up to decipher the speed from the encoder. Using the speed and the current wind speed from the generated wind profile, both the TSR and coefficient of performance are calculated. The TSR curve is approximated with a high order polynomial and limited to a maximum of 15 to avoid false occurrences of positive C_p values above this limit. The coefficient of performance is limited between values of 0 and 0.6 as, theoretically, it will never be outside of these boundaries. From this, the power, torque and current are calculated. The calculation of the current is based on a best fit linear curve for the data in Table 5.2, shown in equation 5.3.

$$I_{DC} = 1.049T_{Turb} \quad (5.3)$$

The calculated current is first put through a threshold block ensuring the current does not go below 1.4 A. This minimum current level is used as it is the point at which no torque is produced in the motor; this is shown in Table 5.2.

The calculations described above are first performed on the Real-Time PXI chassis and the resulting current value is transferred to the FPGA. The FPGA subsequently outputs the current value to the DC power supply for DC motor control. This current value alters the torque in the DC motor, therefore changing the speed to a value pertaining to the current wind speed. The full wind turbine emulation algorithm is given in Figure 5.2, visually describing the method used in the DC motor current control.

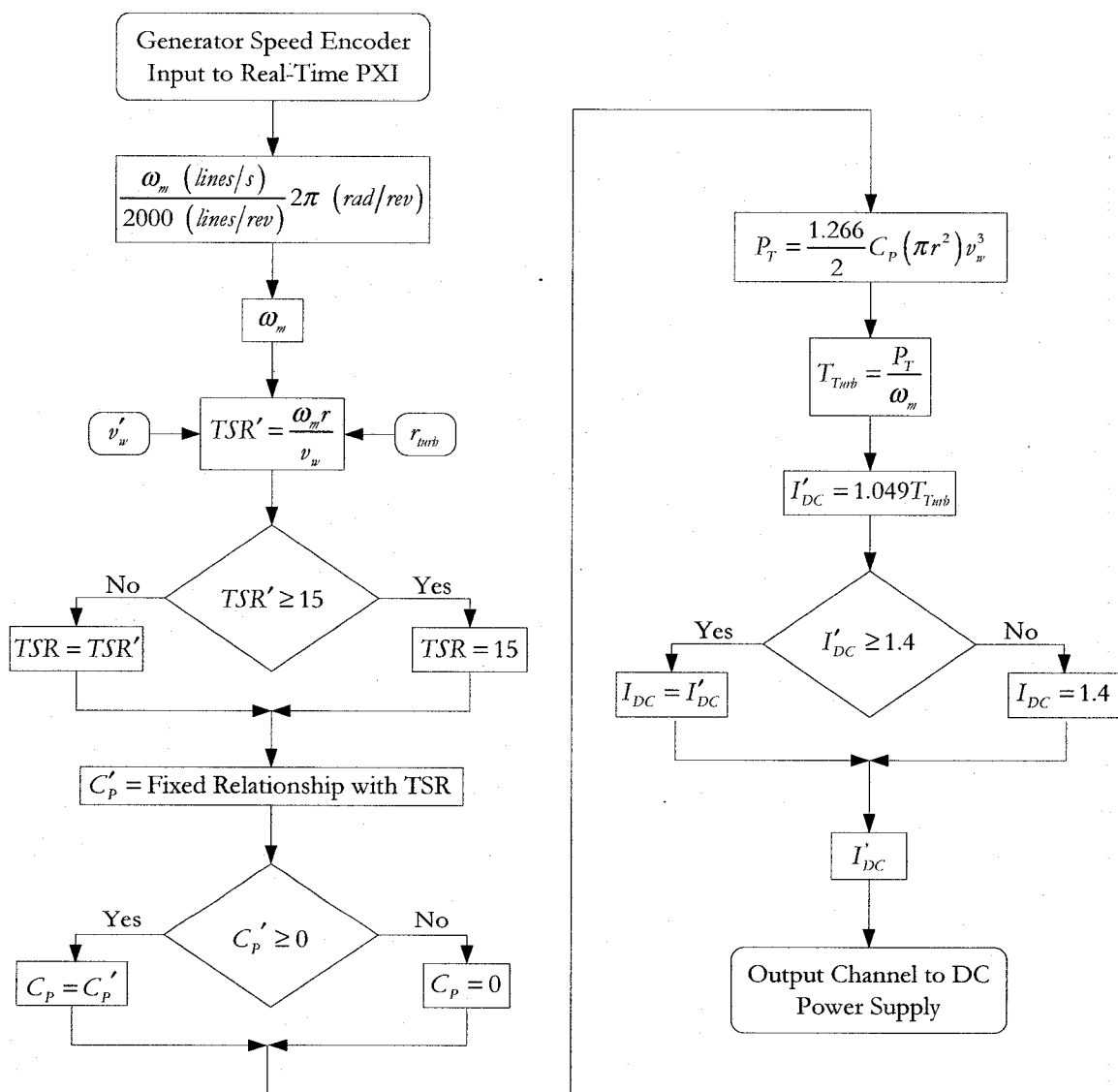


Figure 5.2: Algorithm for the LabView Wind Turbine Emulator

5.2 Brushless Permanent Magnet Generator

A brushless servo motor with an attached speed encoder is chosen to function as the electric generator for the wind energy system. This generator features a high pole number in its rotor construction which is a typical feature of permanent magnet generators employed in wind generation. The high pole number allows for an increase in electrical frequency despite low rotational speeds. Since the system is direct drive and has a high pole number, the wind speed does not force the generator to spin at high speeds. Under the created wind profile, the wind speeds reach a maximum speed of 10 m/s. Therefore if the system is operating at the ideal TSR of 7.9, the generator is predicted to spin at approximately 80 rad/s. Given the machines continuous stall torque of 13 Nm, the amount of power generated at this maximum wind speed will be 1024 W, as desired.

High torque capability at low speeds is an ideal characteristic in choosing a suitable generator for the test rig. The generator is rated for 3.5 kW at a maximum speed of 3000 rpm and is clearly oversized for this application. However due to this oversize, this generator provides the required torque capability at the expected low mechanical speeds. The generator also has a high system inertia giving a slower time response much like practical wind energy systems. A key feature is the addition of a mounted 2000 line optical encoder that is used for the wind emulator control. The electrical generator is rugged and can withstand heavy duty continuous operation; traits that are sought after for wind generation. Several generator properties are outlined in Table 5.4.

Table 5.4: Brushless Servo Motor Specifications

Peak Phase to Phase Torque Constant	$0.71 \frac{Nm}{A}$
Peak per Phase Voltage Constant	$86 \frac{V}{krPM}$
Phase to Phase Winding Inductance	$3.3 mH$
Phase to Phase Winding Resistance	0.51Ω
Rotor Moment of Inertia	$0.064 kgm^2$
Continuous Stall Torque	$13 Nm$
Friction Torque	$0.17 Nm$
Maximum Speed	$3000 rpm$
Poles	8

5.3 Power Electronic Converter

The power electronic converter is comprised of a three phase diode rectifier followed by the flyback DC-DC converter and finally the single phase inverter. The input of the diode rectifier is connected to the output of the brushless permanent magnet generator, essentially rectifying the variable AC voltage to a variable DC voltage. Capacitive DC-links are used to connect both the input of the flyback to the diode rectifier and the output of the flyback to the single phase inverter. Finally, the output of the inverter is connected to the single phase grid through a large line inductance. A standard three phase diode rectifier module is used for generator AC rectification. However, the flyback and its components are custom designed for this application.

5.3.1 Flyback Converter Design

The flyback converter receives a low DC input voltage and outputs a magnified DC voltage to the inverter. The converter contains a single high power metal-oxide-semiconductor field-effect transistor (MOSFET) on the primary side of the circuit. When the MOSFET is in the on-state, energy is stored within the primary winding of the transformer. The energy is later transferred to the secondary winding when the MOSFET is in the off-state. A snubber circuit is used to mitigate the voltage spikes affecting the MOSFET during the transition from on-state to off-state. The final flyback converter schematic, used for the experimental test rig, is provided in Figure 5.3.

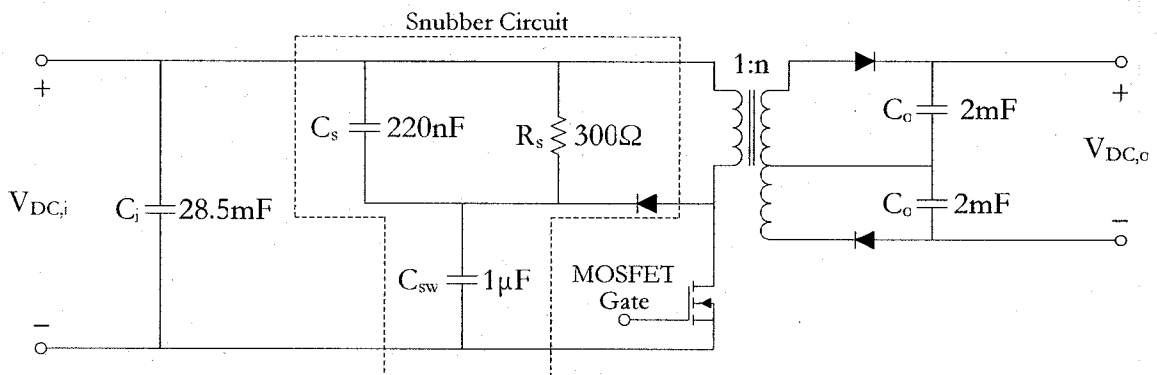


Figure 5.3: Final Flyback DC-DC Converter with Snubber

Flyback Transformer Design

The transformer design is an important factor in the overall composition of the flyback converter. In order to operate within a suitable duty cycle range for the MOSFET, a nominal transformer turns ratio of 14 is selected. In doing so, the duty ratio ranges from 0.343 to 0.819, avoiding the extremes of zero and unity. Refraining from these extremes, the flyback efficiency is optimized and the voltage boost and energy transfer is enhanced. The initial design step is to choose a core size in order to obtain the transformer core magnetizing and winding geometric properties. From the Micrometals transformer core specifications, a flux density of 1.0 T is chosen since this value was slightly below the saturation level on the material B-H curve [35]. The goal of the algorithm is to ensure the core operates near the chosen flux density under the predicted winding current conditions. It is also important to calculate the predicted winding losses to ensure adequate transformer efficiency.

The calculation algorithm for the transformer design is shown in Figure 5.4. The first step is to determine the number of primary and secondary winding turns, which depends on the maximum input DC voltage and flux density, the core magnetizing area and the MOSFET on-time. Next, by splitting the winding window area in half and multiplying by a packing factor of 0.6, the necessary cross sectional areas and diameters of each winding wire are determined. Looking up dimensions for various copper wire gauges, actual wire diameters are chosen nearest to the previously calculated values. An important note in choosing wire gauges is the diameters must be less than the calculated values to ensure the windings will fit within the given core window area. From the actual wire diameters, the resistances of each winding are computed based on the resistivity of copper. Lastly the power losses through each winding are estimated using the predicted DC primary and secondary currents, ensuring acceptable efficiency.

In order to establish the actual flux density achieved through the chosen core, calculation of the amp-turns per length of the primary winding is essential. Carrying over the winding turns (determined in the initial algorithm step), the amp-turns per length is evaluated by using the estimated peak primary current of 37 A. This selected peak primary current is based on the simulations performed for flyback converter circuit verification. Finally the flux density is easily ascertained by simply looking at the flux density versus amp-turns curve (B-H curve) provided for the particular core material.

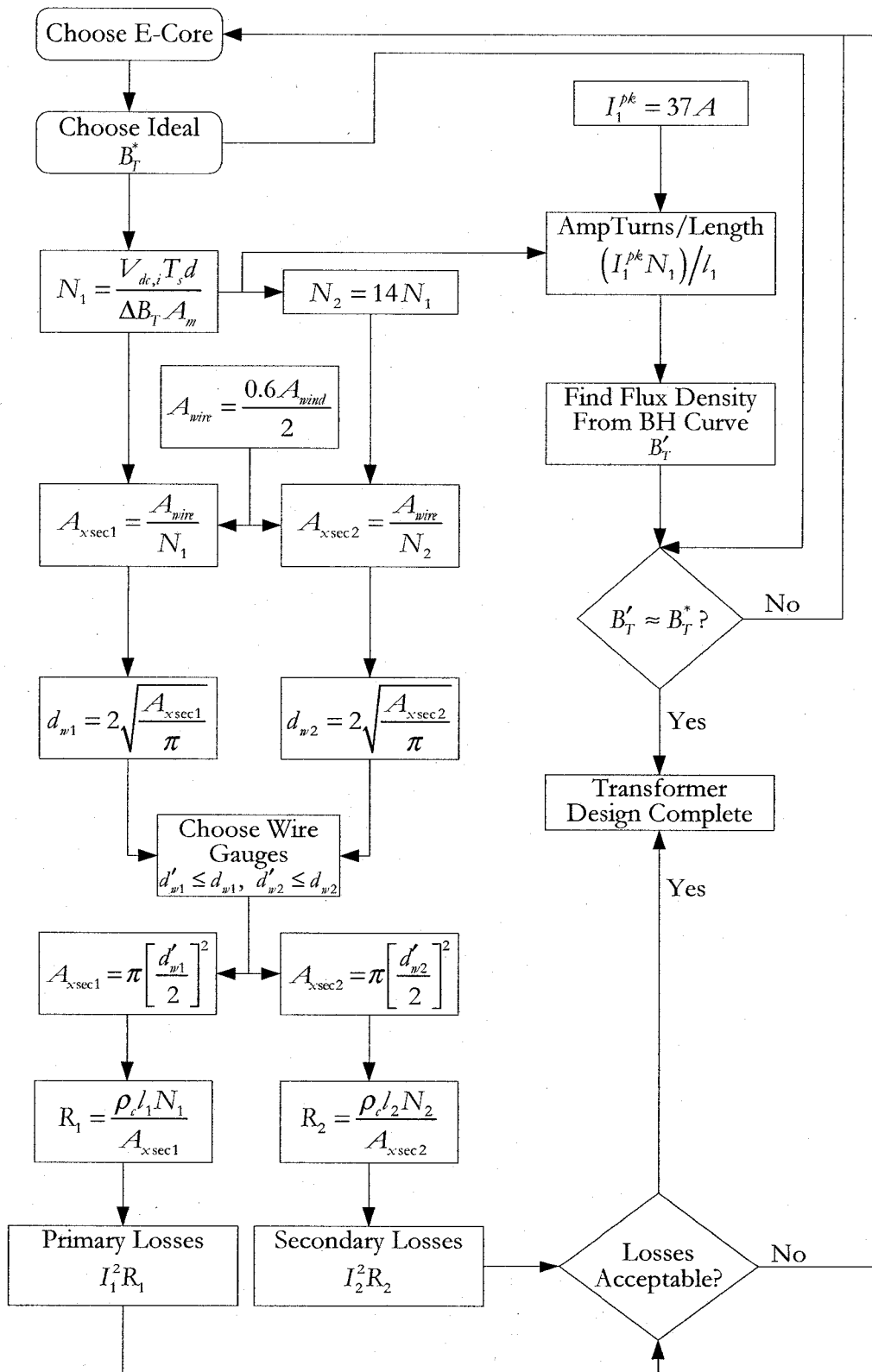


Figure 5.4: Transformer Design Algorithm

Small core sizes are initially used within this algorithm, but it is quickly identified that a larger core is necessary to obtain the required energy and power transfer. A Micrometals E-core, more specifically the E305-26A core, deems to be suitable after increasing the recommended primary and secondary winding turns to 20 and 280 respectively. With 20 primary winding turns, an actual flux density of approximately 0.8T is achieved. Increasing the turns causes a reduction in the winding wire dimensions ensuring the windings fit within the core window area.

The transformer is hand wound with the thinner secondary winding placed first since, because its increased flexibility around the core square corners maximizes the use of the window area. The transformer secondary center tap is created by winding the first 140 turns, cutting the wire, and then continuing the next 140 turns in the same direction. The primary winding is wound directly on top of the secondary winding.

Snubber Circuit Design

The snubber circuit has the sole responsibility to protect the flyback MOSFET from excessive voltage spikes due to leakage inductance in the transformer primary winding. Excess energy stored in the leakage inductance drives current through the transistor, inflicting a surge voltage at the instant the MOSFET is turned off. Consequently, the leakage inductance is an important variable in the design of the snubber circuit. The flyback converter is tested at a low voltage of 15 V without a snubber circuit, in order to identify the magnetizing inductance. The current through the primary winding is then observed and is depicted in Figure 5.5. Utilizing the change in current observed in Figure 5.4 and applying equation 5.4, a calculated magnetizing inductance of $L_m = 321.43 \mu\text{H}$ is obtained.

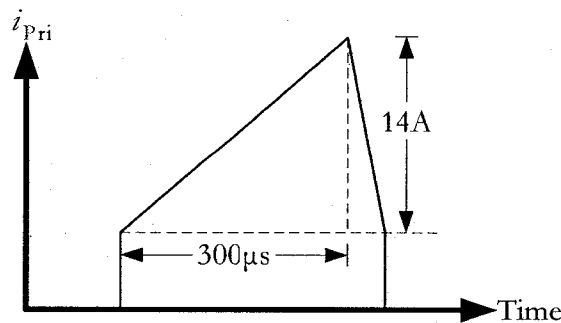


Figure 5.5: Observed Primary Current through the Flyback Transformer

$$L_m = \frac{V_{pri} \delta t}{\delta i_{pri}} \quad (5.4)$$

For a carefully wound transformer, the leakage inductance may be approximated as 3.0% of the magnetizing inductance [36], resulting in a leakage inductance of 8.04 μH . Equation 5.5 gives the energy stored in the leakage inductance as a result of the previously mentioned 37 A peak current expected. Through this calculation a total energy of 5.50 mJ is expected.

$$W_{L_l} = \frac{1}{2} L_l \hat{I}_{pri}^2 \quad (5.5)$$

Equating the total energy in the inductor to the energy dissipated in the snubber capacitance, results in a simple calculation for an appropriate capacitor value. Firstly, however, the maximum allowable transistor voltage must be set to a value of 300V. This voltage is well below the MOSFET voltage rating and well above the voltage output expected from the generator and diode rectifier. This maximum transistor voltage gives a relationship for the snubber capacitor voltage in equation 5.6 and the capacitor value is determined using equation 5.7. In this case a capacitance of 220 nF is chosen for the snubber design.

$$V_s = \hat{V}_T - \hat{V}_{in} \quad (5.6)$$

$$W_{L_l} = W_{C_s} = \frac{1}{2} C_s V_s^2 \quad (5.7)$$

With the snubber capacitance accounted for, only the snubber resistor calculation remains. The goal of the snubber is to accumulate the excess energy from the leakage inductance and dissipate this energy faster than the single switching period of the flyback MOSFET. The flyback switching period is set to 100 μs , thus the dissipation time of the snubber is set to 50 μs . This dissipation time is also known as the resistor-capacitor time constant, τ_{RC} , shown in equation 5.8. Using this equation, a value for the resistor is determined to be 227.27 Ω (for this design a standard 300 Ω resistor is used).

$$R_s = \frac{\tau_{RC}}{C_s} \quad (5.8)$$

An ultrafast, soft recovery diode, specifically suitable for use in snubber circuitry, is selected for this design. In addition the $1\mu\text{F}$ capacitor, connected from the cathode of the snubber diode to the source of the MOSFET, aids in the initial snubber response to the influx of current at the instant the transistor is switched off. With the completion of the snubber circuit design, the flyback converter becomes fully operational within the overall experimental setup.

5.3.2 Single-Phase Inverter

The design of a single-phase inverter is not necessary since a multi-configurable 3-phase power electronic inverter was readily available. The inverter unit was designed and assembled within the power research group, and is suitable for this project since it can handle a maximum of 600 V and 15 A. The inverter module allows both the implementation of a single-phase inverter through alternate connections, and the use of fewer insulated gate bipolar transistors (IGBT). The six-switch device is connected in the manner shown in Figure 5.6, utilizing only the first two transistors in the first inverter leg.

The gate drive and isolation circuitry are also included in the inverter box design. The circuitry includes overcurrent protection which opens all IGBT switches and generates a shut down situation when above rated current conditions occur. The design uses digital optocouplers to create the optical isolation between the switch control logic signals and the inverter circuit. This isolation is absolutely essential for the protection of the National Instruments interfacing hardware used to relay the control signals to the inverter transistors.

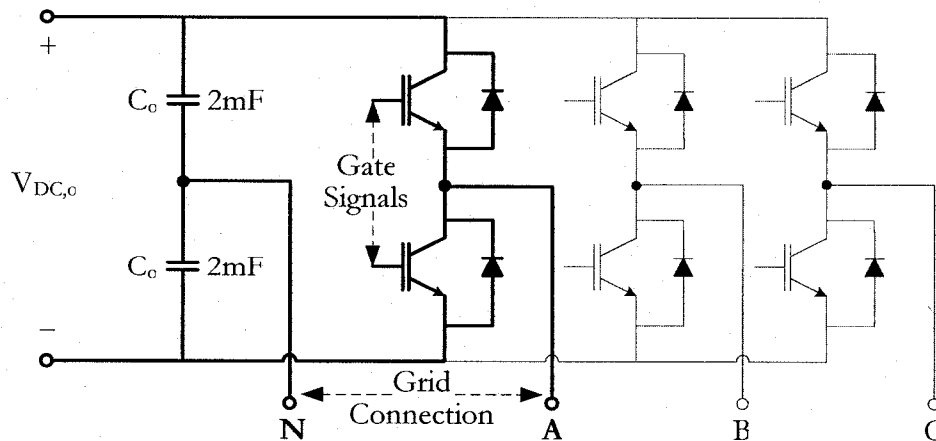


Figure 5.6: Half-Bridge Connection of a 6-Switch Inverter

5.4 Grid Connection

This research considers establishing maximum wind energy capture over a wide range of wind speeds for distribution to a power grid. The power converted by the combination of the diode rectifier, flyback converter and inverter must then be connected to the grid to complete the power transfer. A circuit has been developed to behave in a manner consistent to that of an actual grid. The circuit, shown in Figure 5.7, creates an isolated single-phase AC voltage through a line voltage regulator and variac. A large line inductor is added for current filtering and a 15 A fuse is included for protection.

The line voltage regulator guarantees an isolated and completely constant AC voltage, as the line voltage coming from the outlet may fluctuate slightly. This isolation is only necessary because the DC power supply used to control the generator for turbine emulation is connected to the same supply. In a practical situation this additional isolation is not needed since an actual turbine will be driving the generator. The variac provides an adjustable 0-140 V voltage, giving the system flexibility to operate at lower power levels during testing. Lastly, a large inductor is placed between the grid AC voltage supply and the switching voltage of the inverter. This is performed to minimize both the supply current ripple and the rate of change in the current due to possible inverter and grid voltage differences. The 15 A fuse is used simply as added circuit and inverter protection from any possible damaging overcurrent conditions. This concludes the overall wind energy test rig construction, leaving just the power electronic controller design.

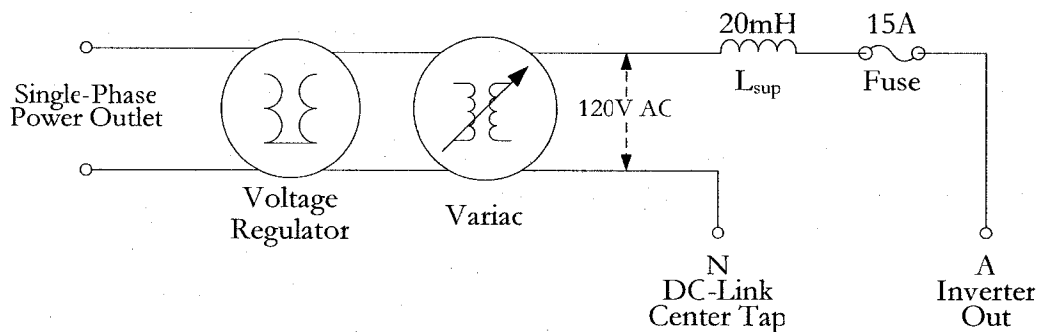


Figure 5.7: Grid Connection Circuit Schematic

5.5 Proposed Converter Controller

The power electronic converter control is implemented through LabView Real-Time software. This software allows for communication between a host computer and the PXI (PCI extensions for Instrumentation) chassis, used for measurement and automation of the variables within the experimental setup. The PXI chassis contains an FPGA data acquisition module that is primarily used for inputting and outputting control signals. The control algorithms for both the flyback converter and inverter are created through the LabView graphical user interface.

5.5.1 Generator Speed Measurement

Maintaining a minimum overall system cost is incredibly important, therefore using the encoder to obtain the generator speed as a control input is unacceptable. Practically, the use of a speed encoder is extremely expensive relative to the cost of power electronic converter. Instead, a circuit can be designed to accept the generator output line-to-line voltage and extract the frequency of this signal. The designed circuit, shown in Figure 5.8, includes an initial resistor divider network for voltage magnitude reduction before entering the instrumentation amplifier. This resistor divider network ensures that the peak of the variable input voltage does not exceed the 15 V power supply at the maximum wind speed. The amplifier is set up to apply a unity gain and provides excellent input noise filtering. The amplifier is set up to apply a unity gain and provides excellent input noise filtering.

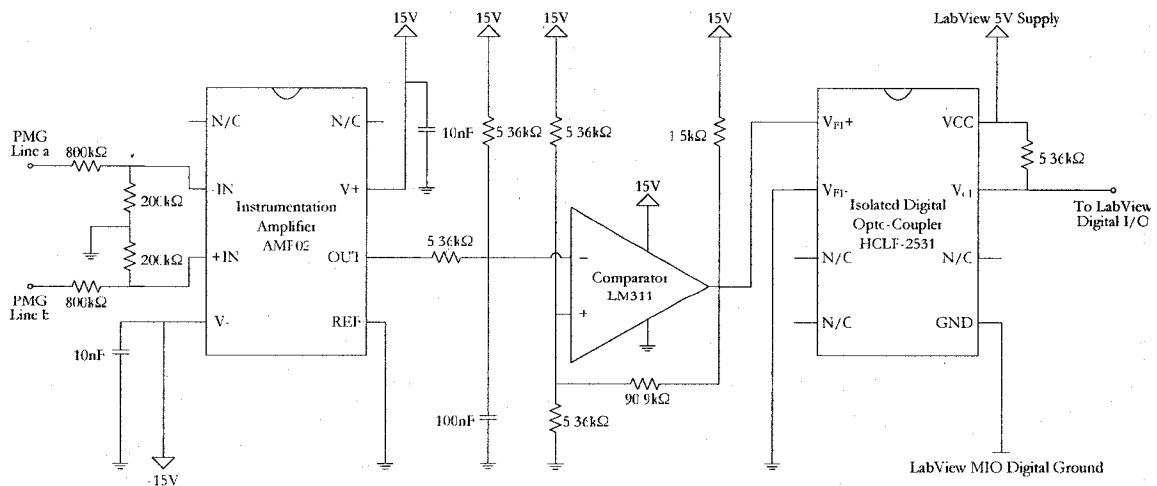


Figure 5.8: Pulse Generation Circuit for Voltage to Frequency Measurement of PMG

The digital optocoupler used for isolation has a maximum reverse breakdown voltage of 5.0V. This specification requires that a single-rail comparator circuit drive the optocoupler, rather than a dual-rail comparator since it will create a reverse input of 15V. The comparator is a special type of op-amp that compares the voltages at the two input pins. The comparator circuit, expanded upon in Figure 5.9, receives the instrumentation amplifier output signal after it has been given a positive offset of 7.5 V. The resistor-divider network of R_1 and R_2 are set to identical 5.36k Ω values to create this voltage offset at exactly half of the 15 V positive supply, shown in equation 5.9. Using the same equation, R_3 and R_4 are also set to 5.36 k Ω , creating the reference voltage at the positive terminal of the op-amp to be 7.5 V. The comparator must also source enough current to turn on the photo diode within the optocoupler. Equation 5.10 shows that for a supply of 15 V, setting R_6 to 1.5 k Ω creates a sufficient source current of 10 mA.

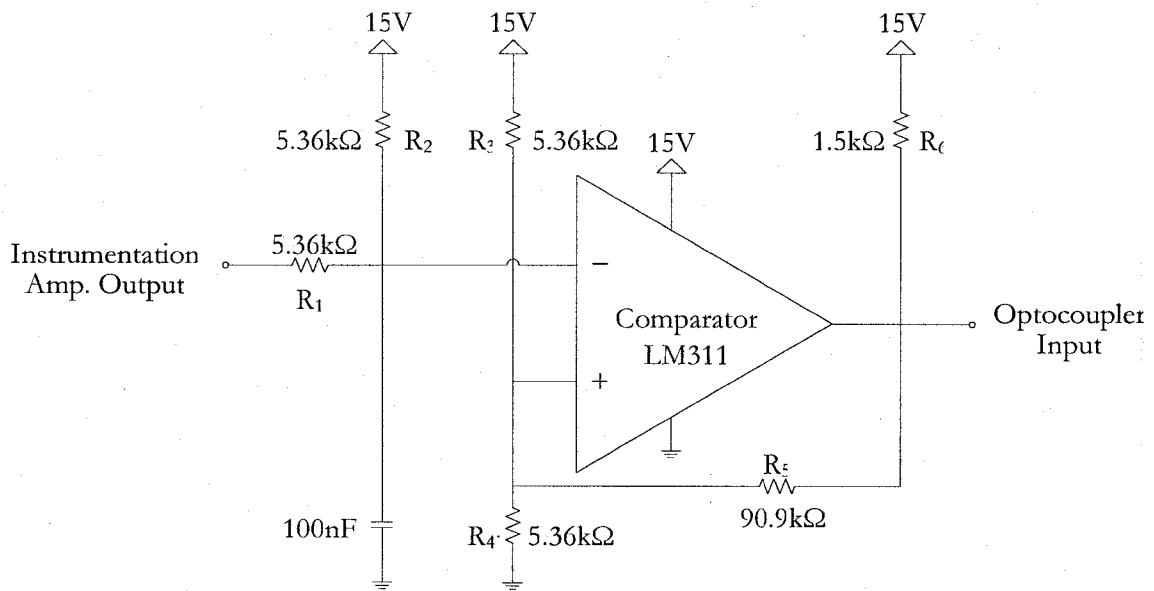


Figure 5.9: Single-Rail Comparator Circuit Design

$$V_{neg} = V_{pos} = 15 \frac{R_2}{R_2 + R_3} \quad (5.9)$$

$$I_{opt} = \frac{15V}{R_6} \quad (5.10)$$

The resistances R_3 - R_6 control the width of a hysteresis band that hovers above and below the reference voltage of 7.5 V. Selecting a 90.90 k Ω resistor for R_5 , the threshold voltages are found to be 7.71 V and 7.29 V, respectively. These values are obtained from equations 5.11 and 5.12. This hysteresis band further nullifies the effect of any noise present on the comparators input pin. This inverting comparator outputs a square wave voltage that is high (15 V) whenever the input voltage is below the low threshold voltage and is low (0 V) whenever it is above the high threshold voltage. Finally, this output is relayed to the optocoupler for isolation purposes to protect the control equipment from the power system.

$$V_{TH_H} = 15 \frac{R_2}{\frac{R_1(R_3 + R_4)}{R_1 + R_3 + R_4} + R_2} \quad (5.11)$$

$$V_{TH_L} = 15 \frac{R_2 R_3}{R_2 R_3 + R_1 (R_2 + R_3)} \quad (5.12)$$

5.5.2 Flyback Control and Driver Circuitry

Flyback Fixed Relationship Controller

The theoretical calculation for a flyback converter duty ratio is relatively simple as it only depends on the presumed constant output voltage, set by the inverter, and the input voltage. Since the input voltage is variable due to the changing wind speed, the theoretical results for the optimal input DC-link voltage found in Figure 4.6 are used instead. The output voltage is fixed at 353.55 V by the inverter switching and constant modulation index of 0.96, evaluated through equation 5.13. Using the theoretical ideal input and output voltages, the duty ratio is calculated at each wind speed using equation 5.14. These calculated duty ratio values, Figure 5.10, became the starting point in evaluating the experimental test rig and determining the actual experimental optimal duty ratio values.

$$V_{DC,o} = \frac{2\sqrt{2}V_s}{m_a} \quad (5.13)$$

$$d = \frac{V_{DC,o}}{n(V_{DC,i}) + V_{DC,o}} \quad (5.14)$$

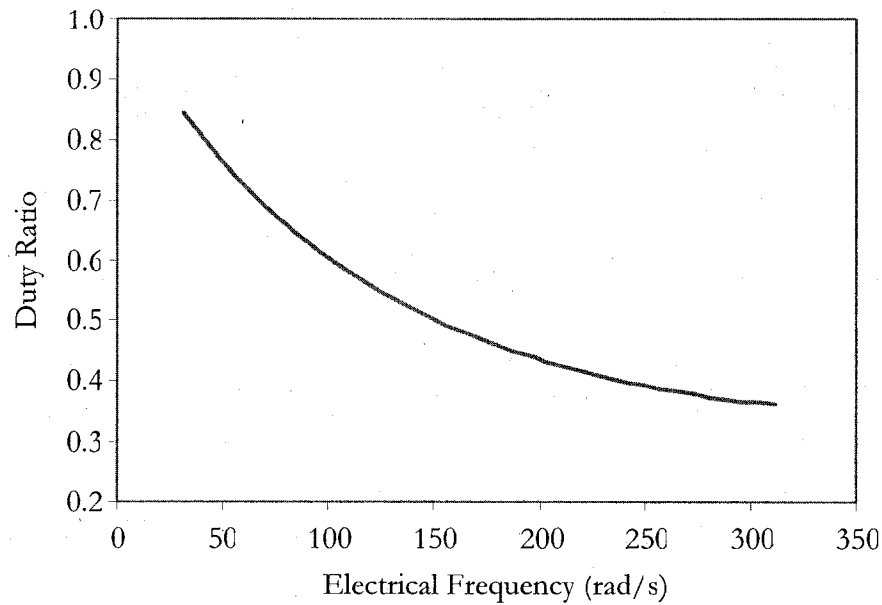


Figure 5.10: Theoretical Duty Ratio vs. Electrical Frequency Fixed Relationship

Using the actual duty ratios found in Chapter 6, a final fixed relationship is found and used in the LabView Real-Time control code. The flyback control code simply takes the generator speed as the sole control input and calculates the optimal duty ratio based on the predetermined fixed relationship. The duty ratio is used to set the pulse width of the 10 kHz square wave switching of the flyback MOSFET.

Flyback Driver Circuitry

In order to operate the flyback MOSFET safely, a proper driver circuit with correct isolation from the LabView control circuitry is developed. The isolation is performed through the use of a digital optocoupler and a dedicated gate driver chip, which forced the MOSFET to turn on and off. The driver circuit also contains a current sensing function that is provided by the gate driver chip. The current sensing circuit allows the chip to identify high current situations that may cause damage to the flyback MOSFET module. High current situations are identified by instances of increased voltage across the MOSFET. Both the entire driver circuit and an expanded look at the current sensing circuit are shown in Figures 5.11 and 5.12 respectively.

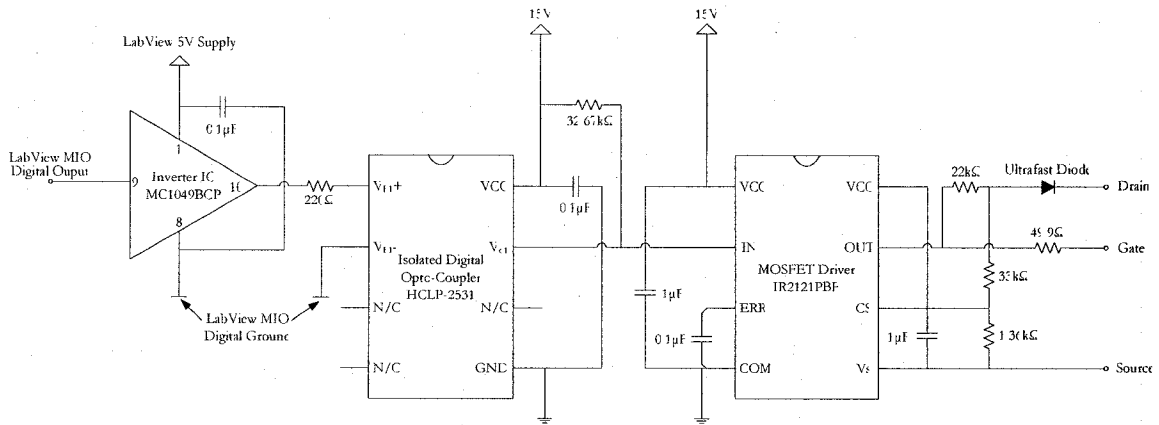


Figure 5.11: Flyback MOSFET Gate Driver Circuit with Current Sensing

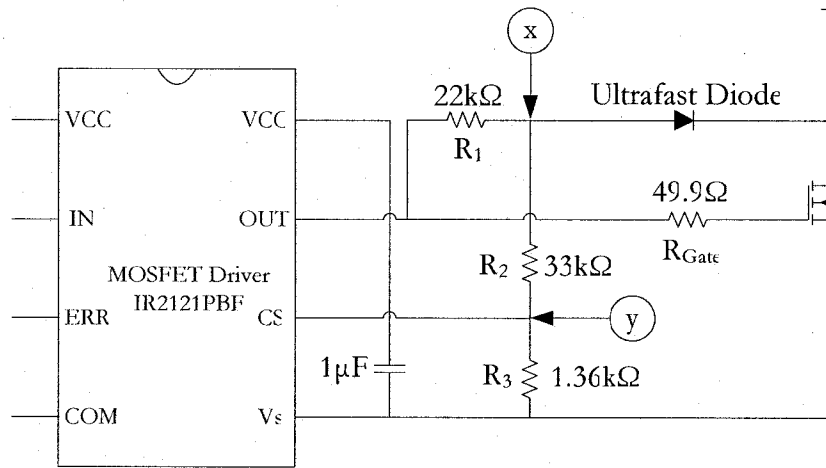


Figure 5.12: Flyback Driver Chip Current Sensing Circuit

Protection of the MOSFET is extremely important; therefore the current sensing design circuitry is an important step in the driver circuit construction process. First, R_1 is chosen to be 22 k Ω since the driver chip provides a 15 V gate-source voltage. Setting R_2 to 33 k Ω simplifies the design leaving just one unknown resistance. The circuit is designed for a peak switch current of 50 A, well above the expected value. It is determined that a drain-source voltage of 4.6 V will occur at this maximum current level. Since the ultrafast diode on-state voltage is 1.2 V (the voltage at point 'x' in Figure 5.12) is 5.8 V, which is shown by equation 5.15. The IR2121 driver chip has a rated current sensing voltage of 230 mV experienced at point 'y'. Therefore with the known values above, equation 5.16 results in a final R_3 resistance value of 1.36 k Ω , completing the current sensing circuit design.

$$V_x = V_D + V_{DS} \quad (5.15)$$

$$R_3 = \frac{V_y R_2}{(V_x - V_y)} \quad (5.16)$$

The gate resistance design is also important, as the value affects the MOSFET turn on time, and it is critical to ensure a fast switching time. Using the MOSFET specification sheet, it is determined that a gate charge of 300 nC is necessary for guaranteeing a fast switching device supplied by a 15 V gate-source voltage. A desired switching on time of 1 μ s is chosen as a reasonable amount since the flyback switching period is established as 100 μ s. At the specified gate charge and desired switch turn-on time, equation 5.17 results in a required gate current of 300 mA.

$$I_{Gate} = \frac{Q_{Gate}}{t_{on}} \quad (5.17)$$

The gate resistance can then be calculated to be 50 Ω for the provided 15 V gate-source voltage, shown by equation 5.18. The closest standard value of 49.9 Ω is chosen for the experimental circuit, concluding the flyback driver circuitry design.

$$R_{Gate} = \frac{V_{GS}}{I_{Gate}} \quad (5.18)$$

5.5.3 Inverter Control and Algorithm

Inverter Theoretical Control

The purpose of the inverter control is to maintain optimal power injection into the grid. This inverter control uses a theoretically defined association involving the generated power, inverter output voltage, grid voltage and the output voltage phase angle. This phase angle, δ , represents the angle difference between the inverter output voltage and grid line voltage. A phasor diagram depicting the magnitudes and directions of the inverter output variables is illustrated in Figure 5.13.

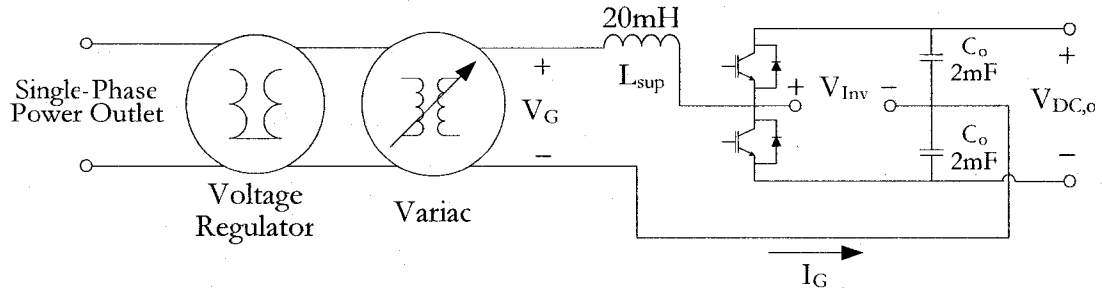


Figure 5.13: Inverter and Grid Output Circuit Diagram

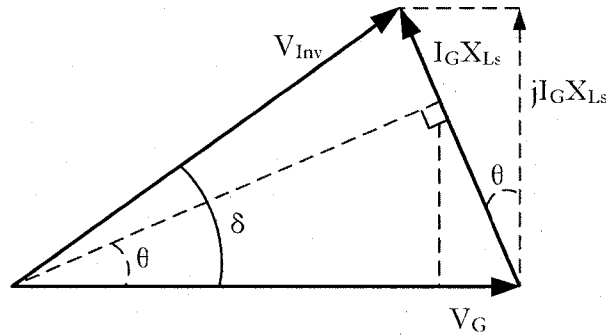


Figure 5.14: Inverter Output Phasor Diagram

From the phasor diagram, the formulas for the power factor angle, θ , and voltage phase angle (δ) are defined as follows

$$\cos(\theta) = \frac{j I_G X_{Ls}}{I_G X_{Ls}} \quad (5.19)$$

$$\sin(\delta) = \frac{j I_G X_{Ls}}{V_{Inv}} \quad (5.20)$$

Combining equations 5.19 and 5.20 results in an equation that relates the power factor angle to the inverter voltage phase angle:

$$\cos(\theta) I_G = \frac{\sin(\delta) V_{Inv}}{X_{Ls}} \quad (5.21)$$

The output real power for the single phase grid is calculated using the well known formula shown by equation 5.22. Assuming negligible losses through the converter a relationship for the power factor angle to the input DC power is established.

$$P_{out} = P_{DC} = V_G I_G \cos(\theta) \quad (5.22)$$

Substituting equation 5.22 into equation 5.21 gives the final equation used to determine the theoretical inverter voltage phase angle needed. This is the angle needed to achieve optimal power flow from the wind turbine, equation 5.23.

$$\delta = \sin^{-1} \left(\frac{P_{DC} X_{Ls}}{V_G V_{Inv}} \right) \quad (5.23)$$

It is once again noted that these values are employed as an experimental starting point. The actual relationship between phase angle and electrical frequency is found experimentally. The theoretical relationship between the inverter voltage phase angle and generator electrical frequency is depicted in Figure 5.14.

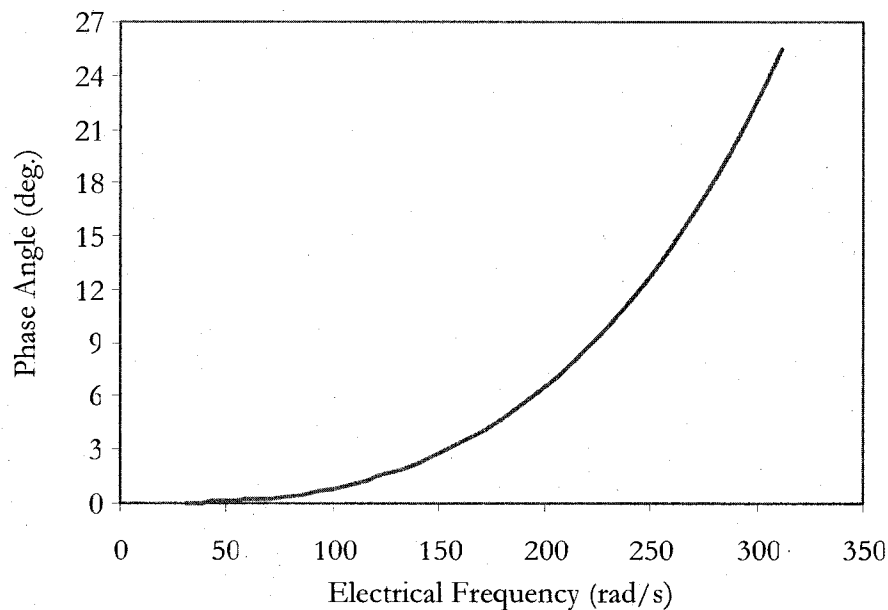


Figure 5.15: Theoretical Phase Angle vs. Electrical Frequency Fixed Relationship

Inverter LabView Control Algorithm

The LabView inverter control algorithm, Figure 5.15, receives the single control input of the instantaneous generator electrical speed. Using this speed input, the algorithm then computes the required optimal phase angle. Since the required phase angle data is obtained experimentally at various wind speeds, a simple second order polynomial curve fit is performed on the data. The computer control employs this polynomial equation during its computation for the required phase angle at the current generator speed. It is noted that the FPGA is used for convenience since it is readily available. In a practical system the controller hardware may be simpler and more cost effective than the FPGA.

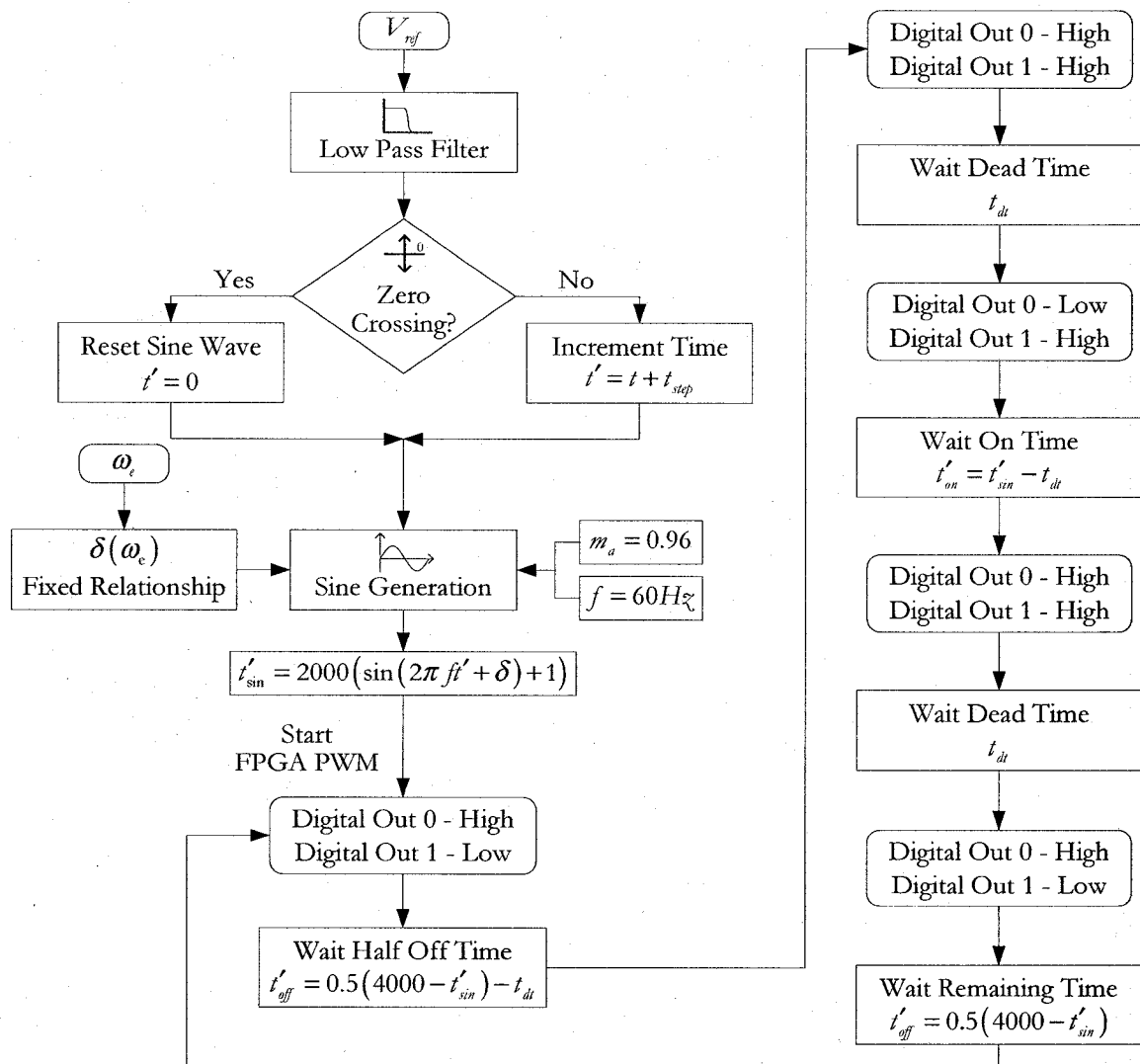


Figure 5.16: LabView Inverter Phase Angle and Switching Algorithm

Simultaneously, the LabView code accepts an analog input voltage as the pulse width modulation reference voltage from the single-phase grid. Applying zero-crossing detection, a 60Hz sine wave is synchronized to the grid voltage at the instance the grid voltage changes from a negative to a positive value. Utilizing a LabView sine wave generation block, the amplitude, hence modulation index, phase shift and DC offset are controllable. The phase shift is controlled using the calculated phase angle that is achieved through the experimental fixed relationship discussed above.

The FPGA implemented PWM generation block uses ticks to control the switching period. In this case 4000 ticks represent 100 μ s while using the 40 MHz internal FPGA clock. The on-time of the inverter switches are determined by the instantaneous amplitude of the reference signal. The signal is first scaled in a manner that assures the maximum amplitude will not exceed 2000 for a modulation index of one. The signal is then shifted upwards creating a DC offset that centers the signal at 2000, making the maximum no larger than 4000. The complete transition of the reference voltage is shown in Figure 5.16, where in this case a modulation index of 0.96 is employed.

When the reference signal reaches its maximum value, the FPGA correlates this value as the high switch on-time in ticks and distributes the switching signals for both inverter transistors accordingly. Since the reference amplitude is sampled at an extremely fast rate, the FPGA outputs appropriate switching signals throughout the sinusoidal transition of the reference signal. For protection of the inverter transistors, a 2 μ s dead-time is included during all state transitions ensuring that both transistors are never on at the same time. Having both switches on together will create a path of zero resistance across the DC-link capacitors. This path will endure a sudden ramp up in current and will undoubtedly destroy the inverter IGBT module. The inverter IGBT's are driven by digital outputs controlled by the LabView real-time FPGA code.

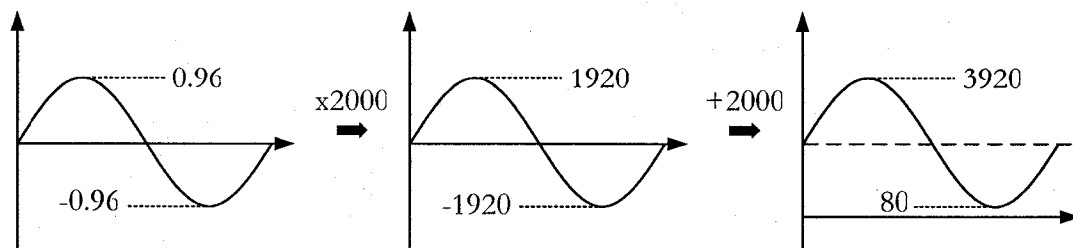


Figure 5.17: Sinusoidal Reference Transition For LabView FPGA PWM Switching

5.6 Chapter Summary

In this chapter the details of the construction of a small scale grid connected wind energy test rig are identified. A controllable DC power supply and permanent magnet DC motor are used for emulation of a wind turbine driving the permanent magnet synchronous generator. The complete design of the flyback converter, including snubber and transformer construction, is also provided. Using the LabView PXI chassis and minimal analog circuitry, control signals for the wind turbine emulation, flyback converter and inverter are easily created. The control algorithms for both the flyback converter and single-phase inverter are given and are later used to produce the experimental results. Chapter six outlines the experiments carried out and the results obtained for verification of the wind turbine control.

Chapter 6

Experimental Results

The experimental results of the proposed grid connected wind turbine are presented in this chapter. The first results provided verification that LabView indeed controls the phase angle of the inverter PWM sinusoidal reference signal. Actual experimental fixed relationships for the duty ratio and phase angle are created and compared to their ideal fixed relationships described in Chapter 5. The controller results for the injection of the variable wind speed profile are shown, including the resulting TSR throughout the changing wind. Lastly the system is subjected to 1 m/s and 2 m/s wind speed step changes and the resulting controller step response results are given.

6.1 Measurement Equipment

Validation of LabView inverter switching and voltage phase angle control is obtained through an oscilloscope. In other experiments, to obtain the dynamic wind speed results, two Yokogawa power meters are used. These meters are inserted into the generator circuit, high DC-link circuit and grid circuit. Each Yokogawa contains three measurement elements allowing for three separate single phase connections or a typical three phase connection. The PXI chassis allows for the connection of both these meters through a single GPIB port. The dynamic results are obtained instantaneously through the LabView computer control for further analysis.

In order to measure the generator 3-phase voltages and currents, the first meter is inserted between the generator output terminals and the input of the 3-phase diode rectifier. The Yokogawa meter requires a three-phase three-wire connection for this particular generator since the generator does not have a neutral connection required for the four-wire connection type. The addition of the power meter is depicted in Figure 6.1, as only two of the three measurement elements on the Yokogawa power meter are needed.

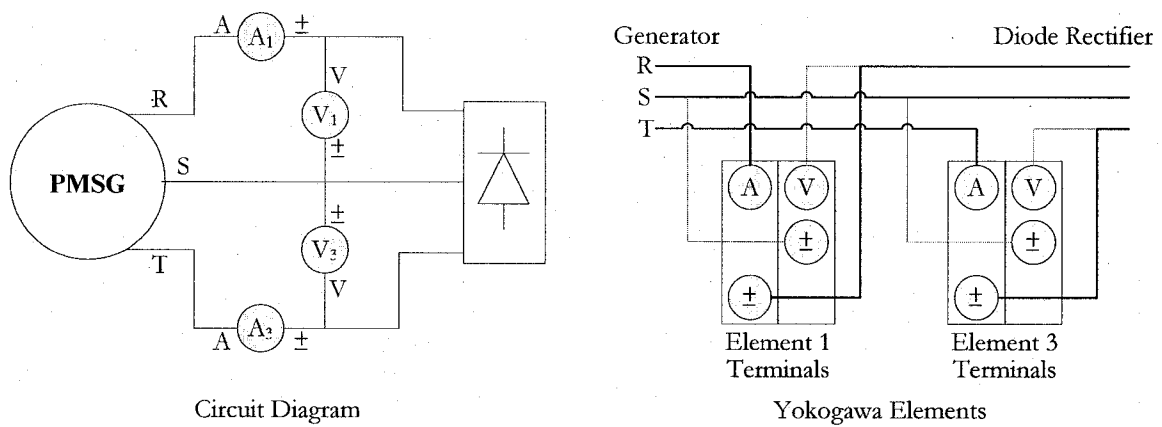


Figure 6.1: Generator Side Connection of Yokogawa Power Meter

It is extremely important to obtain the resulting currents and voltages through the high-side DC-link. Determining the power at this stage gives an accurate distinction between flyback converter losses, and single-phase inverter losses. Since the flyback transformer has a center tapped secondary that is connected at the mid point of two large DC-link capacitors, two separate current measurements are required. The two current loops measured are shown in Figure 6.2, and are used in conjunction with each capacitor voltage to obtain the high-side DC-link power. The final measurement element on the power meter is used for grid power measurement, as both grid voltage and current are obtained. Figure 6.3 outlines how each element is connected to the corresponding portion of the circuit, between the flyback secondary and inverter connections.

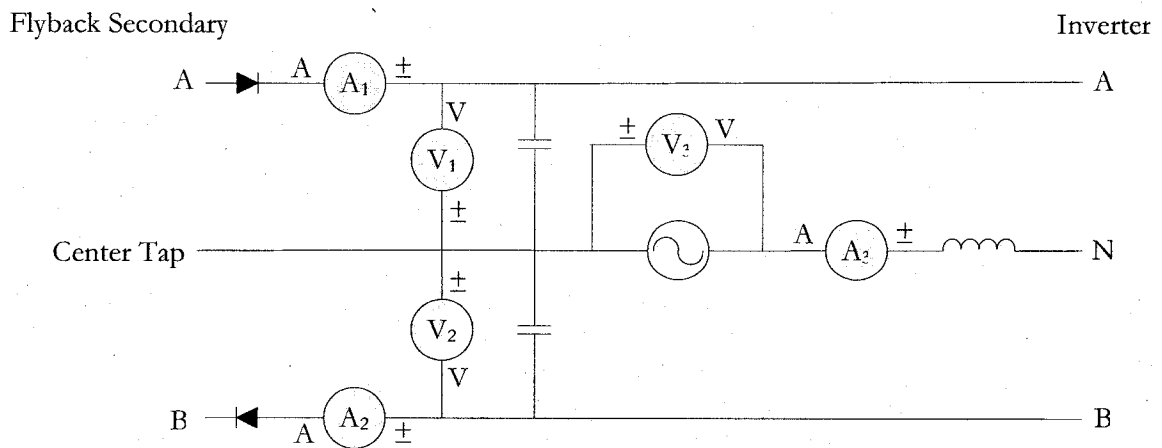


Figure 6.2: High DC-Link and Grid Measurement Circuit

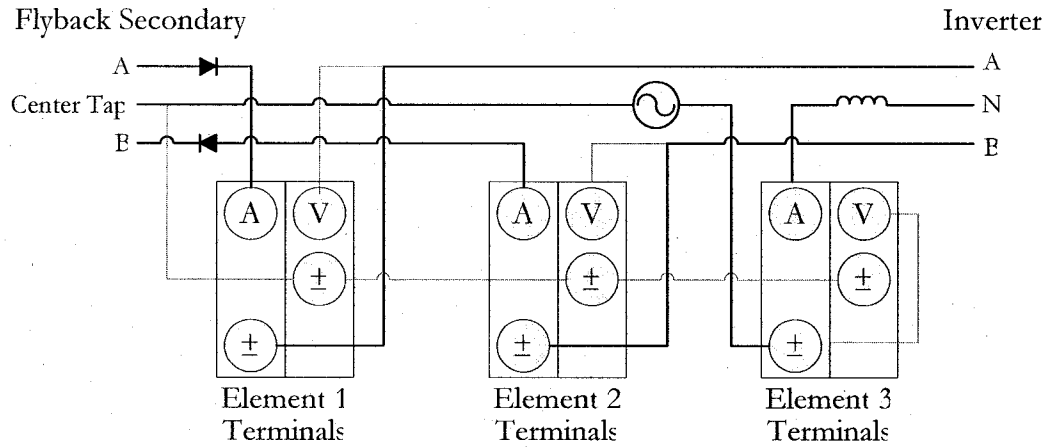


Figure 6.3: Yokogawa Connection for High DC-Link and Grid Measurement

6.2 Controller Verification

Controller verification is completed for both the flyback and inverter stage of the electronic converter. The LabView inverter control is first verified since the sinusoidal PWM switching technique involves the need for a precise phase angle control. It is extremely important that the commanded angle matches the actual produced angle at the output of the inverter. Having the angles match allow the inverter to achieve optimal power flow. Once the inverter control is verified, the calculated ideal flyback duty ratio and inverter phase angle control relationships are investigated.

The experimental fixed relationship are found by stepping the experimental system through steady wind speeds of increasing value and changing both the duty ratio and inverter angle until the optimal TSR is reached. The calculated theoretical optimal values are used as a starting point before performing the aforementioned experiment. From the experimental verification, actual fixed relationships between the control outputs and input generator frequency are created. Using these fixed relationships allows for a simple open-loop control that requires just the mechanical speed as the single control input. This control technique is simpler than the current controller investigated during system simulation verification and thus more cost effective.

6.2.1 Inverter Phase Angle Control

Initially the PWM switching, without phase angle control, is tested by executing the LabView PWM switching control. The inverter output voltage and supply voltage are measured through an oscilloscope. It is expected that the inverter output voltage will resemble a 10 kHz pulsed frequency signal with a peak to peak voltage equalling the DC-link voltage.

During sinusoidal PWM switching, the top level H-bridge inverter switch is on a majority of the time when the reference signal reaches a positive peak. Likewise during the negative peak of the sinusoidal reference signal the low side switch becomes activated for a larger portion of the switching period than the high side switch. This affect can be shown by looking at the inverter output voltage during the period at which the sinusoidal reference voltage is at the positive and negative peak periods. This high-side and low-side switching theory is proven as it is shown in Figure 6.4 and 6.5 respectively. The figure time scales are limited to a shortened period to capture the high switching pattern of the inverter output waveform. This reduced time scale better shows the disparity in switching period between the high and low switch of the inverter. For this particular case a modulation index of 0.6 is used with the DC power supply commanding a DC-link voltage of approximately 300 V, evident in both figures.

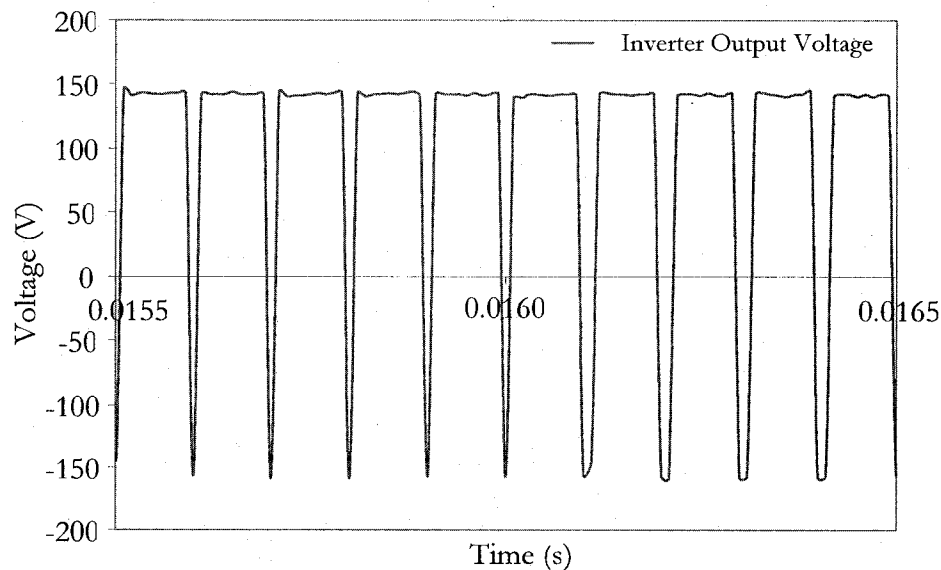


Figure 6.4: Inverter PWM Switching at Positive Peak of Reference Signal

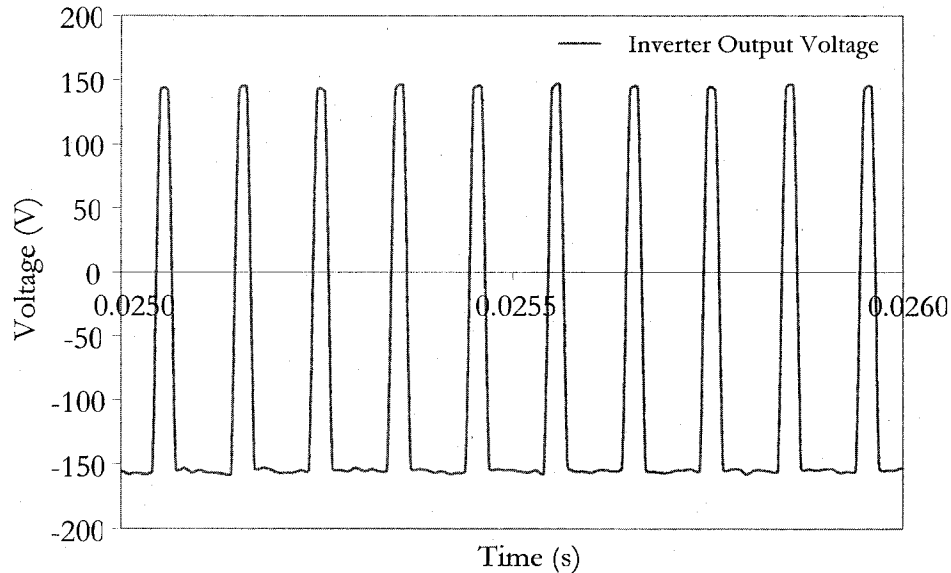


Figure 6.5: Inverter PWM Switching at Negative Peak of Reference Signal

To determine the phase angle produced at the output of the inverter, the grid voltage, grid current, output inductor voltage, power factor angle, and output inverter voltage are simultaneously measured. The 60 Hz fundamental magnitude of each variable is needed and therefore, a Fourier transform is performed on the recorded data using Matlab. It is noted that the commanded angle for this test experiment is set to 26° and the grid voltage is set arbitrarily (not necessarily 120 V) through a single phase variac. Through measurement of the grid current, a 3.1° power factor angle, θ , between grid voltage and current is observed.

The Fourier results, shown in Figure 6.6, display the magnitude of the variables at frequencies ranging from 60 Hz to 500 Hz. The results show that the dominant magnitude of each tested voltage occurs at the fundamental frequency of 60 Hz. The magnitudes of each of the measured voltages are given in Figure 6.7. The magnitude of the inverter output voltage and grid voltage are 112.06 V and 102.86 V respectively. By applying these voltage results to equations 6.1 and 6.2, the actual phase angle is calculated to be 26.67° . The LabView commanded reference angle shift and actual resulting angle are extremely close, showing that the inverter angle control performs excellently.

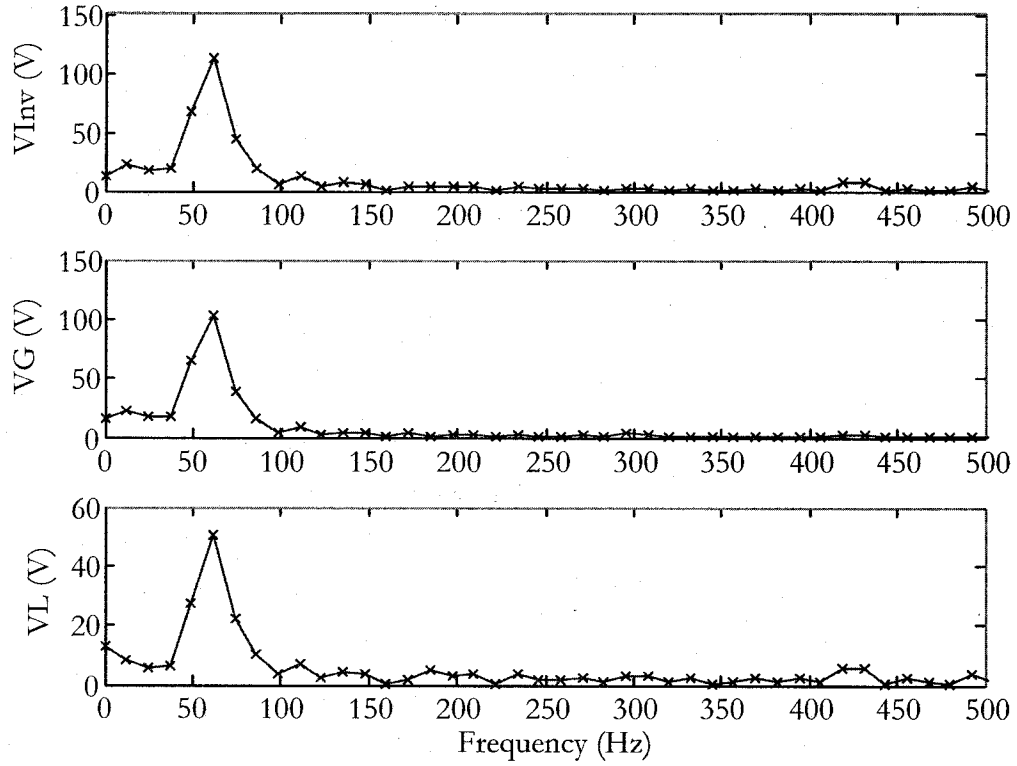


Figure 6.6: Fourier Transform Results for Inverter Angle Verification

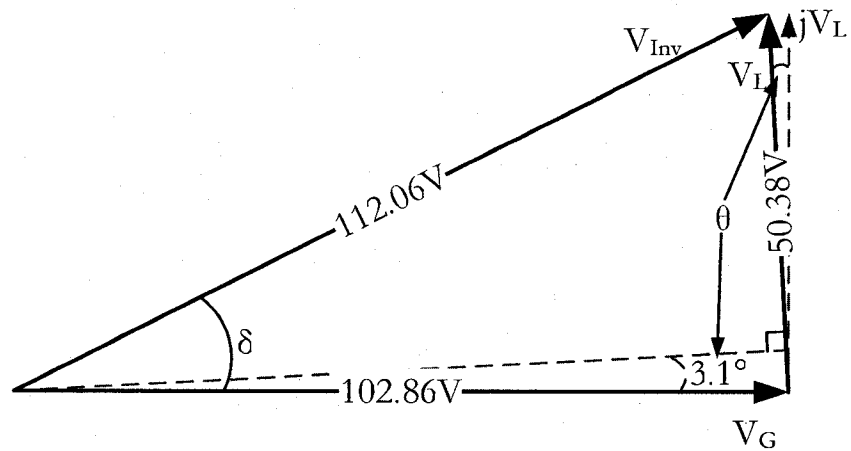


Figure 6.7: Inverter Output Phasor Diagram for Angle Verification

$$jV_L = V_L \cos(\theta) \quad (6.1)$$

$$\delta = \sin^{-1}\left(\frac{jV_L}{V_{Inv}}\right) \quad (6.2)$$

6.2.2 Fixed Relationship Control

In leading up to the implementation of the simple open-loop controller for the conversion system, the theoretical fixed relationships for the duty ratio and angle are first verified. In doing so, the experimental test rig is stepped through a range of wind speeds. At each wind speed the duty ratio and inverter angle are changed until the optimal TSR is reached. The theoretical values, defined in Chapter 5, are used as a starting point in the search for the perfect operating point.

The experimentally defined ideal duty ratio is shown in Figure 6.8 along with the commanded duty ratio and aforementioned theoretical relationship. The experimental optimal duty ratio and commanded duty ratio are almost identical since a 5th order polynomial is used to curve fit the results. This polynomial command relationship is used during the dynamic wind speed control. The large variation between the theoretical and experimental profiles is attributed to assumptions made in the theoretical flyback calculations. The theoretical calculations assume the use of an ideal transformer, and do not account for the snubber circuit added in the test rig. The duty ratio levels off at the end, indicating the need for a much larger MOSFET on-time to cope with the increasing converter losses at the higher power levels.

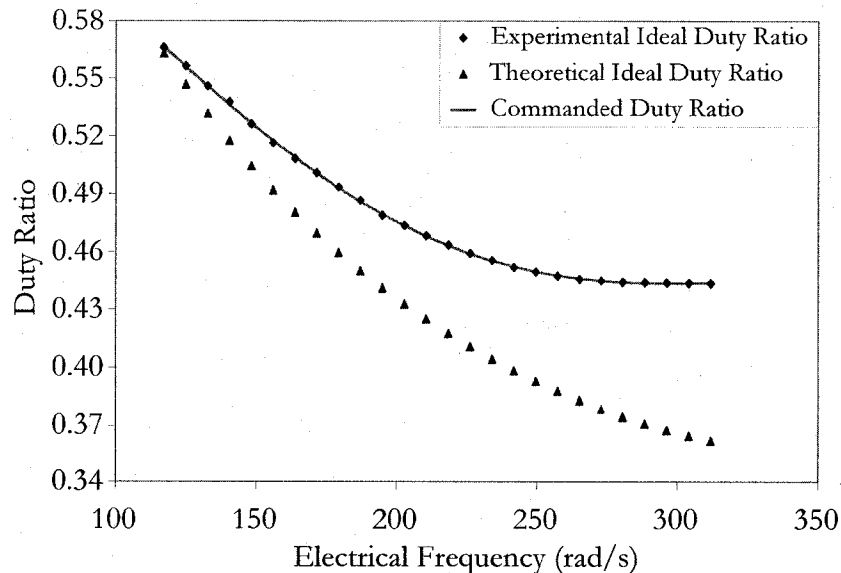


Figure 6.8: Comparison of Optimal Duty Ratio Relationships

Similarly the inverter phase angle relationships are plotted in Figure 6.9. In this case a 2nd order polynomial is used for the commanded phase angle during dynamic control. The discrepancies occur at the higher power range since the theoretical calculations do not take into account any inverter losses. A lower inverter phase angle directly results in an increase in the flyback output voltage and therefore, counters the effect of these inverter losses. Together the two commanded relationships result in optimal power control of the test rig.

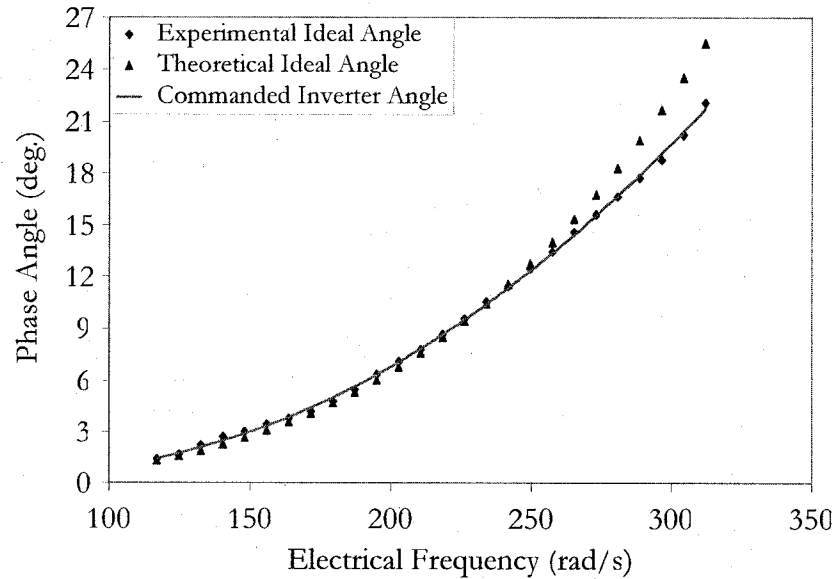


Figure 6.9: Comparison of Optimal Inverter Angle Relationships

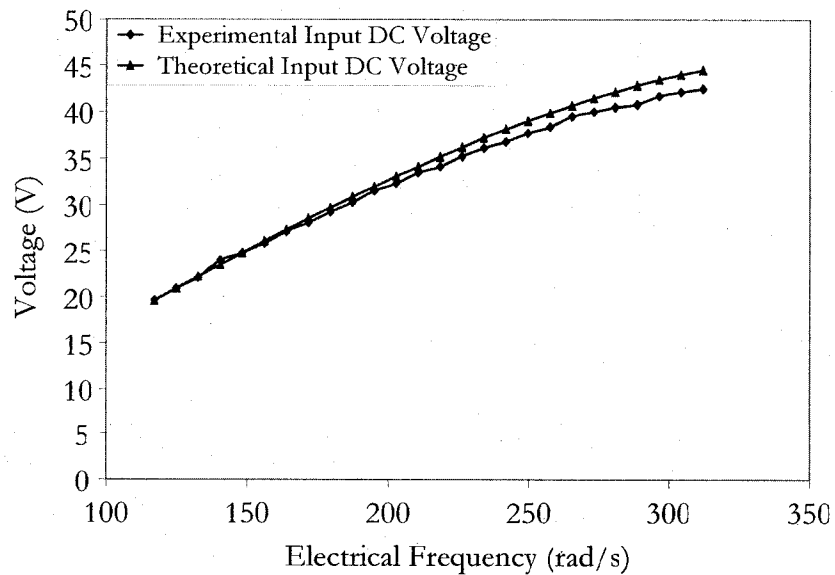


Figure 6.10: Comparison of Theoretical and Experimental Flyback Input DC Voltage

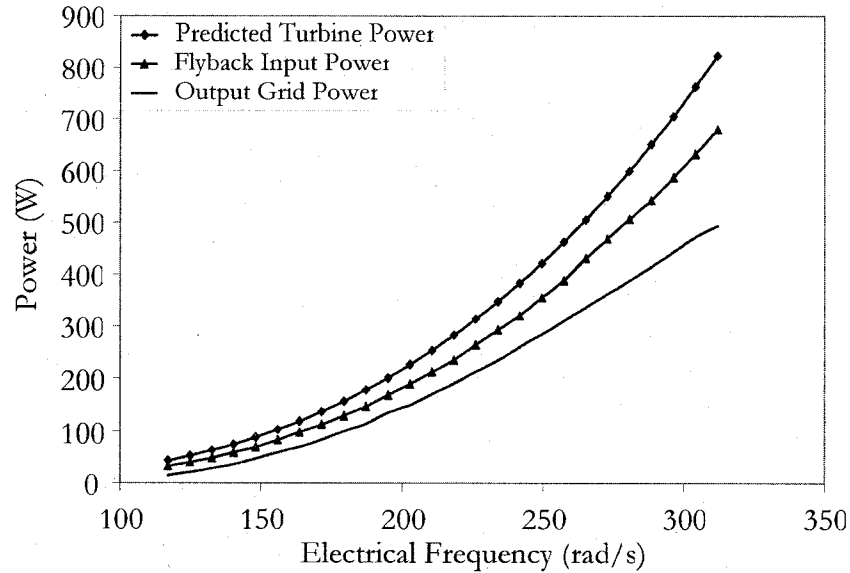


Figure 6.11: Optimal Power Curves at Various System Stages

During the controller verification, the optimal flyback input voltage is also recorded, depicted in Figure 6.10. The plots shown are similar since the theoretical calculations account for the experimental diode rectifier voltage drops and commutation overlap. Figure 6.11 shows that the predicted turbine power, resulting flyback input and grid output power follow the anticipated relationship with generator speed. The evident flyback and inverter losses are further investigated during the controlled variable wind operation.

6.3 Variable Wind Profile Response

The experimental test rig is tested under the conditions of a variable wind profile to determine the performance of the converter open-loop control. Before operating the system under any condition, an initial start up procedure is first implemented. The start-up allows the system to enter steady state before the converter control and wind profile can be activated. The start-up procedure is listed as follows:

1. Ensure all power supplies, grid components and cooling fans are plugged in.
2. Activate LabView code and enable the inverter switching.
3. Set grid RMS supply voltage to 120 V using the single phase variac.
4. Enable the flyback switching with an initial duty ratio of 0.6.

5. Turn on the wind emulator control at an initial constant low wind speed.
6. Activate the power electronic converter duty ratio and angle control.

A variable wind profile that begins at 3.75 m/s and reaches a maximum of 10 m/s is applied to the experimental test rig via equation 6.3.

$$v_w = \left| 5.45 \sin\left(\frac{t}{36}\right) + 0.8 \sin\left(\frac{t}{4}\right) + 3.75 \right| \quad (6.3)$$

Through the control verification it is identified that the controller cut-in wind speed is 3.75 m/s. Due to losses within the power electronic converter the test rig requires a higher than optimal generator speed at wind speeds below 3.75 m/s. Therefore, at these lower wind speeds, an uncontrolled case is ideal. Verification of the open-loop control is of the utmost importance and therefore, wind speeds below 3.75 m/s are disregarded.

The LabView code records the TSR, mechanical speed, generator line-to-line output voltage, and grid output power (Figure 6.12) over two wind cycles. Figure 6.13 shows the controller angle and duty ratio outputs, along with the high-side DC-link voltage.

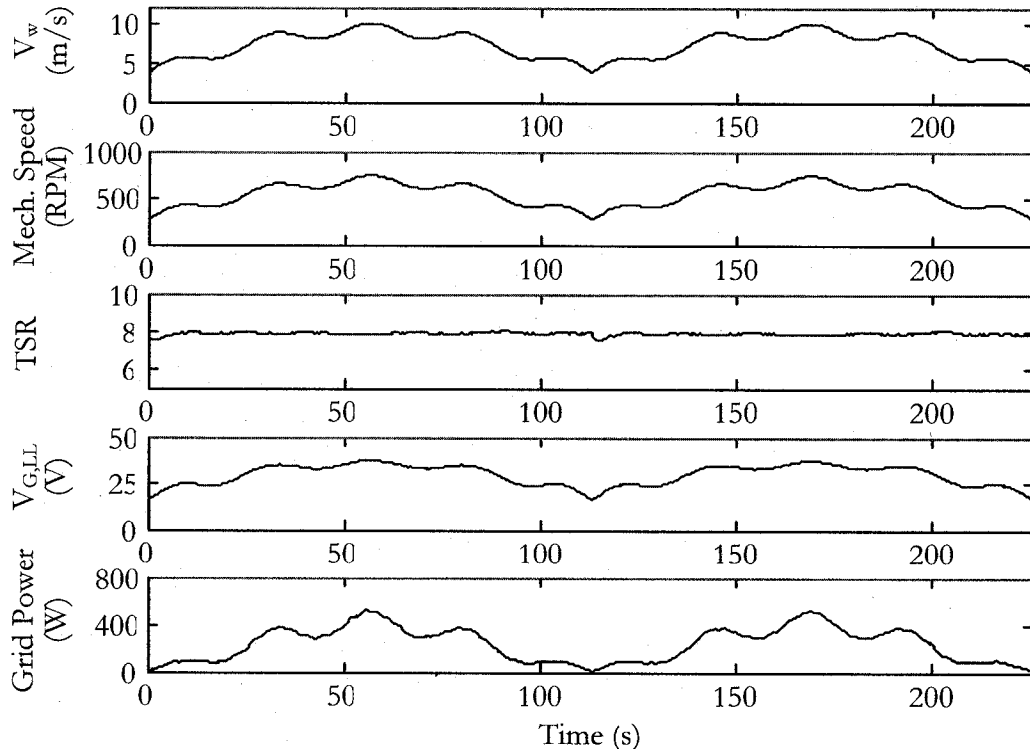


Figure 6.12: Dynamic System Results with a Variable Wind Speed

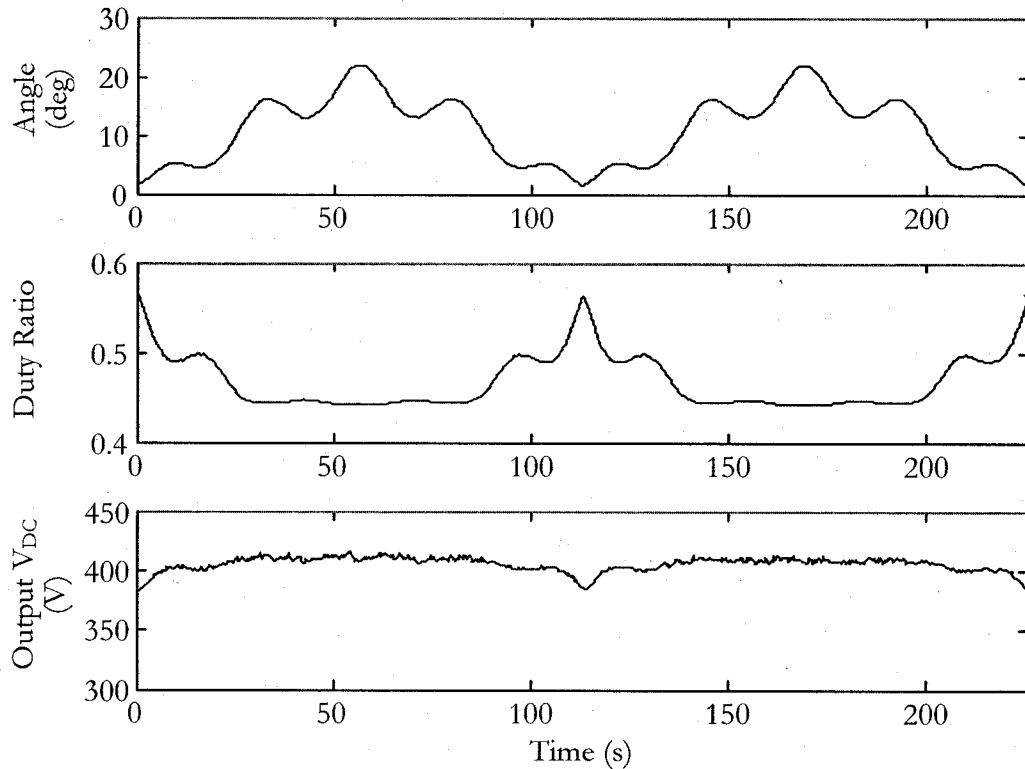


Figure 6.13: V_{DC2} , Commanded Angle and Duty Ratio with a Variable Wind Speed

The controller performance is shown to be excellent since the TSR value remains near the optimal value of 7.8. Although the TSR appears to almost reach 8, this is of little concern since the coefficient of performance (C_p) does not deviate significantly enough to result in a noticeable reduction in power capture. The TSR does slightly decrease at low wind speeds. However, the converter continues to draw power and high wind speed performance is more important. As expected, the generator output voltage and mechanical speed follow a similar form as the wind speed during system control. The converter captures power throughout the entire wind profile, reaching a maximum of approximately 520 W.

The high-side DC-link voltage varies slightly since it is influenced by both the commanded duty ratio and angle. The large output capacitance allows for a relatively constant output DC-link. The slight dip in the DC-link voltage is attributed to the less than optimal generator speed and low TSR at low wind speeds. The commanded controller outputs are smooth, and show the ability of the controller to quickly find the next optimal operating point. The power levels at multiple stages of the test rig are recorded, and are shown in Figure 6.14.

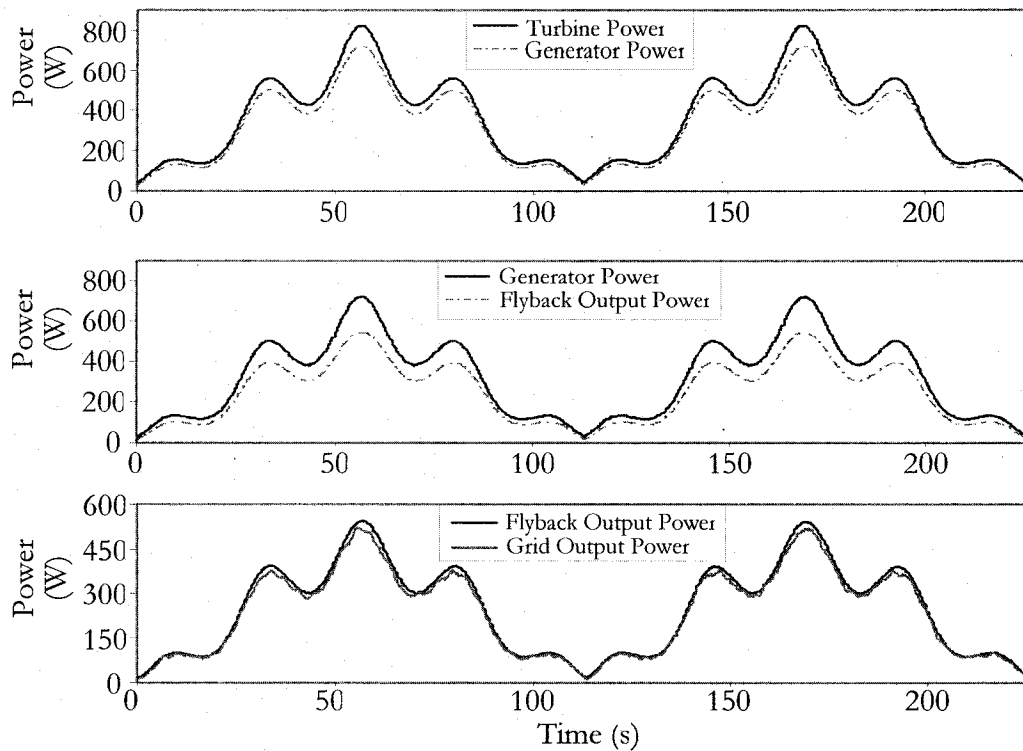


Figure 6.14: Various System Power Results with a Variable Wind Speed

This figure shows and compares the power levels ranging from the expected turbine power, generator output power, flyback output power and finally the grid output power. The results show that the flyback converter contributes most of the loss within the system. The generator efficiency is fairly high during the majority of the wind range, with a slight drop off at the peak power. On the other hand, the inverter proves to perform at the highest efficiency with minimal losses throughout the entire wind profile. The losses shown for the flyback converter also include any losses produced by the three phase diode rectifier, though they are assumed to be minimal.

Figure 6.15 depicts the generator and flyback efficiencies and energy transferred by the flyback converter. The efficiency of the flyback converter reaches a maximum of approximately 80% during high wind speeds. The diminished flyback efficiency may be caused by the MOSFET switching losses and snubber losses due to transformer leakage reactance. The flyback converter receives about 72.53 kJ of energy and is only able to transfer 56.21 kJ of energy, resulting in an overall flyback efficiency of 77%.

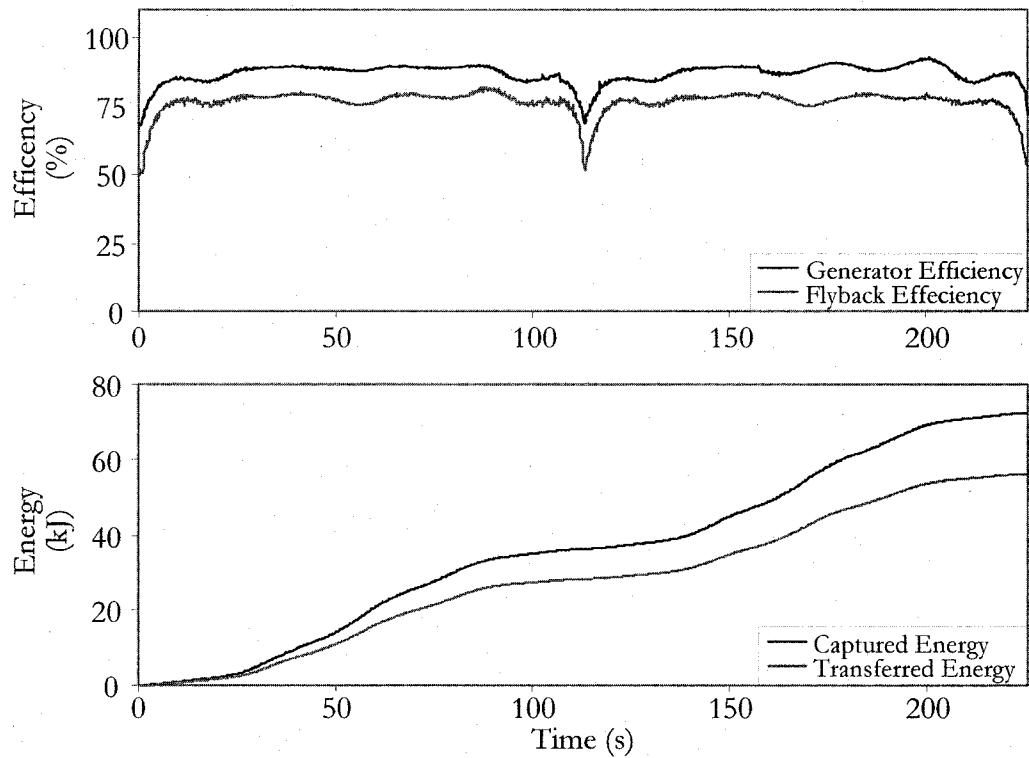


Figure 6.15: Flyback Efficiency and Energy Capture with a Variable Wind Speed

A powdered iron core is used for the transformer since it is readily available. It has been discovered that powdered iron cores are of greater use at higher frequency above 100 kHz and operate at a relatively low permeability. Alloy metal cores have the highest saturation flux density and permeability among ferrites and powder cores. Alloy metal cores are limited to applications with switching frequencies below 30 kHz [37]. The flyback transformer requires a large amount of energy to be transferred at a switching frequency of 10 kHz. The alloy core is a formidable choice in improving the flyback transformer performance under these experimental conditions.

6.4 Controller Step Response

The open-loop controller step response is tested by applying a 1 m/s and 2 m/s step change in wind speed. A rate limit is placed upon the controlled flyback duty ratio and inverter phase angle. This rate limit is implemented for protection of the output DC-link capacitors that are rated at 450 V. Since a slight decrease in the flyback duty ratio heavily affects the DC-link voltage, it is important to not allow this change to occur instantaneously. An

instantaneous change could cause an over-voltage situation to occur. A rate limit of 0.015/s is placed on the duty ratio, and a $5^\circ/\text{s}$ rate limit is placed on the inverter phase angle change.

The system is initiated using the startup steps previously mentioned in order to set the steady state condition. The wind speed is manually controlled and slowly increased to a starting wind speed of 6 m/s. Recording of the data is enabled and a step change of 1 m/s (from 6 m/s to 7 m/s) is forced manually through LabView. The system and controller step response are depicted in Figure 6.16.

The system response is swift after the 1 m/s (3.6 km/h) step change is applied. The TSR quickly drops as the wind speed is stepped up, and the controller responds by altering the angle and duty ratio until the optimal point is reached. The TSR, generator output voltage and mechanical speed settle back to their optimal values. In a similar manner, a step down of 1 m/s is also applied. The system responds similarly however, in this case the TSR suffers a sudden increase. This increase is once again mitigated by the controller action until the optimal value is reached.

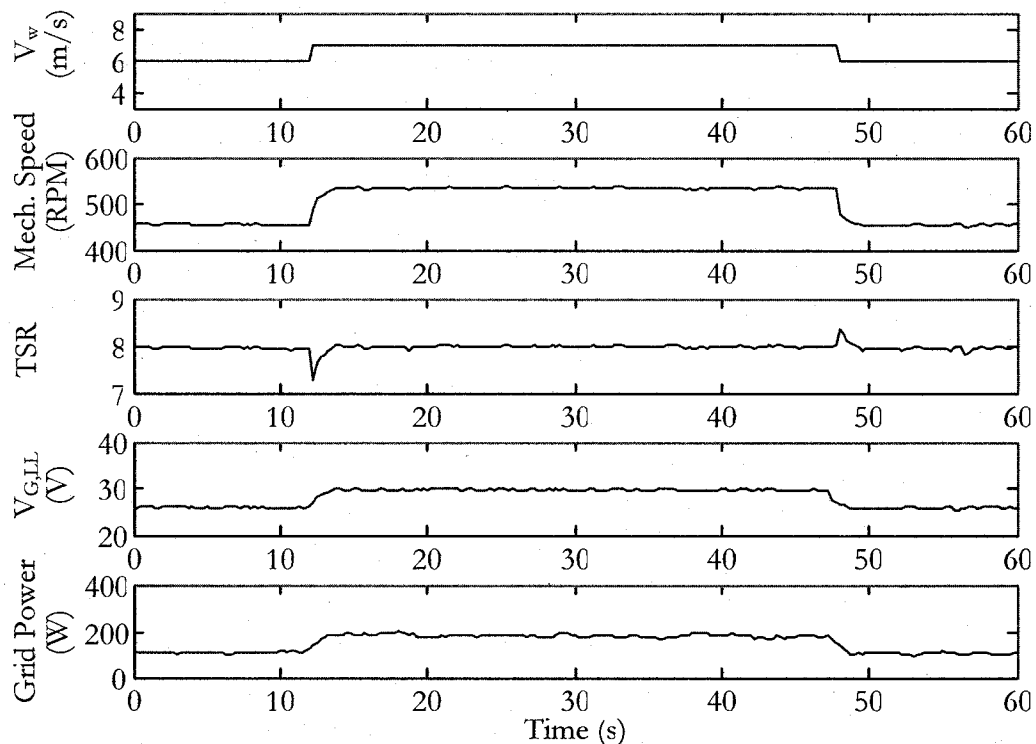


Figure 6.16: Dynamic System Results with a 1 m/s Wind Step Change

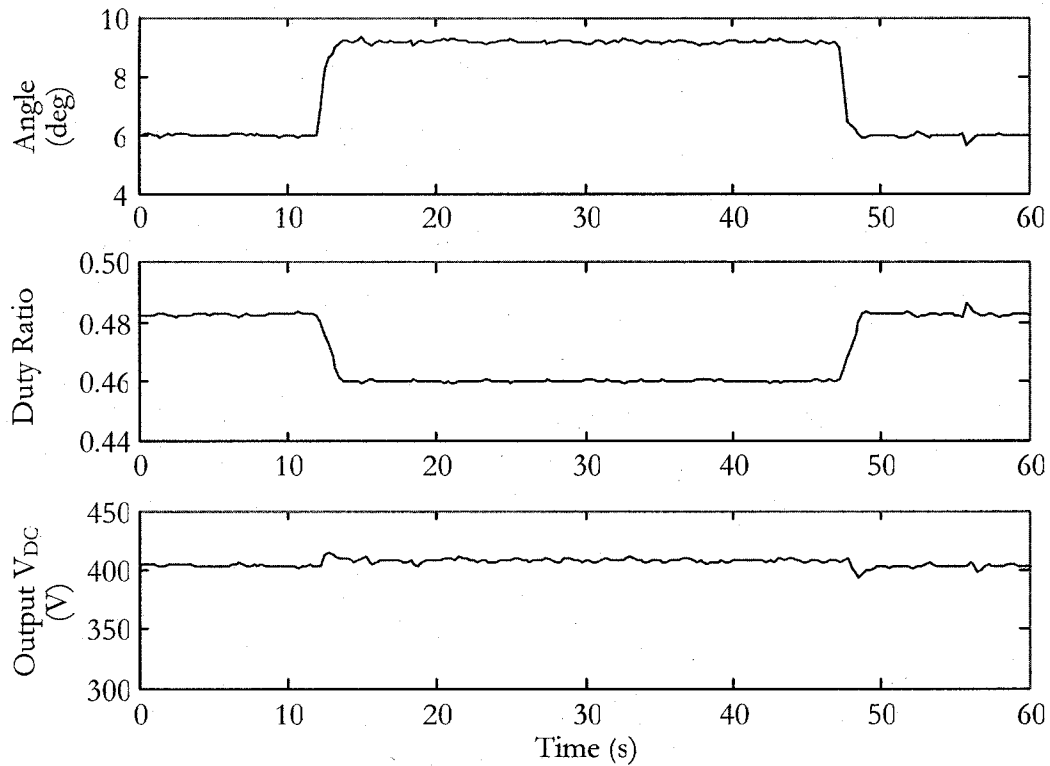


Figure 6.17: V_{DC2} , Commanded Angle and Duty Ratio with a 1 m/s Wind Step Change

The resulting controller action is also recorded. As shown, the duty ratio and angle both under go changes once the step change is employed. A 0.0231 change in duty ratio is required, which, with the rate limit, requires 1.54 s of elapsed time. This change in duty ratio is depicted in the ramp decline and incline shown in Figure 6.17. The angle change requires just 0.638 s, and is a much faster change as expected. An increase in angle will normally decrease the DC-link voltage, and a decrease in duty ratio causes an increase in the same voltage. Although the duty ratio is changed at a much slower rate, it still had a greater affect on the DC-link voltage since voltage increase is observed during the step change.

To further verify the ability of the controller to handle a step change in wind speed, a 2 m/s step change is also applied. In this case the wind speed is stepped from 5 m/s to 7 m/s instantaneously. This is the equivalent to a 7.2 km/h instantaneous wind gust. The system response and control command signals are displayed in Figure 6.18 and Figure 6.19 respectively.

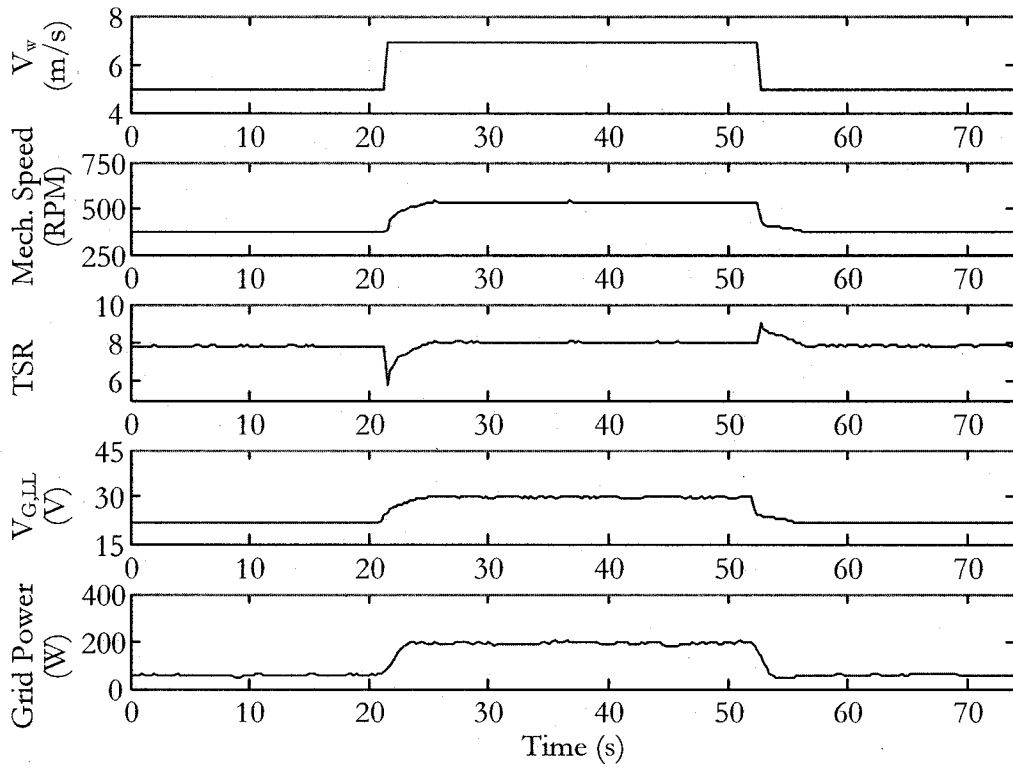


Figure 6.18: Dynamic System Results with a 2 m/s Wind Step Change

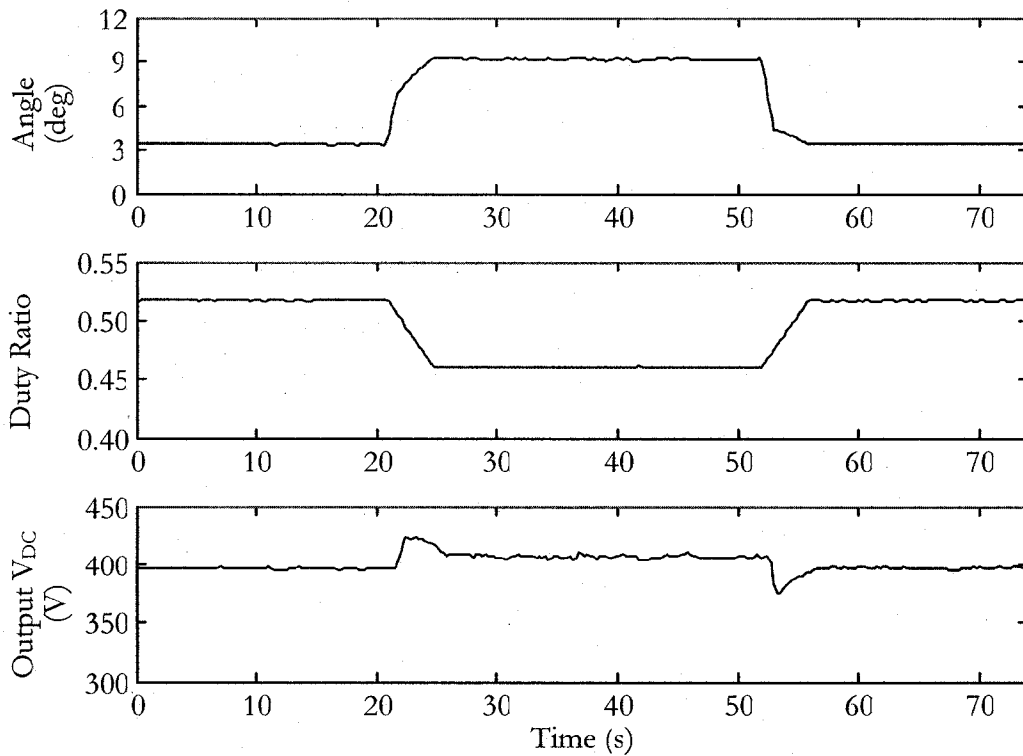


Figure 6.19: V_{DC2} , Commanded Angle and Duty Ratio with a 2 m/s Wind Step Change

The controller shows an excellent response to the change in wind speed. The deviation in TSR during the step changes is again rectified back to the optimal value. The optimal values of mechanical speed, generator voltage and grid power are also achieved, both during step-up and step-down of the wind speed. The angle and duty ratio also change according to the controller command, and are once again rate limited for protection. This rate limit is clearly evident in the figure, which displays a slight ramp in the commanded duty ratio and angle. The DC-link voltage experiences a slightly higher peak during the increase in wind speed. Although it does not reach the maximum of 450 V, this rise is again due to the effect of quickly changing the duty ratio.

A larger step change, for example 3 m/s, may have caused this voltage to exceed the 450 V causing LabView to abruptly shut the system down. Similarly, a step change at higher wind speeds will also cause a larger increase in DC-link voltage. For example, the 2 m/s step change results in an output power change of 124 W. If the change occurs from 8 m/s to 10 m/s, a power change of 240 W would have been experienced. This larger change in power may result in the output DC-link voltage exceeding the 450 V limit.

6.5 Chapter Summary

This chapter provides the experimental results for the wind energy converter test rig. The variable wind dynamic system results are provided, and the validity of the open-loop continual controller is verified. The controller response to a subjected 1 m/s and 2 m/s wind speed step change have also been proven acceptable.

Chapter 7

Conclusions and Future Work

Wind energy continues to grow with, technological advances in power electronic devices leading the way. Wind energy has become a viable source of energy throughout the world, and competes with traditional means of energy production. The goal of this research is to design a cost efficient power electronic converter, for a small-scale grid connected wind turbine. The converter control is designed to achieve maximum power transfer from the wind turbine over a wide speed range. The converter is also low in cost as it only requires the generator speed as an input in controlling the flyback duty ratio and inverter phase angle. The proposed system keeps the cost to a minimum, with just three power electronic switches and a simple open-loop control scheme. In addition it adds the desirable electrical isolation through the flyback high frequency transformer.

Typically, grid connected wind energy systems are comprised of back-to-back controllable converters. However, this configuration causes an increase in cost even though controllability is enhanced. The method of MPPT control has been widely researched, and has proven to provide reasonable performance. However, MPPT encounters issues in reaching the optimal operating point during situations in which the wind speed changes quickly. Other systems employ a constant DC-link voltage, usually set for maximum performance at the site average wind speed. At wind speeds above and below the site average, these systems do not operate at the most ideal point.

The proposed system employs a diode rectifier for the initial AC-DC conversion, an immediate benefit to the overall cost of the system. The system also includes a flyback DC-DC converter in the DC-link. This converter provides the necessary torque control of the generator. The torque control is performed through the manipulation of the commanded flyback duty ratio, which forces an optimal DC-link voltage. The alteration of this voltage, in turn, alters the generator mechanical speed and operation of the wind turbine. In addition, the flyback transformer is designed and constructed to transfer the captured energy, and boost the DC-link voltage for inverter conversion. The flyback transformer also provides isolation between the generator and grid. Other systems require the added cost of a separate

transformer since their converters do not provide the desirable electrical isolation. For flyback MOSFET protection, a snubber circuit is designed to handle large voltage spikes during switch turn off. Finally, the converter is concluded by a single phase inverter that uses phase angle control to provide maximum power transfer to the grid.

The flyback converter control follows a fixed relationship between the optimal duty ratio and generator electrical frequency. Likewise, the inverter control tracks a fixed relationship between the voltage phase angle and electrical frequency. This open-loop method of control proves to follow the optimal turbine TSR excellently for wind speeds ranging from 3.75 m/s to 10 m/s. The controller response to wind step changes of 1 m/s and 2 m/s is exceptional. In both cases the system returns to the optimum point after a brief transient.

The benefits of a controlled system are verified in simulations, with a current controller providing increased power capture over results using a fixed DC-link. The proposed system is experimentally designed and constructed with the wind turbine emulated by a DC power supply and DC motor. The wind emulation is controlled through LabView real-time control. The open-loop control is preferred over the simulated current control due to a reduction in complexity. The control relationships may be easily modified for different wind turbines having different coefficient of performance profiles. LabView real-time control also provides the means to controlling both the flyback and inverter switching. The entire system is extremely cost effective, with a total of only 3 switches used in combination with a simple open-loop control.

The proposed test rig and control operate well throughout the applied wind speed range. Some improvements may be made by first examining other design methods for the flyback transformer. Due to time constraints, and other design obligations, the flyback transformer design is not the main focus of this research. Placing more emphasis on the transformer design may improve the flyback converter performance. Over voltage concerns for the DC-link capacitors hindered the response of the controller. An increase in capacitor voltage limit may allow the controller to shift operating points during wind gusts at a faster rate, if needed.

The use of open-loop control on the inverter and flyback were a means to verifying the ability of using the flyback converter as an option for a DC-DC boost stage. This control option results in a simple control algorithm at a reduced cost. If the cost of current and

voltage sensors are not an issue than future work may entail the use of a current control. Current control may allow for a reduction in the output inductor size and offers more protection as over current situations can be easily monitored. Future work involving the use of a current control may also require a phase lock loop (PLL) in order to accurately match the phase of the grid reference. The PLL will help achieve an accurately controlled PWM switching technique for the current control. Finally, a non-computer control, possibly through analog components or a PIC (Peripheral Interface Controller), is an ideal choice for system practicality and future testing on a real wind turbine.

Bibliography

- [1] Global Wind Energy Council. Global Wind 2005 Report. April 7, 2006.
- [2] P. Fairly. Steady as she blows. *IEEE Spectrum*, 40(8):35-39, August 2003.
- [3] J. Christensen, F. Denton, A. Garg, S. Kamel, R. Pacudan, and E. Usher. Changing Climates – A role of renewable energy in a carbon-constrained world. *The United Nations Environment Programme*, December 2005.
- [4] American Wind Energy Association. “How much does wind energy cost?” Washington, D.C., USA; <http://www.awea.org>, accessed February 22, 2006.
- [5] H. R. Zamot, E. O’Neill-Carrillo, and A. Irizarry-Rivera. Analysis of wind projects considering public perception and environmental impact. In *Proceedings of the 37th Annual North American Power Symposium*, Pages 591–596, October 23–25, 2005. IEEE.
- [6] E. Martinot. Renewables 2005 Global Status Report. *Beijing International Renewable Energy Conference 2005*, November 6, 2005.
- [7] A. Sayigh. World renewable energy. In *Proceedings of 3rd World Conference on Photovoltaic Energy Conversion*, volume 3, pages 2556–2561, May 12–16, 2003. IEEE.
- [8] S. Al-Hallaj. More than enviro-friendly: renewable energy is also good for the bottom line. In *IEEE Power and Energy Magazine*, 2(3), Pages 16–22, May–June 2004. IEEE.
- [9] Bergey Windpower Company. Turbine Product and Prices Information Available at: <http://www.bergey.com>
- [10] Z. Chen and E. Spooner. Current source thyristor inverter and its active compensation system. In *Proceedings on Generation, Transmission and Distribution*, volume 150, pages 447–454, July 2003. IEE.
- [11] N. Yamamura, M. Ishida, and T. Hori. A simple wind power generating system with permanent magnet type synchronous generator. In *Proceedings of the IEEE International Conference on Power Electronics and Drive Systems*, volume 2, pages 849–854, July 27 – July 29, 1999.
- [12] M.G. Simoes, B.K. Bose, and R.J. Spiegel. Fuzzy logic based intelligent control of a variable speed cage machine wind generation system. *IEEE Transactions on Power Electronics*, 12(1):87–95, January 1997.

- [13] S. Mueller, M. Deicke, and Rik W. De Doncker. Double fed induction generator system for wind turbines. *IEEE Industry Applications Magazine*, 8(3):26–33, May–June 2002.
- [14] S. Bhowmik, R. Spee, and J.H.R. Enslin. Performance optimization for doubly fed wind power generation systems. *IEEE Transactions on Industry Applications*, 35(4):949–958, July–August 1999.
- [15] I. Schiemenz, M. Stiebler. Control of a permanent magnet synchronous generator used in a variable speed wind energy system. In *IEEE International Machines and Drives Conference*, pages 872– 877, June 2001.
- [16] S. Bhowmik and R. Spee. Wind speed estimation based variable speed wind power generation. In *Proceedings of the 24th Annual Conference of the IEEE Industrial Electronics Society*, volume 2, pages 596–601, Aug. 31 – Sept. 4 1998.
- [17] L. Zhang, C. Wathanasarn, and W. Shepherd. Application of a matrix converter for the power control of a variable-speed wind-turbine driving a doubly-fed induction generator. In *23rd Annual International Conference on Industrial Electronics, Control and Implementation*, volume 2, pages 906–911, Nov. 1997. IEEE.
- [18] L. Vogel. 1987, The North Dakota wind energy handbook. North Dakota Energy Extension Service Program and North Dakota Office of Intergovernmental Assistance State Energy Program, 1987.
- [19] The Weather Network, Regional Monthly Statistical Information Available at: <http://www.theweathernetwork.com/weather/stats/index.htm>, accessed July 5, 2006.
- [20] R.D. Richardson and G.M. McNerney. Wind energy systems. In *Proceedings of the IEEE*, volume 81, pages 378–389, US Windpower, Livermore, CA, USA, March 1993.
- [21] G.L. Johnson. *Wind Energy Systems*. Prentice–Hall Inc., January 1985.
- [22] Intermediate Technology Development Group. Wind for electricity generation. Bourton on Dunsmore Rugby, United Kingdom; <http://www.itdg.org>, accessed March 10, 2006.
- [23] K. Tan and S. Islam. Optimum control strategies in energy conversion of PMSG wind turbine system without mechanical sensors. *IEEE Transactions on Energy Conversion*, 19(2):392–399, June 2004.
- [24] P. Ledesma and J. Usaola. Doubly fed induction generator model for transient stability analysis. *IEEE Transactions on Energy Conversion*, 20(2):388–397, June 2005.
- [25] S.J. Chapman. *Electric Machines Fundamentals – 3rd Edition*. McGraw–Hill, August 21, 1998.

- [26] R.L. Ames. *AC Generator: Design and Application*. John Wiley and Sons, 1990.
- [27] Chen and E. Spooner. Grid interface options for variable-speed permanent-magnet generators. In *Proceedings on Electric Power Applications*, volume 145, July 1998. IEE.
- [28] P. Wolfgang. *The Challenge of Renewable Energy Market Deployment*. The World Council for Renewable Energy, March 2006.
- [29] M.R. Patel. *Wind and Solar Power Systems*. CRC Press LLC, 1999.
- [30] R.S. Pena, R.J. Cardenas, J.C. Clare, and G.M. Asher. Control strategies for voltage control of a boost type PWM converter. In *32nd Annual Power Electronics Specialists Conference*, volume 2, pages 730–735, June 2001. IEEE.
- [31] Dr. John Salmon. *EE 431 Power Electronics*. Electrical Engineering, University of Alberta, 2nd Floor ECERF, May 2006.
- [32] A.M. Knight and G.E. Peters. Simple wind energy controller for an expanded operating range. *IEEE Transactions on Energy Conversion*, 20(1):459–466, June 2005.
- [33] S. Jiao, G. Hunter, V. Ramsden, and D. Patterson. Control system design for a 20kW wind turbine generator with a boost converter and battery bank load. In *32nd Annual Power Electronics Specialists Conference*, volume 4, pages 2203–2206, June 2001. IEEE.
- [34] A.M. De Broe, S. Drouilhet, and V. Gevorgian. A peak power tracker for small wind turbines in battery charging applications. *IEEE Transactions on Energy Conversion*, 14(4):1630–1635, December 1999.
- [35] Micrometals Iron Powder Cores. PC: General Material Properties Information Available at: http://www.micrometals.com/materials_index.html.
- [36] A. Hren, J. Korelic, and M. Milanovic. RC-RCD clamp circuit for ringing losses reduction in flyback converter, *IEEE Transactions on Circuits and Systems II: Express Briefs*, 53(5): 369–373, May 2006.
- [37] H. L. Chan, K. W. E. Cheng, T. K. Cheung and C. K. Cheung. Study on magnetic materials used in power transformer and inductor. In *2nd International Conference on Power Electronics Systems and Applications*, pages 165–169, November 2006.